A Study on Topology Optimization for Two-Dimensional Steady-State Heat Conduction Problems Using Boundary Element Method

by

Guoxian Jing

A dissertation submitted in partial fulfillment of the requirements

for the degree of Doctor of Engineering

Nagoya University

August 2015

ABSTRACT

Topology optimization is one of the structural optimizations and is a mathematical approach to find the optimal material layout within the given design domain. The objective function appropriately defined reaches its optimum value after optimization under given constraints by using a certain numerical method to solve this optimization problem. It is the most flexible structural optimization compared with other sizing and shape optimizations since it allows appearances of holes in the optimum material layout. Topology optimization has received wide attention and has been implemented through the use of finite element methods based on plenty of optimization techniques, such as homogenization method (HM), solid isotropic material with penalization (SIMP), evolutionary structural optimization (ESO) and level set method (LSM). Based on these popular techniques, topology optimization has been applied to many physical problems and engineering applications such as mechanics, vibration, acoustic, thermal and electromagnetic problems. However, most of the approaches suffered some drawbacks such as checkerboard patterns, intermediate density material and dependency on initial configurations. Moreover, these approaches take much computational time and result in non-smooth boundaries.

This dissertation aims at constructing a level set-based topology optimization method using the boundary element method for heat conduction problems to find the optimal material configuration. The boundary element method is used for the heat conduction analyses by meshing the boundary of the material for each iterative step of optimization to avoid the intermediate density problems.

This dissertation is organized as follows: Chapter 1 includes a classification of structural optimizations and the development of the popular optimization techniques, and reviews starting from their appearance to working principles, applied problems, and advantages and disadvantages. Chapter 2 introduces the concept of the level set method to represent the property (material or void) of design domain, combining the boundary element method which is used to solve heat con-

duction problems, then constructs an time evolution equation for updating the level set function. In the evolution equation, topological derivative or sensitivity concept is introduced and a regularization term is used to control the complexity of the configurations; Chapter 3 provides a topology optimization algorithm and gives a discretization of the time evolution equation for updating level set function. Chapter 4 presents a treatment of the newly generated boundaries as insulating boundaries and derives the topological derivative under the insulating boundary condition for heat conduction problems using boundary element method. The correctness of the topological derivative and its dependency on mesh and initial configuration of the material are validated. Chapter 5 derives the topological derivative under the heat transfer boundary condition using the boundary element method and demonstrates its validation through a numerical example. Also, a topology optimization for two dimensional heat conduction problems under heat transfer boundary condition is developed. Chapter 6, while basing on the topology optimization scheme under heat transfer condition in preceding chapter, considers the cases in which the objective functions for the temperature and heat flux are defined on design-dependent boundaries, which are newly generated ones but evaluated in objective function in this chapter. The topological derivatives of the objective functions both for the temperature and the heat flux are verified through numerical examples. The chapter also presents the topology optimization examples using the corresponding topological derivatives. Finally, Chapter 7 reaches the conclusions of this dissertation.

In conclusion, the level set-based topology optimization for two-dimensional heat conduction problems using the boundary element method under insulating boundary condition, heat transfer boundary condition, as well as morphing boundary considered in the objective functions of temperatures and the heat flux, are proposed. The use of the boundary element method and re-meshing of the boundaries through every iterative step of optimization computation enables this novel characteristic. The proposed method does not suffer checkerboard patterns, intermediate density and zigzag boundaries of the optimum layout of the material. Moreover, it

can provide designers with various optimal configurations with smooth boundaries by adjusting the regularization parameter value. It possesses the advantage of easy meshing compared with the finite element method. Also, the boundary element method is especially convenient and accurate when objective function is defined on boundaries of the configurations. The level set method works well in obtaining boundary element information for solving heat conduction problems using boundary element method. Hereto, the significance of this work lies in the combination of the level set method and the boundary element method in topology optimization for heat conduction problems. Thus, the proposed method will have a great contribution in the designs of thermal devices in engineering applications. Meanwhile, it is suggested that the level set-based topology optimization combining with the boundary element method can be used in other physical problems, such as mechanics, acoustics, and electromagnetic problems, especially in the problems with objective functions defined on boundaries of the new material configurations.

ACKNOWLEDGEMENTS

I would like to express my gratitude and appreciation to Professor Matsumoto, my research supervisor, for offering me the opportunity of conducting the research of topology optimization, which is an quite interesting topic in international forward research fields, and specially to mention that for his suggestion of using the boundary element method, which is not widely researched but has already been proved to be not just an effective and efficient but also superior method to finite element method in solving many physical fields problems.

I would also like to extend my thanks to Dr. Isakari, the Assistant Professor at Matsumoto Lab, for his instructions on derivation of mathematical and physical problems, for his suggestions on writing journals, and particularly for his patience to listen to and communicate with me.

Next, I would like to thank Dr. Yamada, the Assistant Professor at Kyoto University, who specifies in topology optimization and exported his idea into Matusmoto Lab, which makes the possibility of topology optimization combining with the boundary element method, as my research topic.

Besides, I would like to thank Dr. Gao, Mr. Watanabe, Mr. Kourogi, Mr. Matsuda, and other members in Matsumoto Lab, for communication on research.

Finally, I would like to thank my family to the most, for their encouragement and support.

Guoxian Jing

Nagoya, August 26, 2015

Contents

List of Figures

Tables

List of Symbols

$D \backslash \Omega$	Void Domain
D	Design Domain
F	Objective Function
G	Area Constraint
$G_{\max}$	Admissible Upper Limit of Area
$H(\phi(x))$	Heaviside Function
Γ_0	Boundary between Material and Void Domain
Γ_h	Boundary with Robin Boundary Condition
Γ_q	Boundary with Neumman Boundary Condition
Γ_u	Boundary with Dirichlet Boundary Condition
Ω	Material Domain
λ	Lagrange's Multiplier
μ	Adjoint Variable for Adjoint Problems
$\overline{F}(\phi)$	Unconstrainted Optimization Problem
$\phi(x)$	Level Set Function
h	Heat Transfer Coefficient [W/m^2·K]

k	Thermal Conductivity [W/m·K]
q	Heat Flux [W/m^2]
u	Temperature [K]
u_∞	Ambient Temperature [K]
α	Proportional Constant of Reaction Diffusion Equation
β	Proportional Constant of Reaction Diffusion Equation
K	Proportional Constant of Evolution Equation
Γ_{N}	Non-design Boundary
$\mathscr{T}$	Topological Derivative or Sensitivity
τ	Regularization Parameter of Evolution Equation
t	Fictitious Time of Evolution Equation
Δt	Time Increment
$q^*(x,y)$	Fundamental Solution of Laplace's Equation for Flux [W/m^2]
$u^*(x,y)$	Fundamental Solution of Laplace's Equation for Potential [K]
$N_i(\xi,\eta)$	Shape Function, $i = 1,2,3,4$
$\dfrac{\partial N_i}{\partial \xi}$	Derivative of Shape Function, $i = 1,2,3,4$
ω	Weight Residual Function
Γ_ε	Boundary for Newly Generated Hole
Ω_ε	Region of Hole [m^2]
$\bar{\xi}$	Outward Normal Vector to Circle of Hole
$\bar{n}$	Inward Normal Vector to Circle of Hole

ε	Radius of Hole [m]
$\hat{u}$	Target Temperature [K]
Γ_f	Integral Boundary of f
f	Integral Kernel of Objective Function F

Note: Symbols that are not followed with units are dimensionless quantities.

Chapter 1

Introduction

Design optimization is to find a structural configuration to make an objective function reach its maximum or minimum, by which to achieve the best performances of devices, under certain constraints.

1.1 Classification of structural optimization

"Structure" refers how the parts of a thing relate to each other or how a thing is composed of parts. This word is used widely in different branches of research subjects, social, economic, architectural, chemical and physical structures, for example. "Structure", in this dissertation, refers to the physical structure, that is, the state of material layout. Then the structure optimizations can be thought as the process of material redistribution. It is subdivided into Sizing [1, 2, 3, 4, 5], Shape [6, 7, 8, 9] and Topology optimization [10, 11, 12, 13, 14], which are to be introduced in the following paragraphs.

Sizing Optimization: It is to find the optimal size that makes the objective function defined reach to its maximum or minimum under certain constraints. It takes the size of the structure to be optimized as the design variable. Therefore, only the size can be changed in the optimization process. A general view of sizing optimization

is shown as Figure 1.1, in which the obtained configuration is also rectangle, but its length and height have changed.

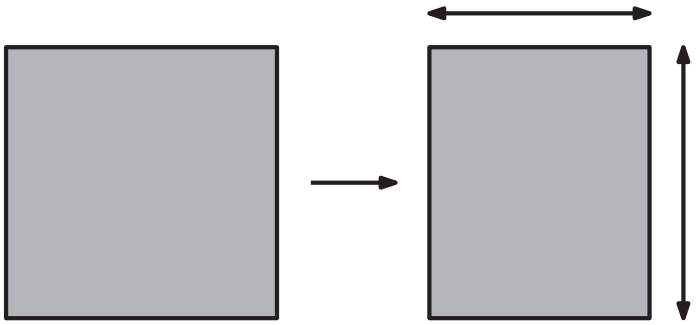

Figure 1.1: Sizing optimization

Shape Optimization: It is to find the optimal shape that makes the objective function defined reach to its maximum or minimum under certain constraints. It takes the boundary shape of the structure to be optimized as the design variable, and allows the boundary shape to change freely under given constrains. This, comparing with sizing optimization, provides designers with more design freedom. The Figure 1.2 gives a general view of shape optimization, in which one can see that the shape has change from rectangle to circle .

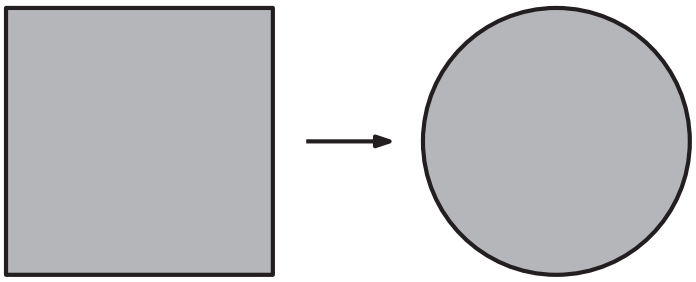

Figure 1.2: Shape optimization

Topology Optimization: It is a mathematical approach by which to find the optimal material layout, such that the objective function reaches its optimum value after optimization under given constraints, within the given design domain. The most important characteristic that differs from the former two is that this method allows

holes to appear in the process of optimization, which, to the max, provides designers with the most design room among the three kinds of optimization. Accordingly, **it is the most flexible structural optimization**. A general view of topology optimization is provided as Figure 1.3, in which one can find there are holes created after optimization.

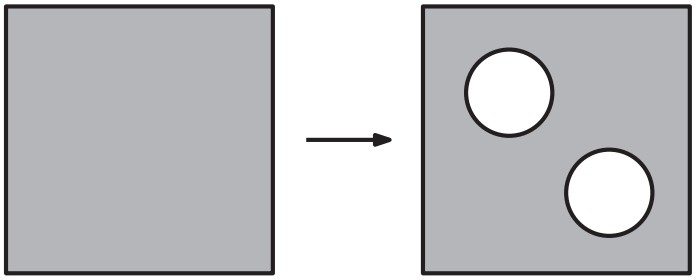

Figure 1.3: Topology optimization

It may be difficult to tell which optimization method is used just by looking at optimized structure. This is because topology optimization allows for appearance of holes and in the process of optimization holes may dissolve boundaries accordingly result the boundary change, which may be mistaken for the result of shape optimization. To avoid these misunderstandings, researchers usually identify what method is used by the practical techniques implemented in the theoretical derivation and its numerical implementation process.

1.2 Development of structural optimization

When it refers to structural optimization, it always dates back to truss layout optimization [15, 16, 17], in which Michell derived analytically the optimality criteria [18] for least weight trusses under the constraint of stress in the year of 1904. This was seen as the milestone contribution to truss layout optimization. However, interests of truss layout optimization was not active until 1950s. Michell's criteria [19] was applied by Cox to some simple layout problems; extended by Prager to other design conditions, say, natural frequency and stationary creep; developed by Hemp

into some other optimality criteria. In 1970s, Michell's optimality criteria was extended to grillages and formulated as the basic principles of optimal layout theory by Prager and Rozvany. In the following 30 years, the research of structural optimization made a great progress and many well-known methods appeared in shape and topology optimization, since sizing optimization is at the lowest level in optimization, which maybe the reason why there is few publications of sizing optimization on Google scholar except the just mentioned optimization of truss, where the length of frames and size of cross sections are variables to be optimized. These methods are named respectively as Homogenization Method [10], Solid Isotropic Material with Penalization, Evolutionary Structural Optimization [20], and Level Set Method [21] . Based on these methods, structural optimization, especially the topology optimization, shows a great potential in exploring ideal and optimized structure. They have been widely applied to many physical problems, such as compliant mechanisms [13, 14, 22], stiffness maximization problems [10, 23, 24], vibration problems [25, 26, 27], acoustic problems [28, 29], thermal problems [30, 31, 32] and electromagnetic design problems [33, 34, 35, 36].

Homogenization Method (HM): It is proposed by Bendsœ and Kikuchi [10] in 1988. Suzuki and Kikuchi have proposed a homogenization method for shape and topology optimization in 1991 [24] in which the mean compliance is considered. Díaaz presented the solutions to shape and topology eigenvalue optimization problems using a homogenization method in 1992 [37] to maximize a single eigenvalue. The homogenization method is also employed in a shape optimization of structures for multiple loading conditions in 1992 [38]. Nishiwaki has proposed topology optimization of compliant mechanisms using the homogenization method in 1998 [14]. Silva and Nishiwaki published a paper on optimization methods applied to material and flextensional actuator design using the homogenization method in 1999 [39]. Tartar has an introduction of the homogenization method in optimal design in 2000 [40]. Allaire has written an book on shape optimization by the homogenization

method in 2002 [41]. The homogenization method acts by representing a finite design space as a cellular body with a periodic microstructure. It has a material property that, in the optimization, the space with cells represents empty space; while the space with cells that holes disappeared represents material space. Based on such a material property, Homogenization Design Method (HDM) [42] appeared and applied to elasticity problems [43, 44], where it extends a finite design domain to a fixed design domain, and replaces the optimization problem with material distribution problem, using the characteristic function. However, it was noted by Campelo [45] that this approach does not need to make finite element again in the next iteration, only needed is to work on the fixed mesh; While, the bad is that a great number of variables comes out during the optimization. **Besides, this approach was found to be a checkerboard-suffering and mesh-dependent method.** An example of checkerboard problem shown in Figure 1.4 can be found in Sigmund's work in 1998 [46], which consists alternating material and void checker. From this figure, one can find that the apparent disadvantage is the boundary of the configuration is not smooth. This can be alleviated, even still not smooth microscopically, by using finer mesh, but will at the expense of increasing in data amount and computational time theoretically, as well as the numerical instabilities of resulting different optimal configuration, which can be in (c) and (d) of the same figure just referred. The instabilities have been studied by discussing the reason for the formation of checkerboard patterns [47]. The similar checkerboard patterns affecting the finite element solution of mixed variational problems have been studied extensively by Brezzi and Fortin [48] in 1991, where the formation of checkerboards is attributed to the relation to the violation of the so-called Babuska-brezzi [49] or LBB condition. Jog and Haber [50] also attributed the patterns in the layout problem to LBB type instability. To ease such instability, different function were suggested in a fashion similar to that suggested by the LBB condition to interpolate the displacement field and density variable, which were two variables in layout optimization problems. Yet the standard Babuska-Brezzi argument that were applied to mixed

variational problems are not met by the layout optimization problem.

Figure 1.4: Example of checkerboards (Cited from [46])

Solid Isotropic Material with Penalization (SIMP): It is also named the density method. It was originally considered by Bendsøe [51] in 1989. Later in 1991 Zhou and Rozvany has developed this method and the term "SIMP" was in fact proposed by Rozvany et al. [52] in 1992. This method is quite attractive in the engineering field. It assumes some explicit relationships between the normalized density and the actual material property in each cell, where the material property can be controlled simultaneously in every iterative step and updated by corresponding mathematical algorithm to reach final design [53]. This approach precludes anisotropic microstructures in problems formulation because it considers just isotropic microstructure, which can result in intermediate density which is shown in Figure 1.5 [54] to form the so-called "gray" area, whose density is less than 1.0 and results in blurred boundaries . Although the material with intermediate density is physically realizable, this method is useful for engineers who are interested in solid-void designs [55]. Some interpolation functions [56] and other restriction method, such as perimeter control [57], explicit density slop constraints [58], adaptive density [59] and regularized density control [60], were used to penalize the intermediate density to "black and white" patterns [52]. Nevertheless, this problem still arise such as in the compliance minimization of thermoelastic structures. Another problem is this method often results local optimal results while using big penalty to avoid the intermediate density as much as possible [61]. Moreover, some penalization on the intermediate material problem is at the expense of increase in finite element mesh. This can be found in an example given in Borrvall and Petersson's work [62]. **In**

a word, it is not only a method suffering intermediate density that does not enable us to have a clear boundary, but also a mesh-dependent one.

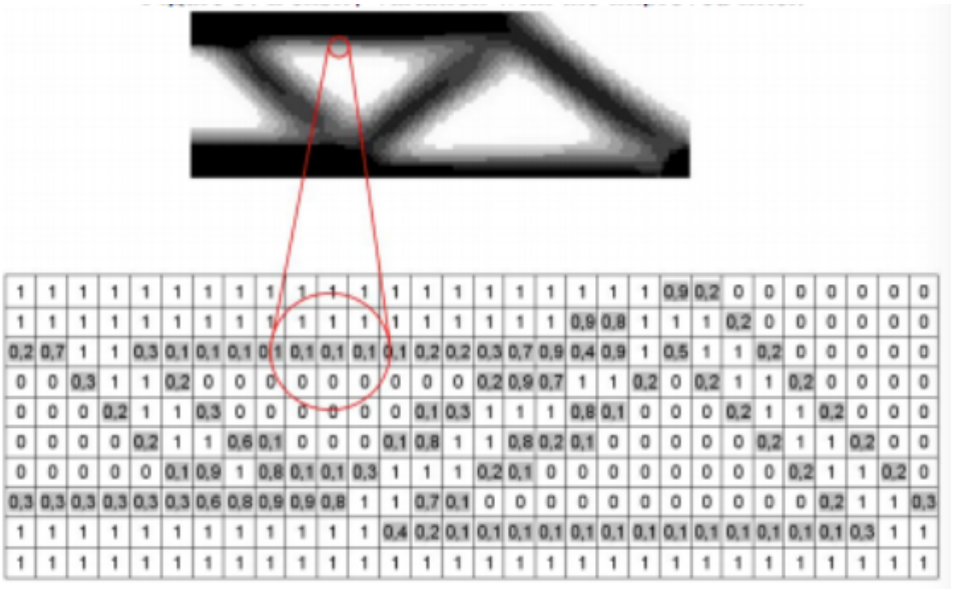

Figure 1.5: Example of Intermediate Density (Cited from [54])

Evolutionary Structural Optimization (ESO): It is introduced by Xie and Steven [20] in 1990s. It is based on the concept of gradually removing unnecessary or inefficient material from a structure to achieve an optimal design, in which corresponding constraints may be imposed on the structure, say, stiffness and frequency. Of course, corresponding criteria for removing material is needed to carry out the optimization under their constraints. In 1993, Xie and Steven proposed a simple evolutionary procedure for structural optimization, which can be seen as the foreshadow of the arise of the ESO concept. In 1996, they applied the evolutionary structural optimization to static problems [64] in which to minimize weight of structure to satisfy stiffness requirements and dynamics problems [63] in which the material is removed at the end of each eigenvalue analysis to realize the aim of maximizing or minimizing a chosen frequency of a structure. Later, this method has been also applied to the shape and topology design for heat conduction [31] in 1999, topology optimization of continuum structures [68] in 2010 and to architecture and urban de-

sign [69] in 2011. However, this method does not allow the deleted elements to be restored. To solve this, another method bi-directional ESO (BESO) [65] came out later, which allows material to be added and removed simultaneously, consequently leads to a more efficient optimization process and has been applied to multiple load case [66], and continuum structures with one or multiple materials [67].

The ESO method is a simple method for structural shape and topology optimization, as stated that the significance of such an evolutionary structural optimization (ESO) method lies in its simplicity in achieving shape and topology optimization in [63]. Meanwhile, since it is based on the simple idea of removing material, its solidness of theoretic basis maybe suspected. Yet, it was proved to have distinct theoretical basis and has potential to become a tool for design engineers [70]. Meanwhile, it is indicated that ESO seems to be producing truss-like topologies, thus it should be applied to structural problems with pin-jointed connections. For other types of structures ESO should be studied further in [70]. Beside, the checkerboard patterns can be also noticed in structural optimization using evolutionary structural optimization method, as observed in some other finite element based optimization problems. Li, Steven and Xie proposed a simple algorithm to suppress this problem rose in evolutionary structural optimization and demonstrated the capabilities of proposed algorithm with a lot of examples [71]. However, people can find the optimal configurations are always with zigzag boundaries, which is an inevitable result of using finite element based method. **One way to relieve this problem may be by increasing the number of discrete finite elements, but will be definitely at the expense of handling large amount data.**

Level Set Method (LSM): It was introduced by S. Osher and J. A. Sethian [21] relying in part on the theory of curve and evolution given in [72] , as a versatile method to implicitly represent evolutional interfaces in an Eulerian coordinate system. It is an useful approach to gain the contour of topological change by using the iso-surface of the level set function. It has been applied to many fields, such as hy-

dromechanics [73, 74, 75], picture processing [76, 77, 78], and CAD [79]. The level set method (LSM) has been seen as an effective numerical technique for tracking interfaces and shapes. It has been widely used in structural optimization.

Sethian and Wiegmann [80] firstly proposed a level set-based structural optimization method where an narrow band level set method [81] is used to represent the design structure through an embedded implicit function in the structural optimization of linear elastostatic structures under user-supplied constraints. Osher and Santosa constructed a numeral approach for optimization problems involving geometry and constraints using level set method which is updated its velocity which is calculated by using the functional gradients [82].

Belytschko et al. proposed a topology optimization with implicit functions, which is thought as the basis of level set methods, but is updated by the integration of hyperbolic conservation equations [83]. This method was applied to problems of optimizing single material and multi-material configurations. And it is linked to the extended finite element method (X-FEM) [84, 85], which enables the design to include features such as interfaces between materials that are not coincident with the mesh arbitrarily positioned cracks, holes, etc. The authors have applied this method in the optimization of cantilever beam structures, where this method was found to be mesh-independent (the results converge to the same configuration), free of the so-called grayscale and checkerboard phenomenon. However, this method is mentioned by the authors to undoubtedly has limitation in the geometries, since implicit surface definitions can result in difficulties at corners.

Wang et al. proposed a structural topology optimization method based on level set models for optimizing linearly elastic structures [86]. In this method, the authors obtained the so-called "Hamilton-Jacobi-type" equation, which defines an initial value problem for the time dependent function. Then "Hamilton-Jocobi-type" equation is used to update the level set function. Later, Wang et al. stretched this method to the optimization problems with multi-materials [87]. In the multi-materials optimizations, m level set functions are employed to represent a structure of $n = 2^m$

different material phases, in a manner as combining colors from three primary colors. Also for this reason, the multi-phase level set method is referred as a "color" level-set method. However, the method they proposed used an implicit, moving boundaries for topology optimization where boundaries (or holes) can emerge with each other to form new boundaries (or holes). For this reason, This method can be thought as a shape optimization method. Moreover, the numerical efficiency is restricted due to the numerical stability condition for discreting level set equation. Xia et al. [88] propose an semi-lagrange method for level set-base topology and shape optimization, in which the total time of optimization process is much less that using simple explicit upwind scheme. Later, Wang and Lim [89] proposed an extended level set method for shape and topology optimization. In this method, a radial basis function (RBF) is introduced construct the implicit level set function with a high level of accuracy and smoothness and to discretize the original initial value problem into an interpolation problem, for which a rapid convergence can be obtained.

Allaire, Jouve, and Toader has proposed a numerical method of shape optimization based on the level set function and on shape differentiation [90, 91], but indicated that the level set method does not solve the inherent problem of ill-posedness of shape optimization that shows itself in the frequent existence of local minima. It is explained that the level set method can easily remove holes but can not make new holes in the middle of a shape. Later, Allaire et al. proposed a structural optimization using topological and shape sensitivity via a level set method where the authors indicated that even the level set method can easily handle boundary propagation with topological changes, it does not allow nucleation of new holes at least in two dimensional case [92, 93]. Thus, the authors introduced the bubble method [94] or topological gradient method [95, 96], which is effective to introduce new holes in the optimization process. Then they coupled it with the level set method and formed an effective algorithm that can escape from local minima problem. To be mentioned, in the optimization algorithm, it is suggested that more level set step

should performed than topological gradients steps, which is implemented with an introduced coupling parameter. This parameter will result irregular shape with too small values and will not nucleate a new hole with too large values.

Yamada et al. [97, 98] proposed a topology optimization method using a level set model incorporating a fictitious interface energy derived from the phase field concept [99, 100]. The authors embedded the level set function in a fixed design domain and added a fictions interface energy term to objective function to regularize the optimization problem. This method is fundamentally different from the traditional level set-based optimization methods proposed by Wang et al. and Allaire et al. It is not a boundary-moving method, thus it can be truly classified as a topology optimization method. Moreover, the fictitious interface energy term acts as a regularization term that enables designers to obtain versatile configurations according to engineering needs. The authors have applied their method to internal heat generation problem where different configurations were obtained with different regularization value, which shows this method is an design-dependent one. Moreover, it is a method that initial configuration does not affect final optimal configuration. In the following, Yamada et al. have this method applied to mean compliance, compliant mechanism [101], vibration, and heat transfer problems.

Topology optimization has been research widely but most research just mentioned are based on finite element method. Besides, Nima Bakhtiary for the first time presented a new interface between CAOSS and MSC/NASTRAN. CAOSS (Computer Aided Optimization System Sauter) is an optional finite element module for the efficient sizing, shape and topology optimization [102]. Zhou et. al. presented a topology optimization for negative permeability metamaterials using level-set algorithm, where the authors used the finite-difference time-domain method to solve both the vector wave equation and its adjoint system [103].

There is no doubt that topology optimization based on finite element method will have disadvantages in computational time, especially for large scale engineering problems. For this reason, some authors started the research of topology op-

timization with boundary element method, which is seen as a boundary-treatment method. Cisilino presented a numerical approach for the topological optimization of 2D potential problems minimizing the total potential energy, where boundary element method is used to solve the potential problems [104]. Xing and Wang presented a topology optimization with level set method based on streamline diffusion finite element method [105]. Matsumoto[106] proposed a level set-based topology optimization for acoustic design problem, in which the topology sensitivity expression are derived combining with the boundary element method. Later, he started a study on topology optimization using level-set function and boundary element method for potential problem [107]. The use of boundary element method generates only elements on boundaries or surfaces and thus makes it easy in handling the mesh compared with FEM.

1.3 Boundary element method

In all optimization methods described in the previous sections, numerical methods are required to solve boundary value problems involved in the process of optimization. The finite element method is usually used but at the expense of mass discrete the whole object. This thesis uses the boundary element method, since it just needs to discrete the boundary of the object.

The boundary element method is a numerical method for the solution of integral equations. It has emerged in the early 19th, then been researched a lot, and by now it already has become an important technique in computational solutions of all kinds of physical problems.

The boundary element method is derived through discretizing the integral equations, which are originally expressed as but equivalent to the partial differential equation. Fredholm [108] discretized the integral equation in potential problems and formed the boundary element approach, which is seen as the indirect boundary element method because of using fictitious density functions that have no physical

meaning. The direct boundary element method was founded by Somigliana [109] in 1886. It is named ”direct” because it formed as boundary values problem.

There was no big breakthrough in the boundary element method until the 1960's when the computers came out. In 1963, Jaswon and Symm [110] took their step into numerical discretization. They discretized the integral equations of two dimensional potential problems governed by Laplace's equation with straight line elements. The elements were described in terms of nodal points and the integrations performed using Simpson's rule, which is a method for numerical approximation of definite integrals. This method is seen as ”semi-direct” method because the functions used to formulate the problems are not fictitious and can be differentiated or integrated to calculated physical quantities. In the late sixties, Rizzo [111] originally developed a numerical method of solving the classical elasticity using the experience of boundary element discretization of potential problem. He also extends it his work into three dimensional one with the surface discretized as flat constant triangular elements. in the early seventies, Cruse [112] widened Rizzo's work and employed more sophisticated elements by allowing the variables to vary linearly over each element. Later, higher-order elements were developed and used by many researchers, say, Lachat, Fenner and Tan [113], in many fields like elastodynamics and mechanics.

The discretization of boundary integral equations has received a fast development. And until 1975, it was coined the name Boundary element method. **This method is a boundary discretisation method. It is an expensive method since it has more interactions to calculate, especially for large scale problems. Some accelerating techniques, say the fast multipole accelerated boundary integral equation methods [114] and the hierarchical matrices methods [115], are developed to resolve this problem. However, it is a convenient method since it is based on the discretisation of the boundary of a domain, while FEM of the interior of a domain. Therefore, it has smaller element data and the mesh can be easily handled. Considering this thesis is to develop topology optimization**

method and does not touch upon large scale problems, the accelerating techniques are not used.

1.4 Motivation, objective and significance

The purpose of this dissertation is to construct level set-based topology optimization algorithms for heat conduction problems using boundary element method. This work's originality lies in the use of boundary element method in the level set-based topology optimization for heat conduction problems. The use of boundary element method is more convenient to generate fewer elements than finite element method. Therefore it can easily handle the mesh than FEM does.

The topology optimization works as a process of material redistribution (holes generate or holes filled with material in a fixed design domain) based on topological derivative under certain given constraint. The difficulty of this work is the derivation of topological derivative or sensitivity. To overcome this, the derivation of topological derivative starts with defining a boundary condition value problem with a certain objective function; then construct a similar boundary condition value problem that is the same as previous defined one but with an infinitesimal hole inside the physical region, which results in a change of the defined objective function. With such two boundary value problems, topological derivative can be obtained by approaching the limit of objective function change, in which an adjoint system is introduced to cancel some unknown quantities. In this work, topological derivatives for insulating boundary condition, heat transfer boundary condition and topological derivatives for heat transfer boundary condition with objective function defined on morphing boundaries are derived. The derived topological derivatives are verified by comparing with the ones obtained by finite difference method. With the verified topological derivative expressions, the thesis forms the topology optimization for heat conduction problems using boundary element method and level set method and applied to many numerical examples to show the availability of the proposed

method.

This work will in large facilitate the development of topology optimization theoretically. It is a flexible (holes can appear or disappear) and convenient method especially when objective function defined on boundaries. Meanwhile, the checkerboard and intermediate material problems do not appear since the use of level set method in the topology optimization process. It is believed that the proposed method will have a great contribution on the structural design of heat conduction devices in engineering field.

1.5 Thesis organization

Since topology optimization belongs to the category of structural optimization, this dissertation starts the first chapter with the classification of structural optimization, in which, three kinds of structural optimization are introduced and compared with each other. Then the development of structural optimization is recalled, where topology optimization as the most prevalent method are described in detail according to the branches. Each branch is processed with its appearing, working principle, applied problems, and in-between followed corresponding advantage and disadvantage and comments to keep consistency. Following the structural optimization, the development of boundary element method is narrated and commented. After the development, the purpose, and objective and significance of this dissertation are stated and the thesis constitution is given as the end of the first chapter.

In the second chapter, a topology optimization is formulated based on the level set method. The distribution of level set function is supposed to have a relationship with the objective function and the change of level set function will change the objective function. Thus a fictitious time is introduced and a time evolution equation for updating the level set function is constructed. In the evolution equation, a topology derivative or sensitivity that needs to be derived combining boundary element method is needed; besides, regularization is introduced to control the complexity of

the topology.

In the third chapter, a topology optimization algorithm flowchart is given and the evolution equation of level set function is numerically discretized.

In chapter four, a topological derivative for heat conduction problem under insulating boundary condition combining with boundary element method is derived. The derived topological derivative correctness, mesh-dependency and initial configuration dependency are checked.

In chapter five, the topological derivative for heat conduction problem under heat transfer boundary condition combining with boundary element method is derived. The derived topological derivative is verified by comparing with the one obtained using finite difference method. Then topology optimization is using this topological derivative is constructed and several numerical examples are provide to show the effectiveness of the proposed method.

In chapter six, while basing on the topology optimization scheme under heat transfer condition in preceding chapter, the cases with the objective functions for the temperature and heat flux defined on the morphing boundaries generated through the iterative steps of the optimization computation are considered. The topological derivatives of the objective functions both for the temperature and the heat flux are derived and verified through numerical examples. The chapter also presents the topology optimization examples using the corresponding topological derivatives.

Chapter 7 reaches the conclusions of this dissertation.

Chapter 2

Level Set-based Topology Optimization Method using BEM

2.1 Introduction

This chapter presents a level set-based topology optimization using boundary element method. In this method, the level set function is supposed to change with respect to fictitious time. The level set function is updated using a reaction-diffusion equation, which is free of re-initialization [117, 118]. This is different from the conferential methods where the level set function is based on the Hamilton-Jacobi equation [119, 120], which is seen as a boundary moving method. The boundary condition value problems with objective function defined on boundary is described.

The boundary element method is used to solve the boundary condition value problem for it generates less elements and its ease to handle the mesh. Besides, the regularization term, which is derived from the concept of the phase field method, works as a reaction-diffusion [121, 122] term but enable designers to obtain various configurations with different complexity.

This chapter firstly described how the level set function defines a material or void property in a fixed design domain, then the optimization problem with an objective function and corresponding constraints are considered. Next, the opti-

mization problem is augmented as an unconstrained problem. In the following, the relationship between level set function and objective function is constructed and formed the reaction-diffusion like time evolution equation [123], in which the regularization term is introduced to control the complexity of the topologies. Secondly, the optimization algorithms for numerical implementation is built up.

2.2 Level set-based topology optimization

The level set method is an approach to represent material shapes by using level set function that is a scalar function of point, $\phi(x)$, defined as follows:

$$\begin{cases} 0 < \phi(x) \leq 1, & x \in \Omega \backslash \Gamma_0, \\ \phi(x) = 0, & x \in \Gamma_0, \\ -1 \leq \phi(x) < 0, & x \in D \backslash \Omega, \end{cases} \tag{2.1}$$

where D, Ω denote the fixed design domain and the material domain, and $D\backslash\Omega$ denotes the void domain, and Γ_0 denotes the boundary between material Ω and void domain $D\backslash\Omega$, as shown in Figure 2.1.

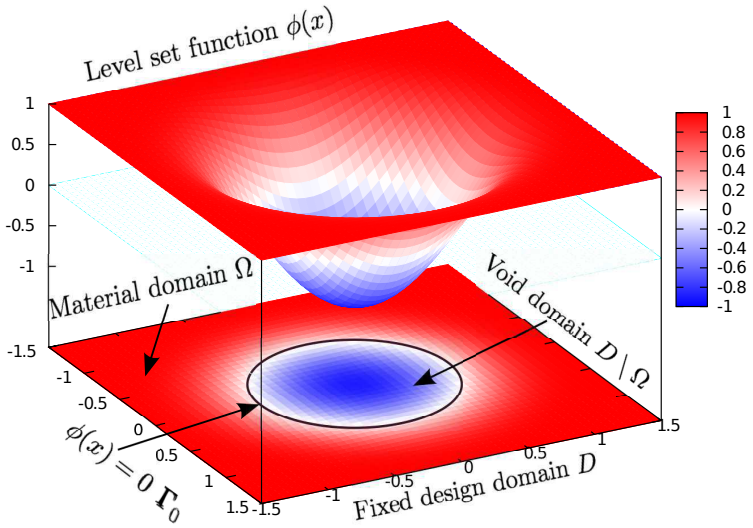

Figure 2.1: Level set function and the fixed design domain D

The following optimization problem is considered with the objective function is

defined on the boundary Γ.

$$\inf F = \int_{\Gamma} f(u,q)\, d\Gamma + \int_{D} g(u,q)\, d\Omega, \tag{2.2}$$

subject to

$$\text{P.D.E.:} \qquad \nabla \cdot (-k\nabla u) = 0 \qquad \text{in } \Omega, \tag{2.3}$$

$$\text{B.C.:} \qquad u = \overline{u} \qquad \text{on } \Gamma_u, \tag{2.4}$$

$$q = -k\frac{\partial u}{\partial n} = \overline{q} \qquad \text{on } \Gamma_q, \tag{2.5}$$

$$q = h(u - u_{\infty}) \qquad \text{on } \Gamma_h. \tag{2.6}$$

and

$$G = \int_{D} H(\phi(x))\, d\Omega - G_{\max} \leq 0, \tag{2.7}$$

where PDE is short for Partial Differential Equation and B.C. is for Boundary Condition. F is an objective function. $f(u,q)$ is a function of u and q defined on Γ or part of Γ and $g(u,q)$ is a function of u and q defined in the fixed design domain. u and $q = -k\frac{\partial u}{\partial n}$ are the temperature on the boundary of Direchlet boundary condition Γ_u and heat flux on the boundary of Neumman boundary condition Γ_q or Robin boundary condition Γ_h, respectively, n is the outward normal direction to Γ, u_{∞} is the ambient temperature, k is the thermal conductivity, h is the heat transfer coefficient, and H is the Heaviside function. G is a constraint used to control the area of the material region no more than $G_{\max}$. $G_{\max}$ is the admissible upper limit of the area of the material region Ω.

The Heaviside function is defined as follows:

$$H(\phi(x)) \begin{cases} 0, & (\phi(x) \leq 0), \\ 1, & (\phi(x) > 0), \end{cases} \tag{2.8}$$

Using Lagrange's method, the optimization problem described by Eqs. (2.2)-(2.7) is turned to be the following unconstrained optimization problem:

$$\overline{F}(\phi) = F(\phi) + I + \lambda G, \tag{2.9}$$

where λ is the Lagrange's multiplier for Eq.(4.3) and I is a function defined as follows:

$$I = \int_D \mu \nabla \cdot (-k \nabla u)\, d\Omega = 0, \tag{2.10}$$

where μ is Lagrange's multiplier that is called here an adjoint variable.

The above optimisation problem has to satisfy the Krush-Kuhn-Tucker (KKT) conditions [98] as follows:

$$F' + I' + \lambda = 0, \quad \lambda G = 0, \quad \lambda \geq 0, \quad G \leq 0, \tag{2.11}$$

where a prime symbol ($'$) denotes a topological derivative, which characterizes a sensitivity of the objective function (3) when a small circular hole is created.

Since it is difficult to solve equations (2.11) in this form for the optimum topology, a fictitious time t [98] is introduced and assumed that the derivative of the distribution of the level set function ϕ with respect to t is proportional to the topological derivative of $\overline{F}$ and the mean curvature of ϕ, can be written like a reaction diffusion equation as follows:

$$\frac{\partial \phi}{\partial t} = \alpha \overline{F}' + \beta \nabla^2 \phi, \tag{2.12}$$

where α and β are the proportional constants of reaction diffusion equation.

Equation (2.12) can be rewritten as an evolution equation:

$$\frac{\partial \phi}{\partial t} = K(\mathscr{T} - \lambda + \tau \nabla^2 \phi) \qquad \text{in } D, \tag{2.13}$$

where t is the introduced fictitious time and K is a constant. t and K are combined to control the updating speed in optimization process. τ is a regularization parameter that can control the curvature distribution of ϕ. Both K and τ are positive constants, and $\mathscr{T}$ is the topological derivative of $F + I$, i.e.,

$$\mathscr{T} = F' + I' \tag{2.14}$$

Equation (2.13) is a diffusion equation determining the distribution of the level set function. Equation (2.13) can be solved under certain boundary conditions and the

initial condition corresponding the the initially assumed distribution of the material in the fixed design domain D. On some part of the boundary, Γ_{N}, noted as non-design boundary for ϕ can not be changed, the value of ϕ can be set as positive, whereas on the other part, although its value can be positive or negative, the normal slope of ϕ can be set to take a constant value. Hence, in this dissertation, the following boundary conditions are considered to solve Eq.(2.13).

$$\frac{\partial \phi}{\partial n} = 0 \qquad \text{on } \partial D \setminus \Gamma_{\mathrm{N}}, \tag{2.15}$$

$$\phi \ = 1 \qquad \text{on } \Gamma_{\mathrm{N}}. \tag{2.16}$$

The initial condition of ϕ can be determined so that the boundary of the material becomes the iso-surface corresponding to $\phi = 0$.

2.3 Optimization algorithms

Since the shape of the optimal configuration is obtained by the distribution of the level set function, firstly, the level set function needs to be initialized; Secondly, the boundary of the configuration inputs will be generated based on the level set function; Thirdly, Combining with the prescribed boundary conditions and values, the temperature field can be constructed and solved using BEM; Fourthly, the adjoint filed of the temperate field is calculated using BEM; Fifth, using the quantities obtained from the calculation of temperature and adjoint field, topological derivative (sensitivity) can be calculated; Sixth, the level set function can be updated with the obtained topological derivative; Seventh, the convergence will be estimated, according to which to repeat or end the optimization process.

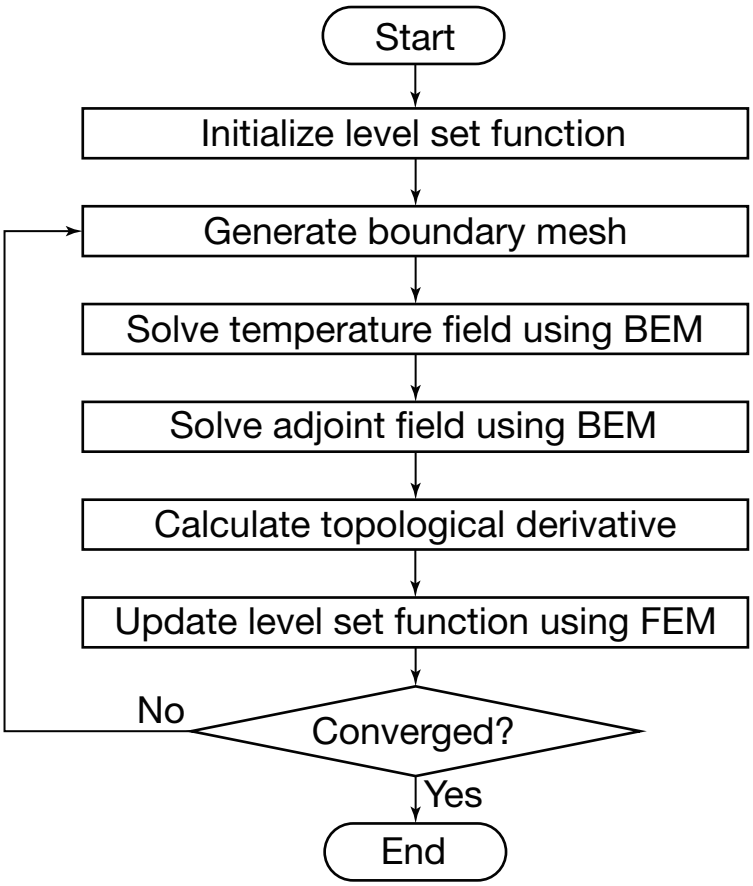

Figure 2.2: Flowchart of topology optimization algorithm

2.4 Conclusions

This chapter firstly introduced the level set function together with characteristic function, then built the topology optimization problem by writing it as an unconstrained problem with regularization parameter introduced to control the complexity of the topology, and last attributed the optimization problem to the form of a time evolution equation. After that, the optimization algorithm for topology optimization for heat conduction problems using boundary element method is built up.

Chapter 3

Numerical Implementations

3.1 Introduction

In this chapter, a numerical implementation method of updating the level-set function is established. After that, the basic formulation of the boundary element method, which is used to solve heat problems in the topology optimization process, is described

3.2 Numerical discretization of evolution equation

The evolution equation in Eq. (2.13) is

$$\frac{\partial \phi}{\partial t} = K(\mathscr{T} - \lambda + \tau \nabla^2 \phi), \tag{3.1}$$

where $\mathscr{T}$ is the topological derivative (sensitivity). Applying Galerkin weighting residual method [130] to Eq. (3.1) over integral domain, the evolution equation becomes as

$$\int_\Omega \frac{\partial \phi}{\partial t} \omega \, d\Omega = \int_\Omega K(\mathscr{T} - \lambda + \tau \nabla^2 \phi) \omega \, d\Omega, \tag{3.2}$$

where ω is weight residual function. Eq. (3.2) can be rearranged as:

$$\int_\Omega \frac{\partial \phi}{\partial t} \omega \, d\Omega = \int_\Omega K(\mathscr{T} - \lambda) \, d\Omega + K\tau \int_\Omega \omega \nabla^2 \phi \, d\Omega, \tag{3.3}$$

In Eq. (3.3), the second term in RHS can be Integrated by parts as:

$$K\tau \int_{\Omega} \omega \nabla^2 \phi \; d\Omega = K\tau \int_{\Gamma} \omega \nabla \phi \cdot n \; d\Gamma - K\tau \int_{\Omega} \nabla \phi \cdot \nabla \omega \; d\Omega, \tag{3.4}$$

Considering ϕ is restricted so as to satisfy the forced boundary condition, the first term in the RHS of Eq. (3.4), the integral taken along the boundary Γ, becomes 0.

Then Eq. (3.2) becomes as:

$$\int_{\Omega} (\frac{\partial \phi}{\partial t} \omega \; + K\tau \nabla \phi \nabla \omega) \; d\Omega = \int_{\Omega} K(\mathscr{T} - \lambda) \omega \; d\Omega. \tag{3.5}$$

Using interpolation method,ϕ and ω can be expressed in Einstein summation shown as

$$\phi = \phi^p N^p \tag{3.6}$$

$$\omega = \omega^q N^q. \tag{3.7}$$

Then Eq. (3.5) can be discretized as

$$\sum_e \int_{\Omega_e} (\frac{\partial \phi^p}{\partial t} N^p N^q + K\tau \phi^p \nabla N^p \nabla N^q) \; d\Omega = \sum_e \int_{\Omega_e} K(\mathscr{T} - \lambda) N^q \; d\Omega. \tag{3.8}$$

It can be simplified to write as

$$M_e \dot{\phi}_e + K_e \phi_e = F_e, \tag{3.9}$$

in which

$$M_e = \int_{\Omega_e} N^p N^q d\Omega \tag{3.10}$$

$$K_e = \int_{\Omega_e} K\tau \nabla N^p \nabla N^q d\Omega \tag{3.11}$$

$$F_e = \int_{\Omega_e} K(\mathscr{T} - \lambda) N^q \; d\Omega, \tag{3.12}$$

where N^p are function of x and y, and ∇N^p are derivatives to x and y, as well as N^q and ∇N^q. It is not easy to directly get the shape function of x,y, but it is noted that the usual method is mapping it to normalized coordinates, then translate it back into actual coordinates when needed.

The whole domain is discretized using 4-node quadrilateral element, shown as Figure 3.1. Each node has two components of displacement, node position and displacement are denoted as (x_i, y_i) and (u_i, v_i) respectively, with $i = 1,2,3,4$.

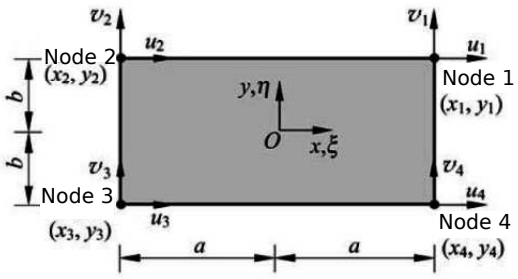

Figure 3.1: 4-node isoparametric element

The components of the displacement at (x,y) can be expressed, with the method of indetermined coefficients, as,

$$u(x,y) = a_0 + a_1 x + a_2 y + a_3 xy \tag{3.13}$$

$$v(x,y) = b_0 + b_1 x + b_2 y + b_3 xy. \tag{3.14}$$

The coefficients a_0, a_1, a_2, a_3 and b_0, b_1, b_2, b_3 can be obtained by solving the equations. Then by substituting them back into the relative equations, the following equations can be obtained:

$$u(x,y) = N^1(x,y)u_1 + N^2(x,y)u_2 + N^3(x,y)u_3 + N^4(x,y)u_4 \tag{3.15}$$

$$v(x,y) = N^1(x,y)v_1 + N^2(x,y)v_2 + N^3(x,y)v_3 + N^4(x,y)v_4, \tag{3.16}$$

in which

$$N^1(x,y) = \frac{1}{4}(1+\frac{x}{a})(1+\frac{y}{b}) \tag{3.17}$$

$$N^2(x,y) = \frac{1}{4}(1-\frac{x}{a})(1+\frac{y}{b}) \tag{3.18}$$

$$N^3(x,y) = \frac{1}{4}(1-\frac{x}{a})(1-\frac{y}{b}) \tag{3.19}$$

$$N^4(x,y) = \frac{1}{4}(1+\frac{x}{a})(1-\frac{y}{b}). \tag{3.20}$$

Their derivatives is derived as:

$$\frac{\partial N^1}{\partial x} = \frac{b+y}{4ab}, \qquad \frac{\partial N_1}{\partial y} = \frac{a+x}{4ab} \tag{3.21}$$

$$\frac{\partial N^2}{\partial x} = \frac{-(b+y)}{4ab}, \qquad \frac{\partial N_2}{\partial y} = \frac{a-x}{4ab} \tag{3.22}$$

$$\frac{\partial N^3}{\partial x} = \frac{-(b-y)}{4ab}, \qquad \frac{\partial N_3}{\partial y} = \frac{-(a-x)}{4ab} \tag{3.23}$$

$$\frac{\partial N^4}{\partial x} = \frac{b-y}{4ab}, \qquad \frac{\partial N_4}{\partial y} = \frac{-(a+x)}{4ab} \tag{3.24}$$

To translate to the dimensionless coordinates with (ξ,η) given $(-1,-1),(1,-1)$, $(1,1),(-1,1)$ at the nodes 1, 2, 3 and 4, individually, it is supposed that

$$\xi = -\frac{x}{a}, \qquad \eta = -\frac{y}{b}. \tag{3.25}$$

Then the shape function is obtained as

$$N_1(\xi,\eta) = \frac{1}{4}(1-\xi)(1-\eta) \tag{3.26}$$

$$N_2(\xi,\eta) = \frac{1}{4}(1+\xi)(1-\eta) \tag{3.27}$$

$$N_3(\xi,\eta) = \frac{1}{4}(1+\xi)(1+\eta) \tag{3.28}$$

$$N_4(\xi,\eta) = \frac{1}{4}(1-\xi)(1+\eta). \tag{3.29}$$

Also the derivative of these shape function is put on here for later use.

$$\frac{\partial N_1}{\partial \xi} = \frac{\eta-1}{4}, \qquad \frac{\partial N_1}{\partial \eta} = \frac{\xi-1}{4} \tag{3.30}$$

$$\frac{\partial N_2}{\partial \xi} = \frac{1-\eta}{4}, \qquad \frac{\partial N_2}{\partial \eta} = \frac{-\xi-1}{4} \tag{3.31}$$

$$\frac{\partial N_3}{\partial \xi} = \frac{1+\eta}{4}, \qquad \frac{\partial N_3}{\partial \eta} = \frac{\xi+1}{4} \tag{3.32}$$

$$\frac{\partial N_4}{\partial \xi} = \frac{-1-\eta}{4}, \qquad \frac{\partial N_4}{\partial \eta} = \frac{1-\xi}{4} \tag{3.33}$$

For isoparametric element, one can also use shape function to make interpolation of coordinates as

$$x = \sum_p^4 N^p x^p, \qquad y = \sum_p^4 N^p y^p \tag{3.34}$$

The term ∇N^p has x and y components. It can be written as Eq. (3.35).

$$\nabla N^p = (\frac{\partial N^p}{\partial x}, \frac{\partial N^p}{\partial y}) \tag{3.35}$$

Usually, the term above cannot be directly calculated, but we note there are such relationships below, which would let us calculate it indirectly.

$$\begin{aligned} \frac{\partial N^p}{\partial \xi} &= \frac{\partial N^p}{\partial x}\frac{\partial x}{\partial \xi} + \frac{\partial N^p}{\partial y}\frac{\partial y}{\partial \xi} \\ \frac{\partial N^p}{\partial \eta} &= \frac{\partial N^p}{\partial x}\frac{\partial x}{\partial \eta} + \frac{\partial N^p}{\partial y}\frac{\partial y}{\partial \eta} \end{aligned} \tag{3.36}$$

The Eq. (3.36) can be written into Matrix as

$$\begin{Bmatrix} \frac{\partial N^p}{\partial \xi} \\ \frac{\partial N^p}{\partial \eta} \end{Bmatrix} = \begin{bmatrix} \frac{\partial x}{\partial \xi} & \frac{\partial y}{\partial \xi} \\ \frac{\partial x}{\partial \eta} & \frac{\partial y}{\partial \eta} \end{bmatrix} \begin{Bmatrix} \frac{\partial N^p}{\partial x} \\ \frac{\partial N^p}{\partial y} \end{Bmatrix} \tag{3.37}$$

which can be written as

$$\begin{Bmatrix} \frac{\partial N^p}{\partial \xi} \\ \frac{\partial N^p}{\partial \eta} \end{Bmatrix} = \Big[J\Big] \begin{Bmatrix} \frac{\partial N^p}{\partial x} \\ \frac{\partial N^p}{\partial y} \end{Bmatrix}. \tag{3.38}$$

Knowing Eq. (3.25), Jacobi Matrix $\Big[J\Big]$ can be calculated easily as

$$\Big[J\Big] = \begin{bmatrix} -a & 0 \\ 0 & -b \end{bmatrix}. \tag{3.39}$$

Then M_e,K_e and F_e can be translated to integrals on dimensionless coordinates with Eq. (3.25) and (3.39), shown as

$$M_e(p,q) = \int_{\Omega_e} N^p N^q \, d\Omega_e = \int_{-1}^{1}\int_{-1}^{1} N_p N_q |[J]| \, d\xi d\eta \tag{3.40}$$

$$K_e(p,q) = \int_{\Omega_e} K\tau \nabla N^p \nabla N^q \, d\Omega_e = \int_{-1}^{1}\int_{-1}^{1} K\tau \nabla N_p \nabla N_q |[J]| \, d\xi d\eta \tag{3.41}$$

$$F_e(q) = \int_{\Omega_e} -K(2\nabla u \nabla \mu + \lambda) N^q \, d\Omega_e = \int_{-1}^{1}\int_{-1}^{1} K(\mathscr{T} - \lambda) N_q |[J]| \, d\xi d\eta. \tag{3.42}$$

Then it substitutes Eqs. (3.13)-(3.16), (3.35)-(3.39) into Eqs. (3.40)-(3.42) to calculate each term of $M_e(p,q)$, $K_e(p,q)$, and $F_e(q)$, the same time, assembles them into corresponding element matrices. Below is the results:

$$M_e = ab \begin{pmatrix} 1/9 & 1/18 & 1/36 & 1/18 \\ 1/18 & 1/9 & 1/18 & 1/36 \\ 1/36 & 1/18 & 1/9 & 1/18 \\ 1/18 & 1/36 & 1/18 & 1/9 \end{pmatrix} \tag{3.43}$$

$$K_e = abK\tau \begin{pmatrix} 2/3 & -1/6 & -1/3 & -1/6 \\ -1/6 & 2/3 & -1/6 & -1/3 \\ -1/3 & -1/6 & 2/3 & -1/6 \\ -1/6 & -1/3 & -1/6 & 2/3 \end{pmatrix} \tag{3.44}$$

$$F_e = abK(\mathscr{T} - \lambda) \begin{pmatrix} 1/4 \\ 1/4 \\ 1/4 \\ 1/4 \end{pmatrix} \tag{3.45}$$

Using receding difference, Eq. (3.9) can be sorted as

$$(\frac{1}{\delta t} M_e + K_e)\phi_{t+\delta t} = \frac{1}{\delta t} M_e \phi_t + F_e. \tag{3.46}$$

Assemble all the element matrix, the global matrix can obtained as

$$(\frac{1}{\delta t} M_a + K)\phi_{t+\delta t} = \frac{1}{\delta t} M_a \phi_t + F_a, \tag{3.47}$$

In which,

$$M_a = \sum_e M_e \tag{3.48}$$

$$K_a = \sum_e K_e \tag{3.49}$$

$$F_a = \sum_e F_e. \tag{3.50}$$

Let $T = (\frac{1}{\delta t} M_a + K_a)$, $B = \frac{1}{\delta t} M_a \phi_t + F_a$, $\phi = \phi_{t+\delta t}$ Eq. (3.47) becomes as

$$T\phi = B. \tag{3.51}$$

Considering ϕ on fixed boundary cannot be changed. Eq. (3.51) can be extended as

$$\begin{bmatrix} T_1 & T_2 \\ T_1 & T_2 \end{bmatrix} \begin{bmatrix} \phi_1 \\ \phi_2 \end{bmatrix} = \begin{bmatrix} B_1 \\ B_2 \end{bmatrix}. \tag{3.52}$$

In Eq. (3.52), ϕ_2 is known. ϕ_1 is on the non-fixed boundary, and is what to be gotten, so it needs to rewrite Eq. (3.52) as

$$\begin{bmatrix} T_1 \end{bmatrix} \begin{bmatrix} \phi_1 \end{bmatrix} = \begin{bmatrix} B_1 \end{bmatrix} - \begin{bmatrix} T_2 \end{bmatrix} \begin{bmatrix} \phi_2 \end{bmatrix}, \tag{3.53}$$

which can be solved to get ϕ_1, the level-set function value on non-fixed boundary.

3.3 Boundary element method

Since boundary element method is a boundary discretization method and has many advantages over finite element method, referred in last chapter, it is used as the solver of heat conduction problems to be solved. Consider that the boundary value problem governed as:

$$\begin{cases} -k\nabla^2 u(x) = 0 & \text{in } \Omega \\ u(x) = \overline{u} & \text{on } \Gamma_u \\ q(x) = \overline{q} & \text{on } \Gamma_q \end{cases} \tag{3.54}$$

where ∇^2 is laplacian operator. Ω is a closed domain with boundary Γ. u is the temperature, q is the heat flux, Γ_u is the temperature boundary and Γ_q is the heat flux boundary. Γ is composed of Γ_u and Γ_q. k is the thermal conductivity. The boundary integral equation is written as follows [130]:

$$c(y)u(y) = \int_\Gamma u^*(x,y)q(x)d\Gamma(x) - \int_\Gamma q^*(x,y)u(x)d\Gamma(x), \quad y \in \Gamma, \tag{3.55}$$

where

$$c(y) = \begin{cases} 1 & y \in \Omega \\ \frac{1}{2} & y \in \Gamma \end{cases} \tag{3.56}$$

with boundary Γ supposed to be smooth; And $u^*(x,y)$ and $q^*(x,y)$ are the fundamental solution of Laplace's equation and its normal derivative, respectively. $u^*(x,y)$ and $q^*(x,y)$ are given as follows [137]:

$$u^*(x,y) = \frac{1}{2\pi}\ln\frac{1}{r}, \tag{3.57}$$

$$q^*(x,y) = -k\frac{-1}{2\pi r}\frac{\partial r}{\partial n}, \tag{3.58}$$

where r denotes the distance between x and y. n is the outward normal vector to the boundary at x.

The Eq. (3.55), can be discretized as follows [131, 132]:

$$c(y)u(y) = \sum_{j=1}^{N}\int_{\Gamma_j} u^*(x,y)q(x)d\Gamma(x) - \sum_{j=1}^{N}\int_{\Gamma_j} q^*(x,y)u(x)d\Gamma(x), \quad y\in\Gamma, \tag{3.59}$$

where Γ_j is the jth boundary element. u and q inside an boundary element can be expressed using quadratic Interpolation function $\phi(\xi)$ as:

$$u(\xi) = \sum_{k=1}^{3}\phi^k(\xi)u_j^k \tag{3.60}$$

$$q(\xi) = \sum_{k=1}^{3}\phi^k(\xi)q_j^k, \tag{3.61}$$

where

$$\phi^1(\xi) = \frac{1}{2}\xi(\xi-1), \tag{3.62}$$

$$\phi^2(\xi) = (1-\xi)(1+\xi), \tag{3.63}$$

$$\phi^3(\xi) = \frac{1}{2}\xi(\xi+1), \tag{3.64}$$

and x inside the element can be expressed as [133]:

$$x(\xi) = \phi^1(\xi)x^1 + \phi^2(\xi)x^2 + \phi^3(\xi) = \sum_{k=1}^{3}\phi^k(\xi)x^k. \tag{3.65}$$

Thus, it has:

$$\int_{\Gamma_j} u^*(x,y)q(x)d\Gamma(x) = \int_{-1}^{1} u^*(\xi)\sum_{k=1}^{3}\phi^k(\xi)q^k G(\xi)\,d\xi \tag{3.66}$$

$$= \sum_{k=1}^{3}\left\{\int_{-1}^{1} u^*(\xi)\phi^k(\xi)G(\xi)\,d\xi\right\}q^k \tag{3.67}$$

$$= \sum_{k=1}^{3} g_{ij}^k q_j^k, \tag{3.68}$$

$$\int_{\Gamma_j} q^*(x,y)u(x)d\Gamma(x) = \int_{-1}^{1} q^*(\xi)\sum_{k=1}^{3}\phi^k(\xi)u^k G(\xi)\,d\xi \tag{3.69}$$

$$= \sum_{k=1}^{3}\left\{\int_{-1}^{1} q^*(\xi)\phi^k(\xi)G(\xi)\,d\xi\right\}u^k \tag{3.70}$$

$$= \sum_{k=1}^{3} h_{ij}^k u_j^k, \tag{3.71}$$

where

$$g_{ij}^k = \int_{-1}^{1} u^*(\xi)\phi^k(\xi)G(\xi)\,d\xi, \tag{3.72}$$

$$h_{ij} = \int_{-1}^{1} q^*(\xi)\phi^k(\xi)G(\xi)\,d\xi. \tag{3.73}$$

Finally, the boundary integral equation can be discretized as:

$$c_i u_i + \left[\begin{array}{cccc} H_{i1} & H_{i2} & \cdots & H_{in} \end{array}\right]\left\{\begin{array}{c} u_1 \\ u_2 \\ \vdots \\ u_n \end{array}\right\} = \left[\begin{array}{cccc} G_{i1} & G_{i2} & \cdots & G_{in} \end{array}\right]\left\{\begin{array}{c} q_1 \\ q_2 \\ \vdots \\ q_n \end{array}\right\}, \tag{3.74}$$

where n is the total number of nodes. The Eq. (3.74) can be written as:

$$[H]\{u\} = [G]\{q\}. \tag{3.75}$$

After moving the unknowns to the left-hand side and the knowns to the right-hand side, it becomes

$$[A]\{x\} = \{y\}, \tag{3.76}$$

where $\{x\}$ is the vector consisting of only unknown nodal values and $\{y\}$ is the vector obtained by multiplying the known nodal values with corresponding parts of the coefficient matrices $[H]$ and $[G]$. Once the temperature and heat flux quantities are obtained, the temperature field u inside the domain Ω can be calculated by the following integral representation [137]::

$$u(y) = \int_\Gamma u^*(x,y)q(x)d\Gamma(x) - \int_\Gamma q^*(x,y)u(x)d\Gamma(x), \quad y \in \Omega, \tag{3.77}$$

as well as the heat flux can be obtained by

$$\frac{\partial u(y)}{\partial y_i} = \int_\Gamma \frac{u^*(x,y)}{\partial y_i}q(x)d\Gamma(x) - \int_\Gamma \frac{q^*(x,y)}{\partial y_i}u(x)d\Gamma(x), \quad y \in \Omega, \tag{3.78}$$

where $i = 1,2$, for two dimensional case.

Note that adjoint problems are also solved using boundary element method in this way.

3.4 Conclusions

In this chapter, the time evolution equation used to update the level set function is numerically discretized. Later, the boundary element method, which is used in each chapter of this thesis, is described.

Chapter 4

Topology Optimization with Insulating Boundary Condition for Heat Conduction Problems using BEM

4.1 Introduction

Heat, in physics, as a kind of energy, can transfer between two bodies of different temperatures. The heat transfer [134] happens at every minute everywhere around our life, in the form of conduction, convection, and radiation. The research on how heat transfer is of great importance, which has an instructive effect on developing devices of all kinds for our society. Therefore, engineers pay much attention on heat transfer and attempt to control the flow of heat through the use of thermal insulation [135], heat exchanges [136].

This chapter presents a level set-based topology optimization under insulating boundary condition for heat conduction problems using boundary element method [137]. That is, the newly generated boundaries are designated as insulating boundary conditions, which can be found as in Figure 4.1. The topological derivative

(sensitivity) under insulating boundary condition, as the core part of the topology optimization in this chapter, is derived. The topological derivative is verified though comparing with the one calculated using finite difference method. The proposed method has been proved efficient with different mesh, different initial configurations.

4.2 Topological derivative

The objective function is defined as:

$$F = \int_{\Gamma_f} f(u,q)\, d\Gamma, \tag{4.1}$$

subject to

$$-k\nabla^2 u = 0 \qquad \text{in } \Omega \tag{4.2}$$

and

$$G = \int_D H(\phi(x))\, d\Omega - G_{\max} \leq 0, \tag{4.3}$$

where $f(u,q) = f\,(u(x), q(x))$ is a function defined on Γ, and Γ_f denotes f's support, i.e., $f(x) = 0$ for $\Gamma \setminus \Gamma_f$, which is introduced to describe the following formulation minutely. Note that Γ_f intersects with Γ_u and/or Γ_q. H is the Heaviside function. $G_{\max}$ is the admissible upper limit of the area of the material region Ω.

To derive the topological derivative, a boundary value problem for a heat conduction problem is defined, then another boundary value problem with an infinitesimal hole created based on the defined boundary value problem is constructed. By comparing the objective function values of two boundary value problems, the topological derivative at the place that the infinitesimal hole is created can be obtained. In a optimization problem, the design domain is meshed and generates many nodes. At each node, there is one topological derivative value needed to be calculated.

Before the hole is created, the boundary value problem [137] (Figure 4.1 (left))

is defined as follows:

$$\begin{cases} -k\nabla^2 u = 0 & \text{in } \Omega \\ u = \overline{u} & \text{on } \Gamma_u \\ q = -k\dfrac{\partial u}{\partial n} = \overline{q} & \text{on } \Gamma_q \end{cases} \tag{4.4}$$

where u and $q = -k\frac{\partial u}{\partial n}$ are the temperature and heat flux, respectively, n is the outward normal direction to Γ, k is the thermal conductivity.

After the hole is created, the temperature and heat flux in Eq. 4.4 subject to a small change defined as δu and δq. Then the boundary value problem (Figure 4.1 (right)) is defined as follows:

$$\begin{cases} -k\nabla^2(u+\delta u) = 0 & \text{in } \Omega \setminus \Omega_\varepsilon \\ u+\delta u = \overline{u} & \text{on } \Gamma_u \\ q+\delta q = -k\dfrac{\partial(u+\delta u)}{\partial n} = \overline{q} & \text{on } \Gamma_q \\ q+\delta q = -k\dfrac{\partial(u+\delta u)}{\partial n} = 0 & \text{on } \Gamma_\varepsilon \end{cases} \tag{4.5}$$

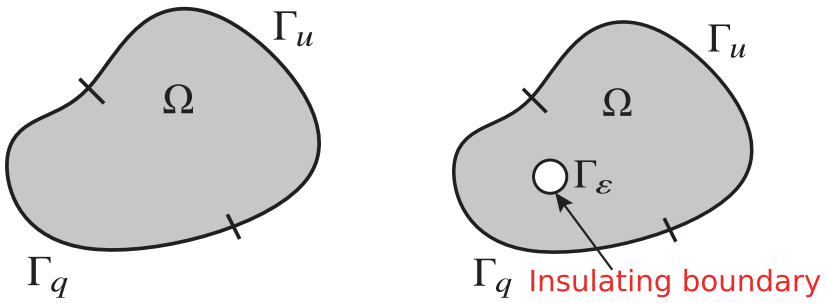

Figure 4.1: (left:) Configuration before a hole is created; (right:) Configuration after a hole is created

By subtracting Eq. (4.4) from Eq. (4.5), one can get the following expression, which will be used later:

$$\begin{cases} -k\nabla^2 \delta u = 0 & \text{in } \Omega \setminus \Omega_\varepsilon \\ \delta u = 0 & \text{on } \Gamma_u \\ \delta q = -k\dfrac{\partial \delta u}{\partial n} = 0 & \text{on } \Gamma_q \\ \delta q = -k\dfrac{\partial \delta u}{\partial n} = -\overline{q} & \text{on } \Gamma_\varepsilon \end{cases} \tag{4.6}$$

The objective function above can be written as an augmented one as:

$$\begin{aligned} J &= \int_{\Gamma_f} f(u,q)\, d\Gamma + \int_{\Omega} \mu \nabla \cdot (-k\nabla u)\, d\Omega \\ &= \int_{\Gamma_f} f(u,q)\, d\Gamma + \int_{\Gamma} \mu(-k\frac{\partial u}{\partial n})\, d\Omega - \int_{\Omega} \nabla\mu \cdot (-k\nabla u)\, d\Omega \\ &= \int_{\Gamma_f} f(u,q)\, d\Gamma + \int_{\Gamma} \mu q\, d\Omega - \int_{\Omega} (-k\nabla\mu)\cdot\nabla u\, d\Omega. \end{aligned} \tag{4.7}$$

When a small hole created in the domain, there is an increment to the objective function:

$$\begin{aligned} J+\delta J = &\int_{\Gamma_f} (f(u,q) + \frac{\partial f}{\partial u}\delta u + \frac{\partial f}{\partial q}\delta q)\, d\Gamma + \int_{\Gamma} \mu(q+\delta q)\, d\Gamma \\ &+ \int_{\Gamma_\varepsilon} \mu(q+\delta q)\, d\Gamma - \int_{\Omega\setminus\Omega_\varepsilon} (-k\nabla\mu)\cdot\nabla(u+\delta u)\, d\Omega. \end{aligned} \tag{4.8}$$

By subtracting Eq. (4.7) from Eq. (4.8), one gets:

$$\begin{aligned} \delta J = &\int_{\Gamma_f} (\frac{\partial f}{\partial u}\delta u + \frac{\partial f}{\partial q}\delta q)\, d\Gamma + \int_{\Gamma} \mu\delta q\, d\Gamma + \int_{\Gamma_\varepsilon} \mu(q+\delta q)\, d\Gamma \\ &- \int_{\Omega\setminus\Omega_\varepsilon} (-k\nabla\mu)\cdot\nabla(\delta u)\, d\Omega + \int_{\Omega_\varepsilon} (-k\nabla\mu)\cdot\nabla u\, d\Omega \\ = &\int_{\Gamma\setminus\Gamma_f} \mu\delta q\, d\Gamma + \int_{\Gamma_f} (\mu + \frac{\partial f}{\partial q})\delta q\, d\Gamma + \int_{\Gamma_f} \frac{\partial f}{\partial u}\delta u\, d\Gamma + \int_{\Gamma_\varepsilon} \mu(q+\delta q)\, d\Gamma \\ &- \int_{\Gamma} (-k\frac{\partial \mu}{\partial n})\delta u\, d\Gamma - \int_{\Gamma_\varepsilon} (-k\frac{\partial \mu}{\partial n})\delta u\, d\Gamma + \int_{\Omega\setminus\Omega_\varepsilon} \nabla\cdot(-k\nabla\mu)\delta u\, d\Omega \\ &+ \int_{\Omega_\varepsilon} \nabla\mu\cdot(-k\nabla u)\, d\Omega \\ = &\int_{\Gamma\setminus\Gamma_f} \mu\delta q\, d\Gamma + \int_{\Gamma_f} (\mu + \frac{\partial f}{\partial q})\delta q\, d\Gamma + \int_{\Gamma_\varepsilon} \mu(q+\delta q)\, d\Gamma \\ &- \int_{\Gamma_f} (-k\frac{\partial \mu}{\partial n} - \frac{\partial f}{\partial u})\delta u\, d\Gamma - \int_{\Gamma\setminus\Gamma_f} (-k\frac{\partial \mu}{\partial n})\delta u\, d\Gamma - \int_{\Gamma_\varepsilon} (-k\frac{\partial \mu}{\partial n})\delta u\, d\Gamma \\ &+ \int_{\Omega\setminus\Omega_\varepsilon} \nabla\cdot(-k\nabla\mu)\delta u\, d\Omega + \int_{\Omega_\varepsilon} \nabla\mu\cdot(-k\nabla u)\, d\Omega \end{aligned} \tag{4.9}$$

According to the boundary value on Γ_ε of Eq. (4.5), the third term of Eq. (4.9) is obtained as:

$$\int_{\Gamma_\varepsilon} \mu(q+\delta q)\, d\Gamma = 0 \tag{4.10}$$

For the 6th term, Taylor expansion is applied to express δu as follows:

$$\delta u(x) = \delta u(x^0 + \varepsilon\overline{\xi}) = \nabla u(x^0)\cdot(\varepsilon\overline{\xi}) + o(\varepsilon), \tag{4.11}$$

where, x^0 is the center of the infinitesimal hole, ε is the radius of the hole and $\overline{\xi}$ is outward normal vector to the circle of the hole at x. The Eq. (4.11) is applied to the sixth term and turn the integral path to the unit circle:

$$\begin{aligned}
-\int_{\Gamma_\varepsilon}(-k\frac{\partial\mu}{\partial n})\delta u\, d\Gamma &= -\int_{\Gamma_c}(-k\frac{\partial\mu}{\partial n})(\nabla u(x^0)\cdot(\varepsilon\overline{\xi}))\varepsilon\, d\Gamma_c \\
&= -\int_{\Gamma_c}(-k\frac{\partial\mu}{\partial n})(\nabla u(x^0)\cdot\overline{\xi})\varepsilon^2\, d\Gamma_c \\
&= -\int_{\Gamma_c}(-k\frac{\partial\mu}{\partial n})(\nabla u(x^0)\cdot(-\overline{n}))\varepsilon^2\, d\Gamma_c \\
&= (\pi\varepsilon^2)(-k\nabla u\cdot\nabla\mu)
\end{aligned} \tag{4.12}$$

where $\overline{n}$ is the inward normal vector the infinitesimal hole, which is opposite to $\overline{\varepsilon}$ By substituting Eq. (4.10) and (4.12) into Eq. (4.9), one can finally obtain that:

$$\begin{aligned}
\delta J = &\int_{(\Gamma\setminus\Gamma_f)\cap\Gamma_q}\mu\,\delta\bar{q}\, d\Gamma + \int_{(\Gamma\setminus\Gamma_f)\cap\Gamma_u}\mu\,\delta q\, d\Gamma \\
&+\int_{\Gamma_f\cap\Gamma_q}(\mu+\frac{\partial f}{\partial q})\delta\bar{q}\, d\Gamma + \int_{\Gamma_f\cap\Gamma_u}(\mu+\frac{\partial f}{\partial q})\delta q\, d\Gamma \\
&-\int_{\Gamma_f\cap\Gamma_u}(-k\frac{\partial\mu}{\partial n}-\frac{\partial f}{\partial u})\delta\bar{u}\, d\Gamma - \int_{\Gamma_f\cap\Gamma_q}(-k\frac{\partial\mu}{\partial n}-\frac{\partial f}{\partial u})\delta u\, d\Gamma \\
&-\int_{(\Gamma\setminus\Gamma_f)\cap\Gamma_u}(-k\frac{\partial\mu}{\partial n})\delta\bar{u}\, d\Gamma - \int_{(\Gamma\setminus\Gamma_f)\cap\Gamma_q}(-k\frac{\partial\mu}{\partial n})\delta u\, d\Gamma \\
&+\int_{\Omega\setminus\Omega_\varepsilon}\nabla\cdot(-k\nabla\mu)\delta u\, d\Gamma + 2(\pi\varepsilon^2)(-k\nabla u\cdot\nabla\mu)
\end{aligned} \tag{4.13}$$

Here, by using the fact $\Gamma_f = \Gamma_f\cap\Gamma_u + \Gamma_f\cap\Gamma_q$ and $\Gamma\setminus\Gamma_f = (\Gamma\setminus\Gamma_f)\cap\Gamma_u + (\Gamma\setminus\Gamma_f)\cap\Gamma_q$, each integral in Eq. (4.9) is split to two parts. Because the variation of known variables is 0, then $\delta u = 0$ and $\delta q = 0$. To eliminate the remaining unknown quantity, the adjoint field μ is determined so that it satisfies the following boundary value problem:

$$\nabla\cdot(-k\nabla\mu) = 0 \qquad \text{in } \Omega\setminus\Omega_\varepsilon \tag{4.14}$$

$$\mu = \begin{cases} 0 & \text{on } (\Gamma \setminus \Gamma_f) \cap \Gamma_u \\ -\dfrac{\partial f}{\partial q} & \text{on } \Gamma_f \cap \Gamma_q \end{cases} . \tag{4.15}$$

$$-k\frac{\partial \mu}{\partial n} = \begin{cases} 0 & \text{on } (\Gamma \setminus \Gamma_f) \cap \Gamma_q \\ \dfrac{\partial f}{\partial u} & \text{on } \Gamma_f \cap \Gamma_q \end{cases} . \tag{4.16}$$

Finally the topological derivative [142, 144] is obtained as:

$$\boxed{\mathscr{T}^{\#} = \lim_{\varepsilon \to 0} \frac{\delta J}{\delta \Omega_\varepsilon} = -2k\, \nabla \mu \cdot \nabla u} \tag{4.17}$$

Note: # is added to $\mathscr{T}$ to mark the topological derivative is obtained under insulating boundary condition. It is used for distinguishing with the topological derivatives obtained in other chapters.

4.3 Numerical examples

4.3.1 Numerical example 1

In this section, several numerical examples are presented to confirm the effectiveness and usefulness of the proposed method. In this example, a steady-state heat conduction problem is considered, shown as Figure 4.2.

The size of fixed design domain Ω is set to be $0.5\,[\mathrm{m}] \times 0.5\,[\mathrm{m}]$. As an initial configuration, the fixed design domain is filled with steel whose thermal conductivity is $k = 17.0\,[\mathrm{W/(m{\cdot}K)}]$. The prescribed temperature and heat flux are given as $\bar{u} = 100\,[\mathrm{K}]$ on Γ_u and $\bar{q} = 1000\,[\mathrm{W/m^2}]$ on Γ_q, respectively, where Γ_u and Γ_q are defined as shown in Figure 4.2. The length of Γ_u and Γ_q are $0.05\,[\mathrm{m}]$. The rest of the boundaries are insulating boundaries.

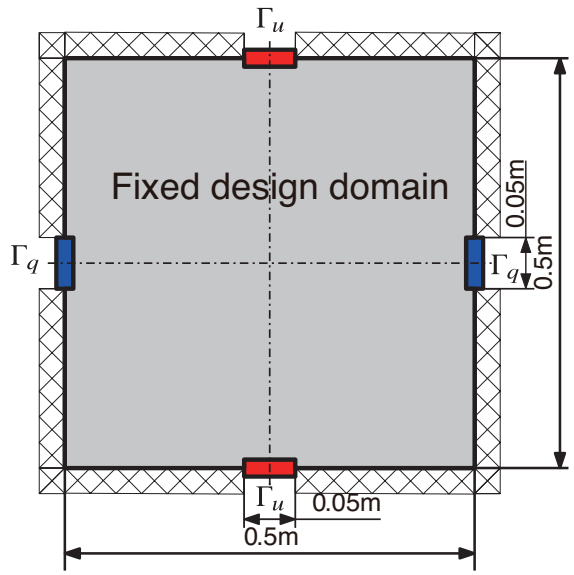

Figure 4.2: Fixed design domain for numerical example 1

The objective is to minimize the objective function defined on Γ_q. The objective function is given as follows:

$$F = \int_{\Gamma_f} (u - \hat{u})^2 \, d\Gamma, \tag{4.18}$$

where $\Gamma_f = \Gamma_q$ and $\hat{u}$ is the target temperature, which is set to be 60 [K].

Verification of topological derivative

It needs to verify the topological derivative expression before starting the topology optimization. According to the definition of topological derivative, the temperature field is calculated to obtain the objective function F_b. Next, material is removed to shape a hole small enough at the position x and calculate the temperature field again to obtain the objective function F_a, then the finite difference method is used to obtain the sensitivity S:

$$S = \frac{F_b - F_a}{A(x)}, \tag{4.19}$$

where, $A(x)$ is the area of the small hole at position x. A comparison of the values of the topological derivative calculated by the proposed method with the ones obtained by the finite difference method is made, shown as Figure 4.3. It can be confirmed by the comparison that the topological derivative expression derived in the proposed method is available.

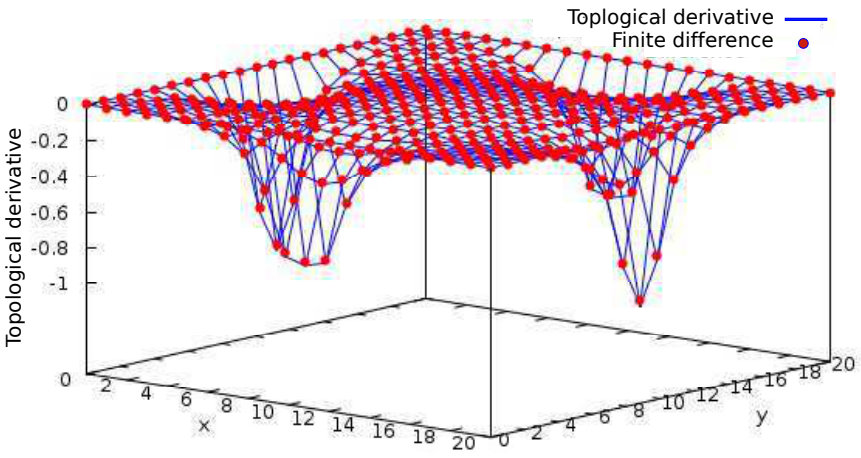

Figure 4.3: Comparison of the topological derivatives calculated by the proposed method with the approximated one by the finite difference

Next, a numerical example is shown with the area constraint set as 20% of the fixed design domain. The regularization parameter is set as $\tau = 3.0 \times 10^{-3}$. The coefficient K of the time evolution equation is set as 5.0. The fictitious time increment Δt is set as 0.1. The fixed design domain is divided into 40 $\times$ 40 cells. The boundary element meshes to solve the boundary value problems of heat field and its adjoint field are created by tracking the zeros of the value of the level set function which is evaluated on the finite element nodes.The obtained optimal distributions of material are shown as Figure 4.4.

Effect of finite element mesh size

The fixed design domain of the present numerical example is divided into 40 $\times$ 40 quadrilateral elements. However, as a numerical method, the finite element mesh

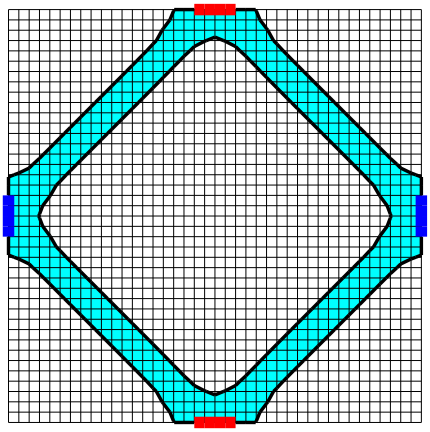

Figure 4.4: Optimal configuration for the numerical example 1

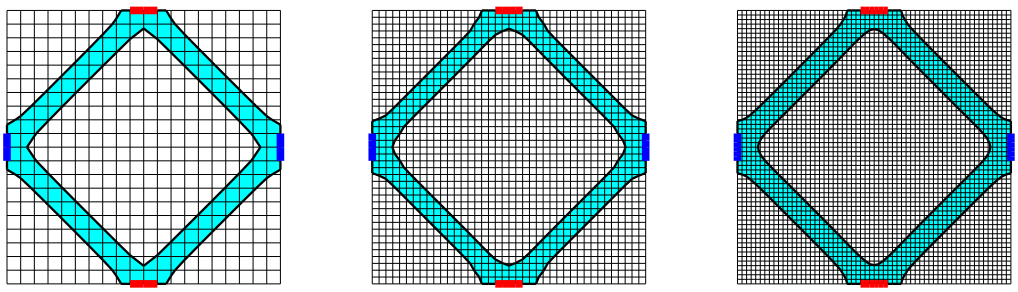

Figure 4.5: (left:) Case A (center:) Case B (right:) Case C for numerical example 1

should not effect the obtained optimal result. To confirm this, three cases of initial, intermediate and obtained optimal configurations of different finite element mesh size are emploied. The three cases are denoted as follows: A (mesh: 20×20 cells), B (mesh: 40×40 cells) and C (mesh: 60×60 cells). Case A and C have the same parameters setting with Case B (the one being discussed) except for the mesh size. The results of three cases are shown as Figure 4.5. From these results, It can be found that same optimal configuration can be obtained regardless of initial configurations. In other words, the finite element mesh does not effect the obtained optimal result.

Effect of initial configuration

Next, whether a numerical method works or not is up to whether it can converge to the same optimal configuration using different initial configurations. To check this, the influence of the initial configuration to the optimal results is investigated. The following 3 initial configurations are considered; (1) the whole fixed design domain is filled with Ω, (2) Ω has 4 holes and (3) Ω has 9 holes. Henceforth the above initial configurations are denoted as "without hole", "with 4 holes" and "with 9 holes", respectively. Figures 4.6–4.8 show initial, intermediate and optimal configurations. For these 3 cases, the regularization parameter is set as $\tau = 5.0 \times 10^{-3}$, the coefficient K of the time evolution equation is set as 5.0, and the fictitious time increment Δt is set as 0.1. From these figures it can be found that the initial configuration has almost no influences on the obtained optimal configuration. This has confirmed that the optimal configuration's obtainment does not depend on the initial configuration.

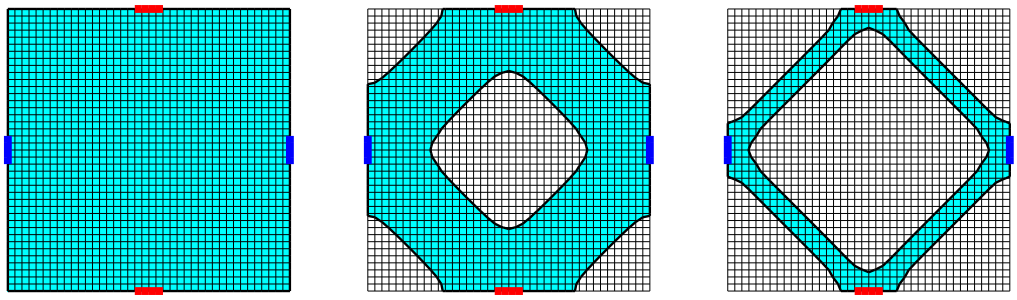

Figure 4.6: (left:) Initial (center:) intermediate (right:) an optimal configuration "without hole" for the numerical example 1

The history of objective function

Because It is not hoped the objective function converge to different value with different finite mesh or initial configurations. Here the objective function history (Figure 4.9) is shown with different initial configurations to show the effect of the initial configuration to objective function.

Figure 4.9 shows the objective function history normalised by its initial value for each initial configuration.

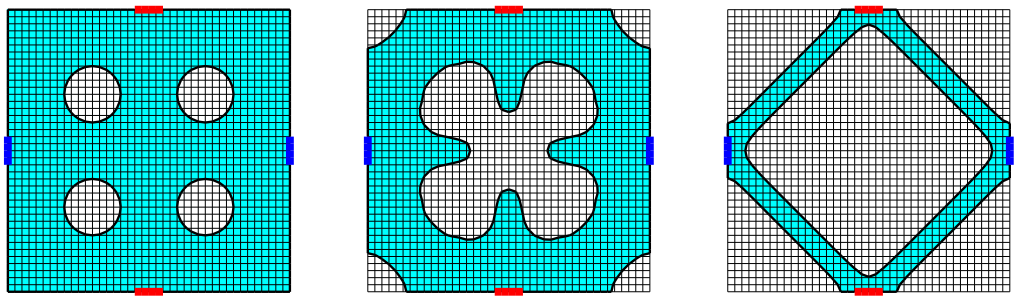

Figure 4.7: (left:) Initial (center:) intermediate (right:) an optimal configuration "with 4 holes" for the numerical example 1

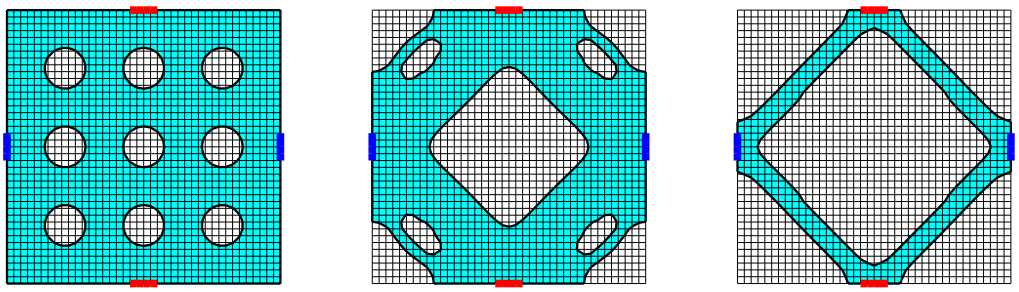

Figure 4.8: (left:) Initial (center:) intermediate (right:) an optimal configuration "with 9 holes" for the numerical example 1

Readers must find that, at the first several step, the objective function drops sharply. This is because holes are generated and the material is removed more that a presupposed mount from the fixed design domain. The objective function has a bounce-back. This is controlled so that the area of material domain changes stalely. Finally, the objective function becomes flat for all initial configurations and converged to similar values.

4.3.2 Numerical example 2

In this numerical example, a problem with boundary conditions different from the previous one is considered to show its availability under diverse boundary conditions. The figure for this example is shown as Figure 4.10. The prescribed tem-

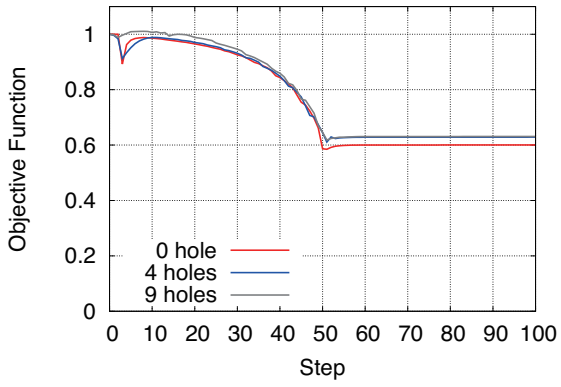

Figure 4.9: Normalized objective function value history for numerical example 1

perature $\bar{u} = 100$[K] on Γ_u, and the prescribed heat flux $\bar{q} = 1000\,[\mathrm{W/m^2}]$ on Γ_q. The rest of the boundaries are insulating boundaries.

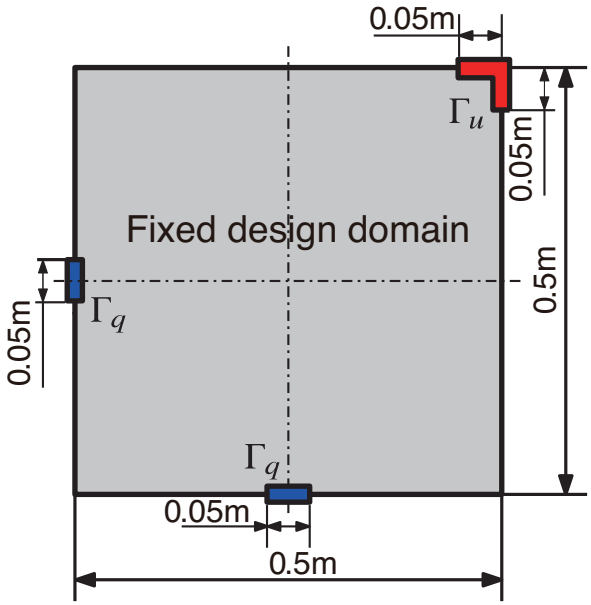

Figure 4.10: Fixed design domain for the numerical example 2

The objective function for this example is same as that for the previous one in Eq. (4.18) with target temperature as $\hat{u} = 60$[K]. The area constraint is set to 20% of the fixed design domain. The regularization parameter is set as $\tau = 5.0 \times 10^{-3}$. The coefficient K of time evolution equation is set as 5.0 and time increment Δt is

set as 0.1.

The boundary elements are generated by searching 0-value level-set function based on the mesh of 40×40 cells. The obtained topology distributions of different initial configurations are shown as Figures 4.11, 4.12 and 4.13. Also, the objective function values of this example with different initial configurations are shown as Figure 4.14. From these figures, it can be concluded the following:

- The objective function decreased enough.
- The obtained configurations have smooth boundaries.
- When the initial configuration is different, the proposed method could give the similar optimal configuration.

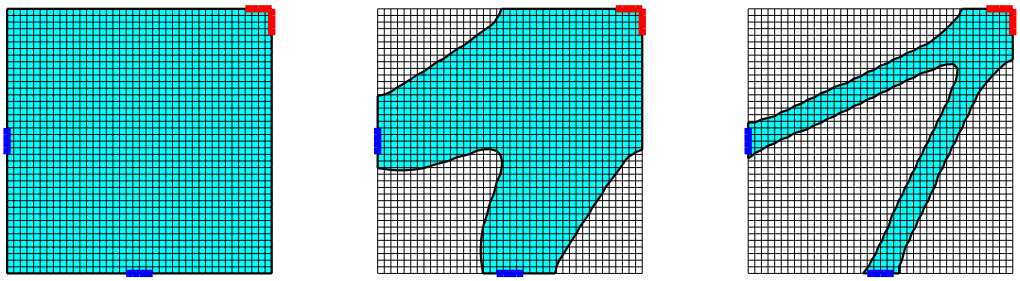

Figure 4.11: (left:) Initial (center:) intermediate (right:) an optimal configuration "without hole" for numerical example 2

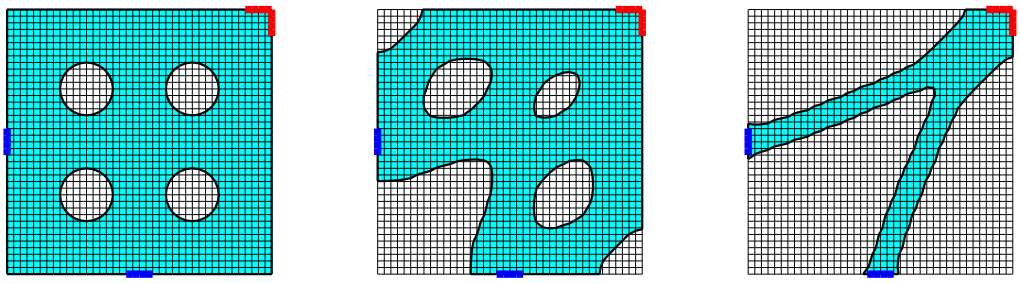

Figure 4.12: (left:) Initial (center:) intermediate (right:) an optimal configuration "with 4 holes" for numerical example 2

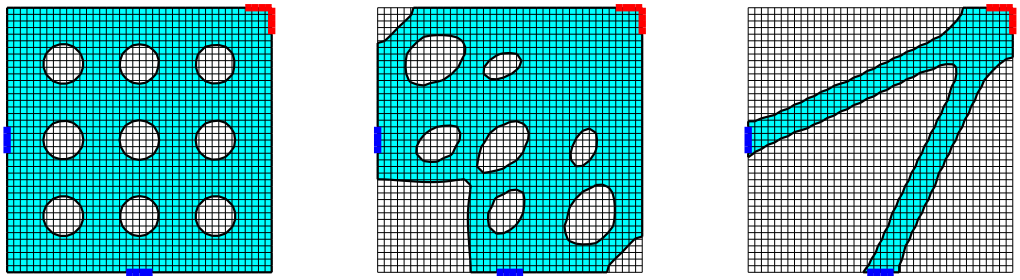

Figure 4.13: (left:) Initial (center:) intermediate (right:) an optimal configuration "with 9 holes" for numerical example 2

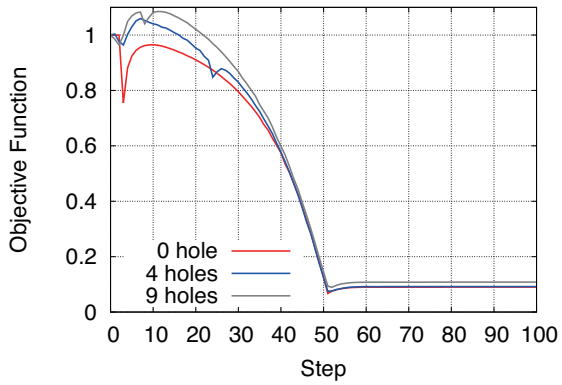

Figure 4.14: Normalized objective function value history for numerical example 2

In Figure 4.14, readers must find that, at the first several step, the objective function drops sharply. This is because holes are generated and the material is removed more that a presupposed mount from the fixed design domain. The objective function has a bounce-back. This is controlled so that the area of material domain changes stalely. While, for the objective functions with 4 and 9 holes initially, the reason that objective functions increase shapely is some void domain is removed or area of holes are decreased. Later, as the updating proceeds, the objective function decrease steady. Finally, the objective function becomes flat for all initial configurations and converged to similar values.

4.4 Conclusions

In this chapter, the topological derivative (sensitivity) under insulating boundary condition using BEM is derived. With the derived topological derivative, a topology optimization method combining with the level set method and the boundary element method for 2D steady-state heat conduction problem is built. Through the numerical examples, the correctness of the topological derivative and the effectiveness of the proposed method has been verified. Besides, It can be concluded that cases of different initial configurations have the same converging tendency, and converged to similar shapes. In particular, A few material shapes with specified temperatures on part of the material boundary are obtained. it is also noted that the obtained shapes are smooth.

Chapter 5

Topology Optimization with Heat Transfer Boundary Condition for Heat Conduction Problems using BEM

5.1 Introduction

Last chapter presented a level set-based topology optimization under insulating boundary condition. It is proved effective through several numerical examples, in one of which the topological derivative or sensitivity derived combining with boundary element method is verified and in others the mesh-dependency and initial configuration dependency are checked, as well as the smoothness of the boundaries of the configuration.

Note that all those in last chapter are based on the assumption that new boundaries are under insulating boundary condition.In this chapter, a topology optimization method for two-dimensional heat conduction problem with heat transfer boundary condition based on the level set method and the boundary element method (BEM) is presented. The newly generated boundary of hole are given as heat trans-

fer boundary shown as Figure 5.1. In this chapter, the objective function is written into an unconstrained problem combining the governing equation of heat transfer boundary value problem. Then The variation of the objective function is obtained when it suffers a change that resulted from removing an infinitesimal circular area. After that, an adjoint system is introduced, which is also a boundary value problem but with the boundary condition and value that can be calculated using the obtained quantities from forward problem, to cancel some unknown quantities so as to write the variation of objective function as an approximation which is so-called topological derivative or sensitivity. The topological sensitivities under heat transfer boundary condition is derived. The topological derivative expression is verified though a numerical example, then applied to a few topology optimization for two dimensional heat conduction problems.

5.2 Topological derivative

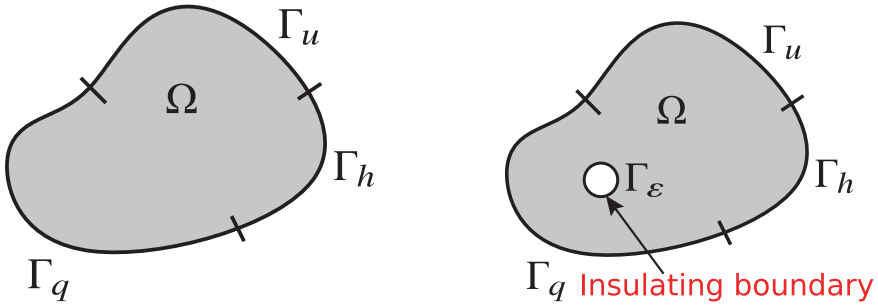

Figure 5.1: (left:) Configuration before a hole is created; (right:) Configuration after a hole is created

A problem is considered the same as the one in Chapter 2 with the newly generated boundary given as heat transfer boundary condition. The augmented objective function J can be rewritten as follows:

$$\begin{aligned} J &= \int_\Gamma f(u,q)\,d\Gamma + \int_\Omega g(u)\,d\Omega + \int_\Omega \mu \nabla\cdot(-k\nabla u)\,d\Omega \\ &= \int_\Gamma f\,d\Gamma + \int_\Omega g\,d\Omega + \int_\Gamma \mu q\,d\Gamma - \int_\Omega \nabla\mu\cdot(-k\nabla u)\,d\Omega, \end{aligned} \tag{5.1}$$

where μ is the adjoint variable considered as the Lagrange multiplier. Γ is the boundary of material domain Ω, and $\Gamma = \Gamma_u \cup \Gamma_q \cup \Gamma_h$. Note that Γ_f, which denotes the support of f and used in the last chapter, is not considered below to simplify the following expressions.

The objective function suffers from a change when an infinitesimal region Ω_ε is removed from Ω, thus one has

$$\begin{aligned} J+\delta J = &\int_\Gamma \left(f + \frac{\partial f}{\partial u}\delta u + \frac{\partial f}{\partial q}\delta q \right) d\Gamma + \int_\Omega \left(g + \frac{\partial g}{\partial u}\delta u \right) d\Omega + \int_\Gamma \mu(q+\delta q)\, d\Gamma \\ &- \int_{\Omega\setminus\Omega_\varepsilon} \nabla\mu\cdot(-k\nabla u)\, d\Omega - \int_{\Omega\setminus\Omega_\varepsilon} \nabla\mu\cdot(-k\nabla\delta u)\, d\Omega + \int_{\Gamma_\varepsilon} \mu(q+\delta q)\, d\Gamma. \end{aligned} \tag{5.2}$$

Therefore, one has

$$\begin{aligned} \delta J = &\int_{\Gamma_u\cup\Gamma_q\cup\Gamma_h} \left(\frac{\partial f}{\partial u}\delta u + \frac{\partial f}{\partial q}\delta q \right) d\Gamma + \int_\Omega \frac{\partial g}{\partial u}\delta u\, d\Omega + \int_{\Gamma_u\cup\Gamma_q\cup\Gamma_h} \mu\delta q\, d\Gamma \\ &- \int_{\Omega\setminus\Omega_\varepsilon} \nabla\mu\cdot(-k\nabla\delta u)\, d\Omega + \int_{\Gamma_\varepsilon} \mu(q+\delta q)\, d\Gamma + \int_{\Omega_\varepsilon} \nabla\mu\cdot(-k\nabla u)\, d\Omega \\ = &\int_{\Gamma_q} \frac{\partial f}{\partial u}\delta u\, d\Gamma + \int_{\Gamma_u} \frac{\partial f}{\partial q}\delta q\, d\Gamma + \int_{\Gamma_h} \left(\frac{\partial f}{\partial u}\delta u + \frac{\partial f}{\partial q}\delta q \right) d\Gamma \\ &+ \int_{\Gamma_u} \mu\delta q\, d\Gamma + \int_{\Gamma_h} \mu\delta q\, d\Gamma - \int_{\Gamma_q} \eta\delta u\, d\Gamma - \int_{\Gamma_h} \eta\delta u\, d\Gamma \\ &- \int_{\Omega\setminus\Omega_\varepsilon} \left[\nabla\cdot(-k\nabla\mu) - \frac{\partial g}{\partial u} \right] \delta u\, d\Omega \\ &- \int_{\Gamma_\varepsilon} \eta\delta u\, d\Gamma + \int_{\Gamma_\varepsilon} \mu(q+\delta q)\, d\Gamma + \int_{\Omega_\varepsilon} \nabla\mu\cdot(-k\nabla u)\, d\Omega, \end{aligned} \tag{5.3}$$

where δJ is the variation of the augmented objective function, Γ_u, Γ_q and Γ_h denote the temperature boundary, heat flux boundary and heat transfer boundary, respectively; And

$$\eta = -k\frac{\partial\mu}{\partial n} = -k\nabla\mu\cdot\mathbf{n}. \tag{5.4}$$

and Γ_h is heat transfer boundary.

From the heat transfer boundary condition on Γ_h, one finds

$$\delta q = h\delta u \qquad \text{on } \Gamma_h. \tag{5.5}$$

Thus, one has

$$\begin{aligned}
\delta J &= \int_{\Gamma_u} \left(\mu + \frac{\partial f}{\partial q}\right) \delta q \, d\Gamma - \int_{\Gamma_q} \left(\eta - \frac{\partial f}{\partial u}\right) \delta u \, d\Gamma \\
&\quad + \int_{\Gamma_h} \left(\frac{\partial f}{\partial u} + h\frac{\partial f}{\partial q} + h\mu - \eta\right) \delta u \, d\Gamma - \int_{\Omega\setminus\Omega_\varepsilon} \left[\nabla\cdot(-k\nabla\mu) - \frac{\partial g}{\partial u}\right] \delta u \, d\Omega \\
&\quad - \int_{\Gamma_\varepsilon} \eta \, \delta u \, d\Gamma + \int_{\Gamma_\varepsilon} \mu(q+\delta q)\, d\Gamma + \int_{\Omega_\varepsilon} \nabla\mu\cdot(-k\nabla u)\, d\Omega \\
&= \int_{\Gamma_u} \left(\mu + \frac{\partial f}{\partial q}\right) \delta q \, d\Gamma - \int_{\Gamma_q} \left(\eta - \frac{\partial f}{\partial u}\right) \delta u \, d\Gamma \\
&\quad - \int_{\Gamma_h} \left[\eta - h\left(\mu + \frac{1}{h}\frac{\partial f}{\partial u} + \frac{\partial f}{\partial q}\right)\right] \delta u \, d\Gamma - \int_{\Omega\setminus\Omega_\varepsilon} \left[\nabla\cdot(-k\nabla\mu) - \frac{\partial g}{\partial u}\right] \delta u \, d\Gamma \\
&\quad - \int_{\Gamma_\varepsilon} \eta \, \delta u \, d\Gamma + \int_{\Gamma_\varepsilon} \mu(q+\delta q)\, d\Gamma + \int_{\Omega_\varepsilon} \nabla\mu\cdot(-k\nabla u)\, d\Omega. \qquad (5.6)
\end{aligned}$$

Let us define the adjoint system, as follows:

$$\text{D.E.:} \qquad \nabla\cdot(-k\nabla\mu) - \frac{\partial g}{\partial u} = 0 \qquad \text{in } \Omega, \qquad (5.7)$$

$$\text{B.C.:} \qquad \mu = -\frac{\partial f}{\partial q} \qquad \text{on } \Gamma_u, \qquad (5.8)$$

$$\eta = \frac{\partial f}{\partial u} \qquad \text{on } \Gamma_q, \qquad (5.9)$$

$$\eta = h\left(\mu + \frac{1}{h}\frac{\partial f}{\partial u} + \frac{\partial f}{\partial q}\right) \qquad \text{on } \Gamma_h. \qquad (5.10)$$

Then, δJ results in

$$\delta J = -\int_{\Gamma_\varepsilon} \eta \, \delta u \, d\Gamma + \int_{\Gamma_\varepsilon} \mu(q+\delta q)\, d\Gamma + \int_{\Omega_\varepsilon} \nabla\mu\cdot(-k\nabla u)\, d\Omega. \qquad (5.11)$$

In the neighborhood of infinitesimal Ω_ε, u and μ can be expanded about the center of Ω_ε, as follows:

$$u = u^0 + \nabla u^0\cdot\mathbf{r} + O(r^2) \approx u^0 + r(u^0_{,1}\cos\theta + u^0_{,2}\sin\theta), \qquad (5.12)$$

$$\mu = \mu^0 + \nabla\mu^0\cdot\mathbf{r} + O(r^2) \approx \mu^0 + r(\mu^0_{,1}\cos\theta + \mu^0_{,2}\sin\theta), \qquad (5.13)$$

$$q \approx -k\nabla u^0\cdot\mathbf{n} = k\left.\frac{\partial u}{\partial r}\right|_{r=0} = k(u^0_{,1}\cos\theta + u^0_{,2}\sin\theta), \qquad (5.14)$$

$$\eta \approx -k\nabla\mu^0\cdot\mathbf{n} = k\left.\frac{\partial \mu}{\partial r}\right|_{r=0} = k(\mu^0_{,1}\cos\theta + \mu^0_{,2}\sin\theta), \qquad (5.15)$$

where $\mathbf{r}$ is the position vector of the point in the neighborhood of the center of Ω_ε, and $r = |\mathbf{r}|$, as shown in Figure 5.2. A superscript '0' denotes the value at the center

of Ω_ε. $u^0_{,1}$ and $u^0_{,2}$ are the gradients of u at the center of Ω_ε in x and y directions, respectively, and $\mu^0_{,1}$ and $\mu^0_{,2}$ are defined in the same way. θ is the counter clockwise angle from x-axis. $\mathbf{n}$ is the outward normal vector to Γ_ε, in opposite direction of $\mathbf{r}$.

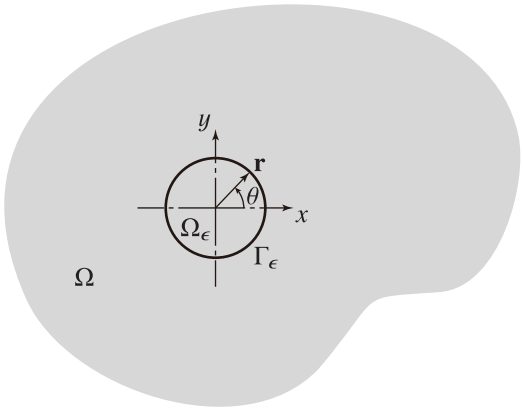

Figure 5.2: The neighborhood of the infinitesimal circular domain removed from the material.

The heat transfer boundary condition is considered on Γ_ε as

$$q + \delta q = h(u + \delta u - u_\infty), \tag{5.16}$$

where h is the heat transfer coefficient and u_∞ is the ambient temperature.

For sufficiently small Ω_ε, δu behaves as the main part of the solution of Laplace's equation in the neighborhood of the center of Ω_ε, as follows:

$$\delta u = a \ln r + \frac{b}{r}\cos\theta + \frac{c}{r}\sin\theta + O\Big(\frac{d}{r^3}\Big). \tag{5.17}$$

where a, b, c, and d are coefficient constants. Since δu vanishes when $r \to 0$, δu cannot contain a constant term in the general solution, and d should behave as $O(r^3)$. The term proportional to $\ln r$ can exist if the coefficient a vanishes as $\Gamma_\varepsilon \to 0$.

Thus, the following term can be obtained:

$$\begin{aligned}\delta q &= -k\frac{\partial \delta u}{\partial n} = k\frac{\partial \delta u}{\partial r} \\ &= \frac{ka}{r} - \frac{kb}{r^2}\cos\theta - \frac{kc}{r^2}\sin\theta + O\Big(\frac{d}{r^4}\Big).\end{aligned} \tag{5.18}$$

Therefore, for $r=\varepsilon$, Eq. (5.16) becomes as:

$$\begin{aligned} &ku^0_{,1}\cos\theta + ku^0_{,2}\sin\theta + \frac{ka}{\varepsilon} - \frac{kb}{\varepsilon^2}\cos\theta - \frac{kc}{\varepsilon^2}\sin\theta \\ &\quad = hu^0 + h\varepsilon u^0_{,1}\cos\theta + h\varepsilon u^0_{,2}\sin\theta + ha\ln\varepsilon + \frac{h}{\varepsilon}b\cos\theta + \frac{h}{\varepsilon}c\sin\theta - hu_\infty. \end{aligned} \tag{5.19}$$

By rearranging the above equation, one has

$$\begin{aligned} &\left(\frac{k}{\varepsilon} - h\ln\varepsilon\right)a - \left(\frac{k}{\varepsilon^2}+\frac{h}{\varepsilon}\right)b\cos\theta - \left(\frac{k}{\varepsilon^2}+\frac{h}{\varepsilon}\right)c\cos\theta \\ &\qquad = h(u^0-u_\infty) + (h\varepsilon - k)u^0_{,1}\cos\theta + (h\varepsilon-k)u^0_{,2}\sin\theta. \end{aligned} \tag{5.20}$$

By comparing the coefficients, the followings are obtained as

$$a = \varepsilon\frac{h(u^0-u_\infty)}{k-h\varepsilon\ln\varepsilon}, \tag{5.21}$$

$$b = \varepsilon^2\frac{k-\varepsilon h}{k+\varepsilon h}u^0_{,1}, \tag{5.22}$$

$$c = \varepsilon^2\frac{k-\varepsilon h}{k+\varepsilon h}u^0_{,2}. \tag{5.23}$$

Finally, the variation of δu and δq on Γ_ε is obtained as

$$\delta u = \varepsilon\frac{h(u^0-u_\infty)}{k-h\varepsilon\ln\varepsilon}\ln r + \frac{\varepsilon^2}{r}\frac{k-\varepsilon h}{k+\varepsilon h}u^0_{,1}\cos\theta + \frac{\varepsilon^2}{r}\frac{k-\varepsilon h}{k+\varepsilon h}u^0_{,2}\sin\theta, \tag{5.24}$$

$$\delta q = \frac{\varepsilon}{r}\frac{kh(u^0-u_\infty)}{k-h\varepsilon\ln\varepsilon} - \frac{\varepsilon^2}{r^2}\frac{k(k-\varepsilon h)}{k+\varepsilon h}u^0_{,1}\cos\theta - \frac{\varepsilon^2}{r^2}\frac{k(k-\varepsilon h)}{k+\varepsilon h}u^0_{,2}\sin\theta. \tag{5.25}$$

Let us evaluate the variation δJ next.

$$\begin{aligned} \delta J &= -\int_{\Gamma_\varepsilon}\eta\,\delta u\,d\Gamma + \int_{\Gamma_\varepsilon}\mu(q+\delta q)\,d\Gamma + \int_{\Omega_\varepsilon}\nabla\mu\cdot(-k\nabla u)\,d\Omega \\ &\equiv A + B + C, \end{aligned} \tag{5.26}$$

where

$$A = -\int_{\Gamma_\varepsilon}\eta\,\delta u\,d\Gamma, \tag{5.27}$$

$$B = \int_{\Gamma_\varepsilon}\mu(q+\delta q)\,d\Gamma, \tag{5.28}$$

$$C = \int_{\Omega_\varepsilon}\nabla\mu\cdot(-k\nabla u)\,d\Omega, \tag{5.29}$$

and

$$
\begin{aligned}
A = &-\int_0^{2\pi} (k\mu_{,1}^0 \cos\theta + k\mu_{,2}^0 \sin\theta) \\
&\times \left[\varepsilon \frac{h(u^0 - u_\infty)}{k - h\varepsilon \ln\varepsilon} \ln\varepsilon + \varepsilon \frac{k - \varepsilon h}{k + \varepsilon h} u_{,1}^0 \cos\theta + \varepsilon \frac{k - \varepsilon h}{k + \varepsilon h} u_{,2}^0 \sin\theta \right] \varepsilon \, d\theta \\
&= -\pi k \varepsilon^2 \frac{k - \varepsilon h}{k + \varepsilon h} \left(\mu_{,1}^0 u_{,1}^0 + \mu_{,2}^0 u_{,2}^0 \right). \qquad (5.30)
\end{aligned}
$$

$$
\begin{aligned}
B = &\varepsilon \int_0^{2\pi} \left(\mu^0 + \varepsilon \mu_{,1}^0 \cos\theta + \varepsilon \mu_{,2}^0 \sin\theta \right) \times \left(k u_{,1}^0 \cos\theta + k u_{,2}^0 \sin\theta \right. \\
&+ \frac{kh(u^0 - u_\infty)}{k - \varepsilon h \ln\varepsilon} - \frac{k(k - \varepsilon h)}{k + \varepsilon h} u_{,1}^0 \cos\theta - \frac{k(k - \varepsilon h)}{k + \varepsilon h} u_{,2}^0 \sin\theta) \, d\theta \\
&= 2\pi\varepsilon \mu^0 h(u^0 - u_\infty) \frac{k}{k - \varepsilon h \ln\varepsilon} + \pi \varepsilon^3 \frac{2kh}{k + \varepsilon h} \left(\mu_{,1}^0 u_{,1}^0 + \mu_{,2}^0 u_{,2}^0 \right). \qquad (5.31)
\end{aligned}
$$

Also, one has

$$
C = \int_{\Omega_\varepsilon} \nabla\mu \cdot (-k \nabla u) \, d\Omega \approx -\pi \varepsilon^2 k \left(\mu_{,1}^0 u_{,1}^0 + \mu_{,2}^0 u_{,2}^0 \right). \qquad (5.32)
$$

Therefore, δJ becomes as

$$
\begin{aligned}
\delta J = &-\pi k \varepsilon^2 \frac{k - \varepsilon h}{k + \varepsilon h} \nabla\mu^0 \cdot \nabla u^0 + 2\pi\varepsilon \mu^0 h(u^0 - u_\infty) \frac{k}{k - \varepsilon h \ln\varepsilon} \\
&+ \pi \varepsilon^3 \frac{2kh}{k + \varepsilon h} \nabla\mu^0 \cdot \nabla u^0 - \pi \varepsilon^2 k \nabla\mu^0 \cdot \nabla u^0. \qquad (5.33)
\end{aligned}
$$

Thus, it is able to define the topological derivative with heat transfer boundary condition [140, 146] as follows:

$$
\boxed{\mathscr{T}^\circ = \lim_{\varepsilon \to 0} \frac{\delta J}{2\pi\varepsilon} = \mu^0 h(u^0 - u_\infty).} \qquad (5.34)
$$

Note that we have used the fact that $\frac{k}{k - \varepsilon h \ln\varepsilon}$ behaves as

$$
\frac{k}{k - \varepsilon h \ln\varepsilon} = \varepsilon + \frac{h \ln\varepsilon}{k} \varepsilon^2 + O(\varepsilon^3) \qquad (5.35)
$$

in the limit $\varepsilon \to 0$.

Note: $^\circ$ is added to $\mathscr{T}$ to mark the topological derivative is obtained under heat transfer boundary condition. It is used for distinguishing with the topological derivatives obtained in other chapters.

5.3 Numerical examples for verifying the topological derivative

In this example, we demonstrate the correctness of the topological derivative.

Let us consider a design domain initially filled with the material entirely in the area of $4.0\,[\mathrm{m}] \times 4.0\,[\mathrm{m}]$ as shown in Figure 5.3. Temperature boundary condition is given for the left and top edges of the design domain, with prescribed temperature $\bar{u} = 100[\mathrm{K}]$, while heat flux boundary condition is given for the bottom and right edges with prescribed heat flux $\bar{q} = 50\,[\mathrm{W/m^2}]$. The thermal conductivity of the domain is assumed as $k = 1.0\,[\mathrm{W/(m{\cdot}K)}]$. We compare the topological derivative value calculated by Eq. (5.34) with the approximate one calculated by a finite difference of the values of objective function for the original domain and the domain from which a small circular hole is removed. Heat transfer boundary condition with the ambient temperature $u_\infty = 30[\mathrm{K}]$ and the heat transfer coefficient $h = 0.001\,[\mathrm{W/(m^2{\cdot}K)}]$ is considered on the circular hole.

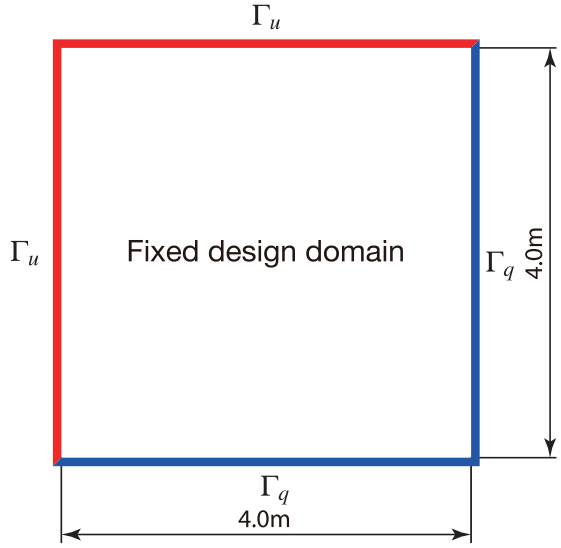

Figure 5.3: Fixed design domain for example 1

The objective function for this example is defined as

$$F = \int_{\Gamma_q} (u - \hat{u})^2 \, d\Gamma, \tag{5.36}$$

where $\hat{u} = 40$[K] is the target temperature.

The boundary of the square domain is discretized with 40×40 uniformly with quadratic continuous elements. Also, 40×40 grids are generated in the fixed design domain, the topological derivative values are calculated at the sample internal grid points shown in Figure 5.4. The approximate values of the topological derivative is calculated by the following formula:

$$F'_{\text{approx}} = \frac{F_{\text{original}} - F_{\text{hole}}}{2\pi\varepsilon}, \tag{5.37}$$

where, F_{original} and F_{hole} denote the values of the objective function before and after the hole is created. $\varepsilon = 0.0001$ [m] is the radius of the hole, and the boundary of the hole is divided into 32 quadratic elements when F_{hole} is calculated using the boundary element method. As shown in Figure 5.5, the topological derivative values obtained using the proposed approach are in good agreement with those obtained with the finite difference formula, thus the present formulae of the topological derivative is verified.

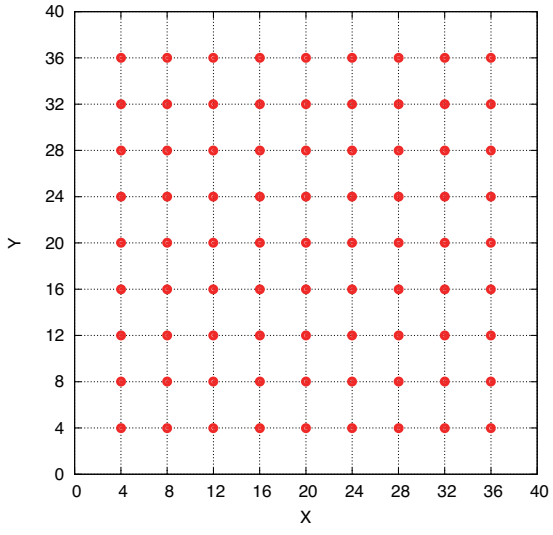

Figure 5.4: Sample points for verifying the topological derivative

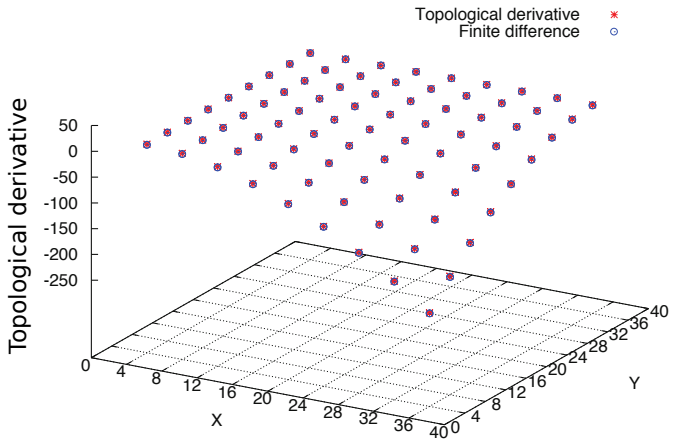

Figure 5.5: Comparison of the topological derivatives obtained by the proposed approach with the one by the finite difference

5.4 Numerical examples for the topology optimizations

5.4.1 Numerical Example 1

In this example a topology optimization based on the present topological derivative is demonstrated. We consider a fixed design domain of $4.0\,[\mathrm{m}] \times 4.0\,[\mathrm{m}]$. The thermal conductivity of the domain is $k = 1.0\,[\mathrm{W/(m{\cdot}K)}]$. We arrange the boundary conditions as shown in Figure 5.6. The length of each Γ_u is $0.8\,[\mathrm{m}]$. On Γ_u, temperature is given as $\bar{u} = 100[\mathrm{K}]$, while on Γ_h, heat transfer boundary condition with $h = 1.0[\mathrm{W/(m \cdot K)}]$ and $u_\infty = 0[\mathrm{K}]$ is specified. The objective function for this example is defined as

$$F = \int_{\Gamma_h} (u - \hat{u})^2 \, d\Gamma, \tag{5.38}$$

which is defined on the fixed heat transfer boundary Γ_h. $\hat{u}$ is the target temperature prescribed as $\bar{u} = 10[\mathrm{K}]$.

The area constraint $G_{\max}$ is set to be 70% of the fixed design domain. The regularization parameter is set as $\tau = 5.0 \times 10^{-1}$. The proportional coefficient and

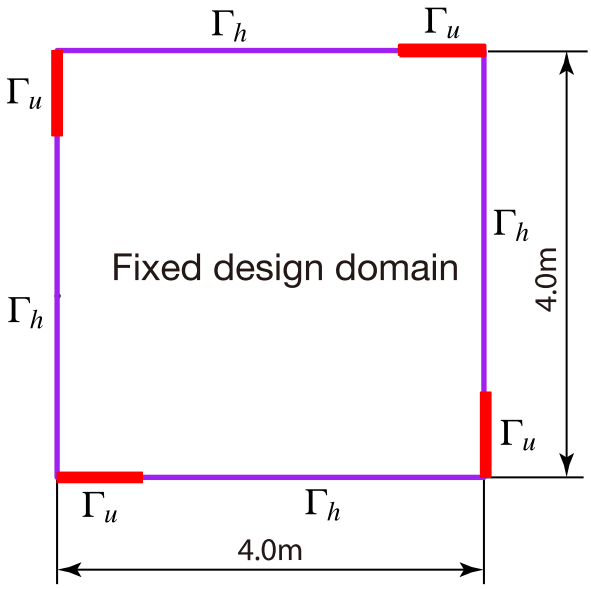

Figure 5.6: Fixed design domain for example 2

the fictitious time interval are given as $K = 10.0$ and $\Delta t = 0.2$, respectively. The boundary element is generated automatically by searching isosurface of zero-value of the level set function. The initial configuration of the domain and the obtained intermediate and optimum configurations are shown in Figure 5.7.

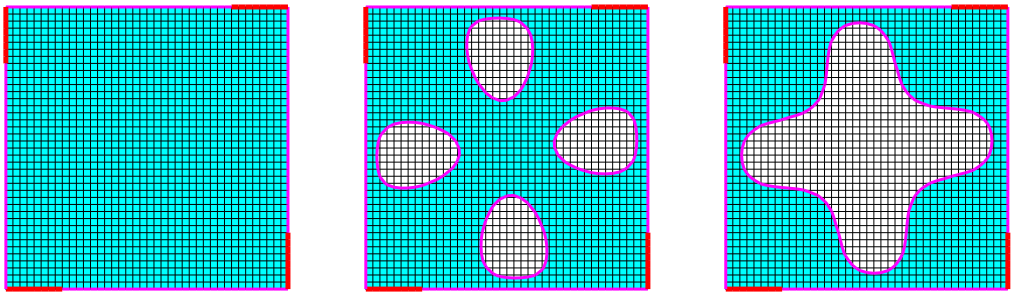

Figure 5.7: Initial (left), intermediate (middle) and optimal (right) configurations for example 2

From the obtained intermediate and optimum configurations, we find that cavities emerge in the are close to the edges of the fixed design domain, extend to the central area of the domain, then join together to be like a crisscross pattern.

The area constraint 70% is satisfied as found in Figure 5.8. Corresponding history of the value of the objective function, normalized by the initial value of the function, is shown in Figure 5.9. It is observed that the objective function value decreases step by step to 75.0% of its initial value.

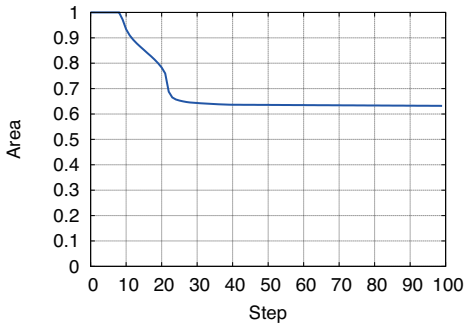

Figure 5.8: Area for example 2

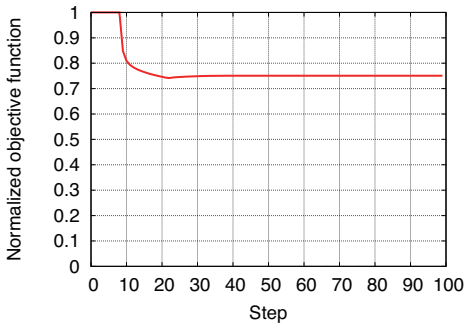

Figure 5.9: Normalized objective function for example 2

Readers must find that, at the first several step, the objective function does not change. This is because no holes appear during these steps. However, the distribution of the level set function changes also during these steps, just not enough to produce a hole. After that, the objective function does decrease sharply, where the fixed design domain suffers a rapid topology change. At the 22nd step, the objective function reaches its lowermost value, but the area constraint 70% is not yet satisfied. Thus, more material should be removed in the later steps. Later the area constraint is satisfied and objective function converged.

Next the effects of regularization parameter τ to the results are demonstrated. In Figure 5.10, the optimum configurations obtained with different values of the regularization parameter, $\tau = 2.5 \times 10^{-1}$, 5.0×10^{-1} and 7.5×10^{-1} are shown.

As the regularization parameter increases, the configuration of the obtained optimum result becomes simpler. This gives more suggestion to application for manufacture.

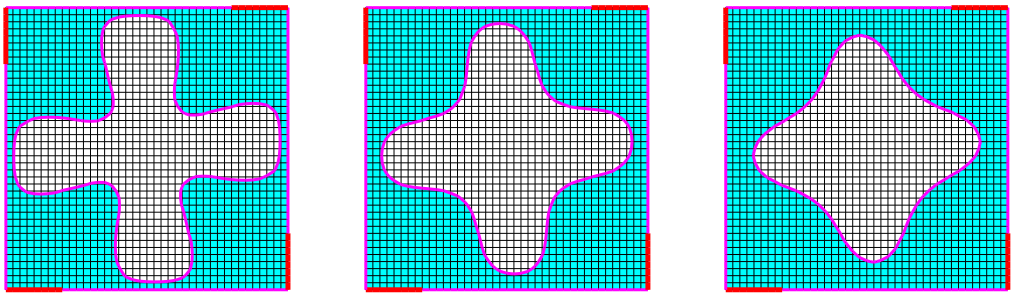

Figure 5.10: Various optimal results for the regularization parameters: $\tau = 2.5 \times 10^{-1}$ (left), 5.0×10^{-1}(middle) and 7.5×10^{-1} (right) for example 2

Certainly, attention should be paid to the histories of the objective function, because the minimum value of objective function under corresponding constraints is pursued. Meanwhile, it is noticed that the complexity of optimal configuration has some effect on the objective function. In Figure 5.11 are compared the profiles of the objective function for $\tau = 2.5 \times 10^{-1}$, 5.0×10^{-1}, and 7.5×10^{-1}. The corresponding achieved normalized objective function values are 74.1%, 75.0% and 76.3% of the initial value, respectively.

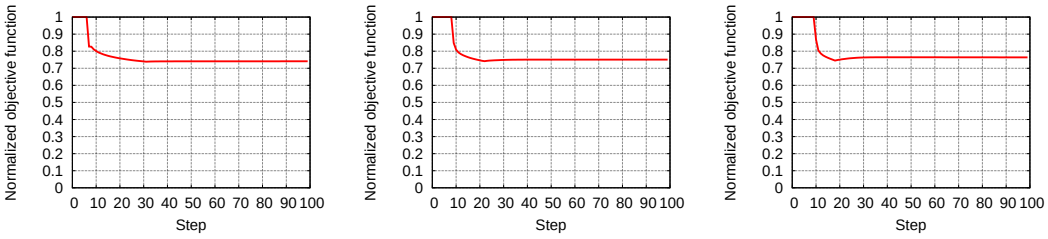

Figure 5.11: Comparison of the histories of the objective function values for example 2 with $\tau = 2.5 \times 10^{-1}$ (left), 5.0×10^{-1} (middle) and 7.5×10^{-1} (right)

5.4.2 Numerical Example 2

In last example, optimal configurations are obtained with temperature and heat transfer boundary. For generality, this example considers the optimization under heat flux and heat transfer boundary. This will further manifest the availability of

the proposed method under other boundary conditions.

In this example, the fixed design domain is set as 4.0m $\times$ 4.0m, whose thermal conductivity is $k = 1.0\,[\mathrm{W/(m{\cdot}K)}]$, as those of the previous examples, but heat flux boundary conditions on Γ_q and heat transfer boundary conditions on Γ_h are prescribed as shown in Figure 5.12. Γ_q is centred at each corresponding edge of the square domain and its length is set as $1.6\,[\mathrm{m}]$.

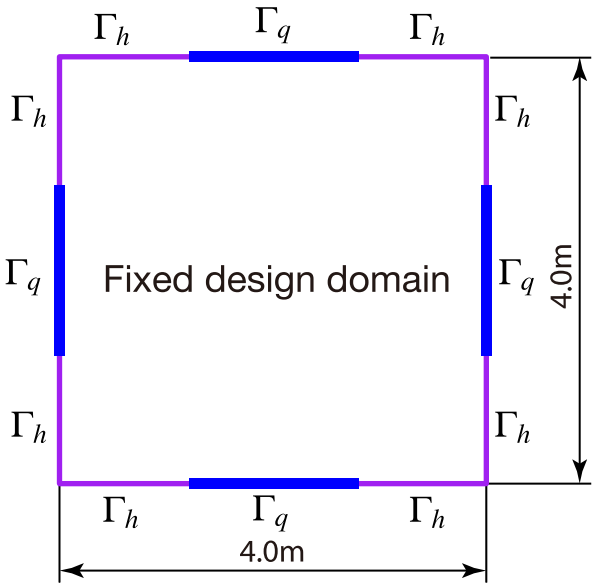

Figure 5.12: Fixed design domain for example 3

The heat flux on Γ_q is given as $\bar{q} = 100.0\,[\mathrm{W/m^2}]$, and on Γ_h the heat transfer coefficient and ambient temperature are given $h = 1.0\,[\mathrm{W/(m^2{\cdot}K)}]$ and $u_\infty = 80[\mathrm{K}]$, respectively. The heat conductivity and heat transfer coefficient are given as $k = 1.0\,[\mathrm{W/(m\cdot K)}]$.

The objective function assumed for this example is the same as that given by Eq. (5.38), but the target temperature is now assumed as $\bar{u} = 30[\mathrm{K}]$, and the area constraint $G_{\max}$ is set as 60% of the area of the fixed design domain. Also, $K = 10.0$ and $\Delta t = 0.8$ are used. The level set function whose values are calculated on a 40 40 mesh.

The initial, intermediate and optimum configurations of the result are shown

Figure 5.13 as for $\tau = 5.0 \times 10^{-1}$.

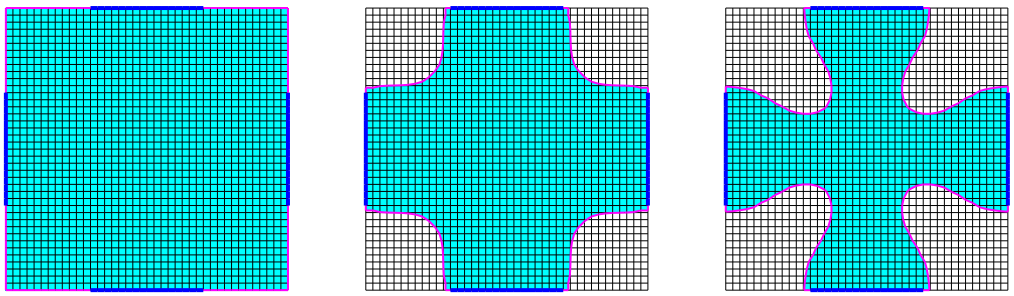

Figure 5.13: Initial (left), intermediate (middle) and optimal (right) configurations for example 3

In Figures 5.14 and 5.15 are shown the history of the normalized area and objective function. The area constraint is satisfied. It can be found that the objective function coverages to 20.0% where it's history curve becomes flat.

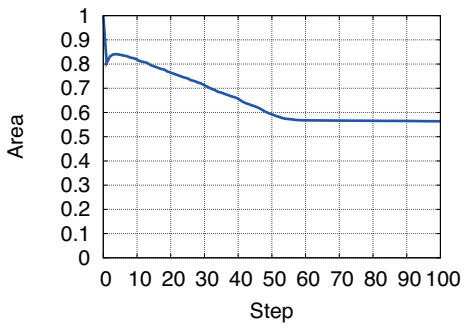

Figure 5.14: Area for example 3

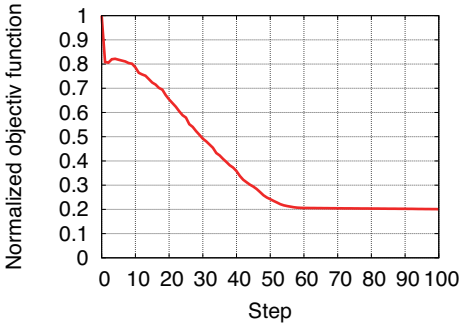

Figure 5.15: Normalized objective function for example 3

In Figure 5.16, the optimal configurations obtained for various regularization parameter values: $\tau = 1.0 \times 10^{-1}$, 5.0×10^{-1} and 10.0×10^{-1}, are compared. The various optimal configurations can satisfy more requirement for manufacture.

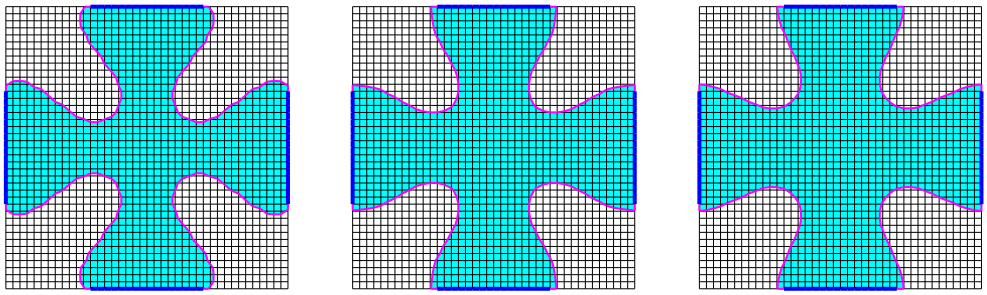

Figure 5.16: Various optimal results for the regularization parameters: $\tau = 1.0 \times 10^{-1}$ (left), 5.0×10^{-1}(middle) and 10.0×10^{-1} (right) for example 3

In Figure 5.17 are compared the profiles of the objective function for $\tau = 1.0 \times 10^{-1}$, 5.0×10^{-1}, and 10.0×10^{-1}. All the cases give almost 80% reduction of the initial value. The objective functions' value are almost the same, because their configurations are almost the same. This is different from the previous example, in which the objective functions are different with much difference in obtained configurations.

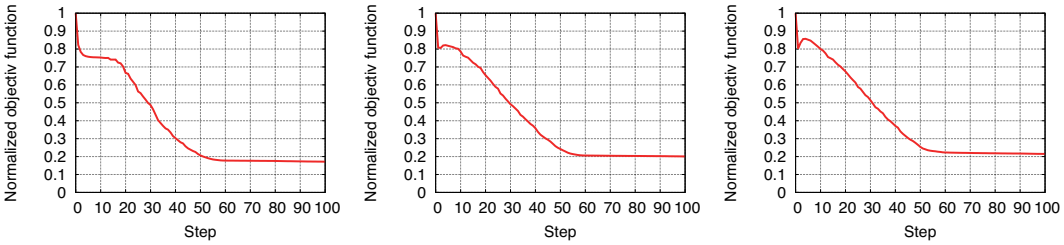

Figure 5.17: Comparison of the histories of the objective function values for example 3 with $\tau = 1.0 \times 10^{-1}$ (left), 5.0×10^{-1} (middle) and 10.0×10^{-1} (right) for example 3

5.5 Conclusions

This chapter presented a new level-set based topology optimization method for two-dimensional heat conduction problems using the boundary element method. Analytically the topological derivative (sensitivity) expression is derived for the heat

transfer boundary condition on the boundary corresponding to a topology change. The topological derivative expressions are verified through corresponding numerical examples. The same time, topology optimizations using the topological derivative has been built and applied in many numerical examples for various boundary conditions. It is emphasized that, with the present approach, the heat transfer boundary condition can be precisely considered without any approximation on the newly generated boundaries of the optimal shape of the material, because the exact expression of the topological derivative considering the heat transfer boundary condition is used and also the newly generated boundary is actually discretized and this boundary condition is given in the analysis.

Chapter 6

Topology Optimization with Objective Function Defined on Design-dependent Boundary with Heat Transfer Boundary Condition using BEM

6.1 Introduction

In last chapter, we presented a level set-based topology optimization under heat transfer boundary condition. It is proved effective through several numerical examples, in one of which the topological derivative or sensitivity derived combining with boundary element method is verified.

However, the morphing heat transfer boundaries are not included in the evaluation of objective function. Since the evaluation with newly generated heat transfer boundaries included can express the trend of the objective function as a whole, this chapter, on the basis of last chapter, presents a topology optimization method under heat transfer boundary condition with the newly generated boundaries included

in the estimation of objective function. Here the newly generated boundary evaluated in objective function is named as design-dependent boundary. The design-dependent boundary can be described that the boundary may changes but still evaluated in objective function as shown in Figure 6.1. Then we extended to the case that the objective function as of heat flux. For both cases, the topological derivative or sensitivity is different from the one derived in last chapter, since the definitions of the objective functions are changed. Also we verified each topological sensitivity expression though a numerical example, then applied to a few two dimensional topology optimization for heat conduction problems.

6.2 Topological derivatives

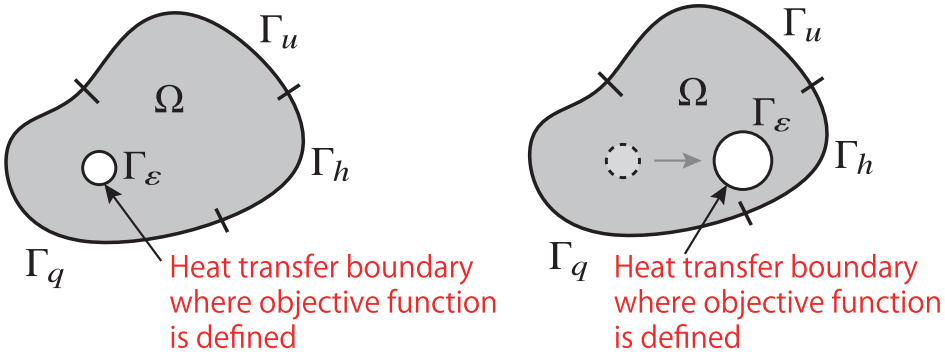

Figure 6.1: (left:) Configuration before a hole is created; (right:) Configuration after a hole is created

We consider a problem the same as the one in Chapter 2 with the newly generated boundary evaluated in objective function with heat transfer boundary condition. The augmented objective function J can be rewritten, after integrating by parts, as follows:

$$J = \int_\Gamma f \, d\Gamma + \int_\Omega \nabla\mu \cdot (-k\nabla u) \, d\Omega. \tag{6.1}$$

The objective function suffers from a change, denoted by δJ, when an infinites-

imal region Ω_ε is removed from Ω. After some manipulations, we obtain as

$$\begin{aligned}\delta J = &\int_{\Gamma_u}\left(\mu+\frac{\partial f}{\partial q}\right)\delta q\,d\Gamma - \int_{\Gamma_q}\left(\eta-\frac{\partial f}{\partial u}\right)\delta u\,d\Gamma \\ &- \int_{\Gamma_h}\left[\eta - h\left(\mu+\frac{1}{h}\frac{\partial f}{\partial u}+\frac{\partial f}{\partial q}\right)\right]\delta u\,d\Gamma \\ &+ \int_{\Gamma_\varepsilon}\left(f+\frac{\partial f}{\partial u}\delta u+\frac{\partial f}{\partial q}\delta q\right)d\Gamma - \int_{\Omega\setminus\Omega_\varepsilon}\left[\nabla\cdot(-k\nabla\mu)\right]\delta u\,d\Gamma \\ &- \int_{\Gamma_\varepsilon}\eta\,\delta u\,d\Gamma + \int_{\Gamma_\varepsilon}\mu(q+\delta q)\,d\Gamma + \int_{\Omega_\varepsilon}\nabla\mu\cdot(-k\nabla u)\,d\Omega, \end{aligned} \tag{6.2}$$

where

$$\eta = -k\frac{\partial\mu}{\partial n} = -k\nabla\mu\cdot\mathbf{n}, \tag{6.3}$$

It is assumed that the adjoint variable μ is the solution of the following boundary value problem:

$$\nabla\cdot(-k\nabla\mu) = 0 \qquad \text{in } \Omega, \tag{6.4}$$

$$\mu = -\frac{\partial f}{\partial q} \qquad \text{on } \Gamma_u, \tag{6.5}$$

$$\eta = \frac{\partial f}{\partial u} \qquad \text{on } \Gamma_q, \tag{6.6}$$

$$\eta = h\left(\mu+\frac{1}{h}\frac{\partial f}{\partial u}+\frac{\partial f}{\partial q}\right) \qquad \text{on } \Gamma_h. \tag{6.7}$$

In the following, the derivation is the same as that carried on in last chapter is omitted for simplicity. Here directly use the equation of δJ obtained in last chapter:

$$\begin{aligned}\delta J = &-\pi k\varepsilon^2\frac{k-\varepsilon h}{k+\varepsilon h}\nabla\mu^0\cdot\nabla u^0 + 2\pi\varepsilon\mu^0 h(u^0-u_\infty)\frac{k}{k-\varepsilon h\ln\varepsilon} \\ &+ \pi\varepsilon^3\frac{2kh}{k+\varepsilon h}\nabla\mu^0\cdot\nabla u^0 - \pi\varepsilon^2 k\nabla\mu^0\cdot\nabla u^0. \end{aligned} \tag{6.8}$$

Next, $f(u,q)$ is considered to be evaluated also on Γ_ε. Let the variation of J in

this case be written as δJ^*. Then, we have

$$\begin{aligned}
\delta J^* &= \delta J + \int_{\Gamma_\varepsilon} f(u,q)\, d\Gamma \\
&\approx 2\pi\varepsilon\mu^0 h(u^0-u_\infty) + \int_{\Gamma_\varepsilon} \left(f + \frac{\partial f}{\partial u}\delta u + \frac{\partial f}{\partial q}\delta q \right) d\Gamma \\
&= 2\pi\varepsilon\mu^0 h(u^0-u_\infty) + \varepsilon \int_0^{2\pi} f\, d\theta \\
&\quad + \varepsilon \int_0^{2\pi} \frac{\partial f}{\partial u} \left[\frac{h(u^0-u_\infty)\varepsilon\ln\varepsilon}{k-h\varepsilon\ln\varepsilon} + \frac{k-\varepsilon h}{k+\varepsilon h}(u^0_{,1}\cos\theta + u^0_{,2}\sin\theta) \right] d\theta \\
&\quad + \int_0^{2\pi} \frac{\partial f}{\partial q} \left[\frac{kh(u^0-u_\infty)}{k-h\varepsilon\ln\varepsilon} - \frac{k(k-\varepsilon h)}{k+\varepsilon h}(u^0_{,1}\cos\theta + u^0_{,2}\sin\theta) \right] d\theta. \qquad (6.9)
\end{aligned}$$

Therefore, the topological derivative becomes as

$$\begin{aligned}
\mathscr{T} &= \lim_{\varepsilon\to 0} \frac{\delta J^*}{2\pi\varepsilon} \\
&= \mu^0 h(u^0-u_\infty) + \lim_{\varepsilon\to 0} \frac{1}{2\pi} \int_0^{2\pi} f\, d\theta \\
&\quad + \lim_{\varepsilon\to 0} \frac{1}{2\pi} \int_0^{2\pi} \frac{\partial f}{\partial u} \left[\frac{h(u^0-u_\infty)\varepsilon\ln\varepsilon}{k-h\varepsilon\ln\varepsilon} + \frac{k-\varepsilon h}{k+\varepsilon h}(u^0_{,1}\cos\theta + u^0_{,2}\sin\theta) \right] d\theta \\
&\quad + \lim_{\varepsilon\to 0} \frac{1}{2\pi\varepsilon} \int_0^{2\pi} \frac{\partial f}{\partial q} \left[\frac{kh(u^0-u_\infty)}{k-h\varepsilon\ln\varepsilon} - \frac{k(k-\varepsilon h)}{k+\varepsilon h}(u^0_{,1}\cos\theta + u^0_{,2}\sin\theta) \right] d\theta \\
&= A + B + C + D, \qquad (6.10)
\end{aligned}$$

where

$$A = \mu^0 h(u^0-u_\infty) \qquad (6.11)$$

For the case that the objective function is defined as of temperature:

$$f = (u-\hat{u})^2 = \left[u^0 - \hat{u} + \varepsilon(u^0_{,1}\cos\theta + u^0_{,2}\sin\theta) \right]^2 \qquad \text{on } \Gamma_\varepsilon, \qquad (6.12)$$

where $\hat{u}$ is the target temperature. Then, we have

$$\frac{\partial f}{\partial u} = 2(u-\hat{u}) = 2\left[u^0 - \hat{u} + \varepsilon(u^0_{,1}\cos\theta + u^0_{,2}\sin\theta) \right] \qquad \text{on } \Gamma_\varepsilon \qquad (6.13)$$

$$\frac{\partial f}{\partial q} = 0 \qquad \text{on } \Gamma_\varepsilon \qquad (6.14)$$

and

$$B = \lim_{\varepsilon\to 0}\frac{1}{2\pi}\int_0^{2\pi} f\,d\theta = \lim_{\varepsilon\to 0}\frac{1}{2\pi}\int_0^{2\pi}\left[u^0-\hat{u}+\varepsilon(u^0_{,1}\cos\theta+u^0_{,2}\sin\theta)\right]^2 d\theta$$
$$= (u^0-\hat{u})^2 \tag{6.15}$$

$$C = \lim_{\varepsilon\to 0}\frac{1}{2\pi}\int_0^{2\pi}\frac{\partial f}{\partial u}\left[\frac{h(u^0-u_\infty)\varepsilon\ln\varepsilon}{k-h\varepsilon\ln\varepsilon}+\frac{k-\varepsilon h}{k+\varepsilon h}(u^0_{,1}\cos\theta+u^0_{,2}\sin\theta)\right]d\theta = 0 \tag{6.16}$$

$$D = \lim_{\varepsilon\to 0}\frac{1}{2\pi\varepsilon}\int_0^{2\pi}\frac{\partial f}{\partial q}\left[\frac{kh(u^0-u_\infty)}{k-h\varepsilon\ln\varepsilon}-\frac{k(k-\varepsilon h)}{k+\varepsilon h}(u^0_{,1}\cos\theta+u^0_{,2}\sin\theta)\right] = 0\,d\theta \tag{6.17}$$

Therefore, we obtain the following derivative (sensitivity) [138, 139]:

$$\boxed{\mathscr{T}^* = \mu^0 h(u^0-u_\infty)+(u^0-\hat{u})^2} \tag{6.18}$$

Note: * is added to $\mathscr{T}$ to mark the topological derivative is obtained with objective function of temperature defined on design-dependent boundary with heat transfer boundary condition. It is used for distinguishing with the topological derivatives obtained in other places.

For the case that the objective function is defined as of heat flux:

$$f = (q-\hat{q})^2 = \left[k(u^0_{,1}\cos\theta+u^0_{,2}\sin\theta)-\hat{q}\right]^2$$
$$= k^2\left[(u^0_{,1})^2\cos^2\theta+(u^0_{,2})^2\sin^2\theta\right]+\hat{q}^2$$
$$+2k^2u^0_{,1}u^0_{,2}\cos\theta\sin\theta-2k\hat{q}(u^0_{,1}\cos\theta+u^0_{,2}\sin\theta)\quad\text{on }\Gamma_\varepsilon. \tag{6.19}$$

$$\frac{\partial f}{\partial u} = 0\quad\text{on }\Gamma_\varepsilon. \tag{6.20}$$

$$\frac{\partial f}{\partial q} = 2(q-\hat{q}) = 2\left[k(u^0_{,1}\cos\theta+u^0_{,2}\sin\theta)-\hat{q}\right]\quad\text{on }\Gamma_\varepsilon. \tag{6.21}$$

Therefore, we have

$$B = \lim_{\varepsilon\to 0}\frac{1}{2\pi}\int_0^{2\pi} f\,d\theta\ = \lim_{\varepsilon\to 0}\frac{1}{2\pi}\int_0^{2\pi}\left\{k^2\left[(u^0_{,1})^2\cos^2\theta+(u^0_{,2})^2\sin^2\theta\right]+\hat{q}^2\right\}d\theta$$
$$= k^2\left|\nabla u^0\right|^2+\hat{q}^2. \tag{6.22}$$

and

$$C = \lim_{\varepsilon \to 0} \frac{1}{2\pi} \int_0^{2\pi} \frac{\partial f}{\partial u} \left[\frac{h(u^0 - u_\infty)\varepsilon \ln \varepsilon}{k - h\varepsilon \ln \varepsilon} + \frac{k - \varepsilon h}{k + \varepsilon h} (u^0_{,1} \cos\theta + u^0_{,2} \sin\theta) \right] d\theta = 0. \tag{6.23}$$

Also, using Eq. (6.21), D can be obtained as:

$$\begin{aligned} D &= \lim_{\varepsilon \to 0} \frac{1}{2\pi} \int_0^{2\pi} \frac{\partial f}{\partial q} \left[h(u^0 - u_\infty) - k(u^0_{,1} \cos\theta + u^0_{,2} \sin\theta) \right] d\theta \\ &= -2\hat{q}h(u^0 - u_\infty) - k^2 \left| \nabla u^0 \right|^2. \end{aligned} \tag{6.24}$$

Then the topological derivative with objective function defeined as of heat flux [141] is obtained as:

$$\boxed{\mathscr{T}^\star = h(u^0 - u_\infty)(\mu^0 - 2\hat{q}) + \hat{q}^2.} \tag{6.25}$$

Note: * is added to $\mathscr{T}$ to mark the topological derivative is obtained with objective function of heat flux defined on design-dependent boundary with heat transfer boundary condition. It is used for distinguishing with the topological derivatives obtained in other places.

6.3 Numerical examples for verifying the topological derivatives

6.3.1 Numerical Example 1

This example is used to verify the correctness of the derived topological derivative of heat conduction problems with objective function of temperature defined on design-dependent boundary with heat transfer boundary condition in Eq. (6.18).

Let us consider a design domain initially filled with the material entirely in the area of $4.0\,[\mathrm{m}] \times 4.0\,[\mathrm{m}]$ as shown in Figure 6.2. Temperature boundary condition is given for the left and top edges of the design domain, with prescribed temperature $\bar{u} = 50[\mathrm{K}]$, while heat flux boundary condition is given for the bottom and

right edges with prescribed heat flux $\bar{q} = 50\,[\mathrm{W/m^2}]$. The thermal conductivity of the domain is assumed as $k = 1.0\,[\mathrm{W/(m{\cdot}K)}]$. We compare the topological derivative value calculated by Eq. (6.18) with the approximate one calculated by a finite difference of the values of objective function for the original domain and the domain from which a small circular hole is removed. Heat transfer boundary condition with the ambient temperature $u_\infty = 45[\mathrm{K}]$ and the heat transfer coefficient $h = 0.001\,[\mathrm{W/(m^2{\cdot}K)}]$ is considered on the circular hole.

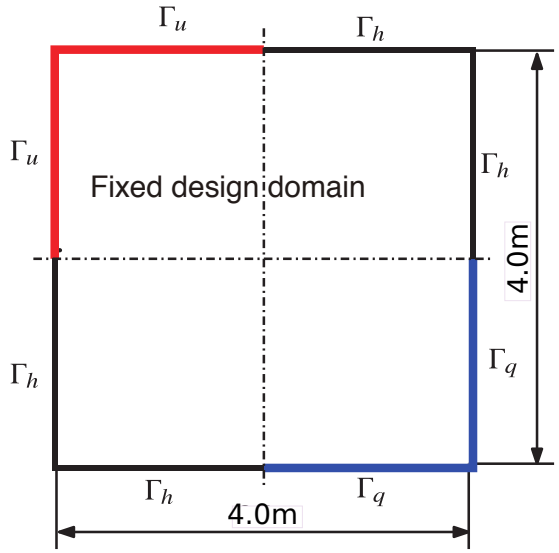

Figure 6.2: Fixed design domain for example 1

The objective function for this example is defined as

$$F = \int_{\Gamma_h \cup \Gamma_\varepsilon} (u - \hat{u})^2 \, d\Gamma, \tag{6.26}$$

where $\hat{u} = 15[\mathrm{K}]$ is the target temperature.

The boundary of the square domain is discretized with 40×40 uniformly with quadratic continuous elements. Also, 40×40 grids are generated in the fixed design domain, the topological derivative values are calculated at the sample internal grid points shown in Figure 6.3. The approximate values of the topological derivative is calculated by the following formula:

$$F'_{\mathrm{approx}} = \frac{F_{\mathrm{original}} - F_{\mathrm{hole}}}{2\pi\varepsilon}, \tag{6.27}$$

where, F_{original} and F_{hole} denote the values of the objective function before and after the hole is created. $\varepsilon = 0.0001\,[\text{m}]$ is the radius of the hole, and the boundary of the hole is divided into 32 quadratic elements when F_{hole} is calculated using the boundary element method. As shown in Figure 6.4, the topological derivative values obtained using the proposed approach are in very good agreement with those obtained with the finite difference formula, of which the maximum error is less than 1%, thus the present formula of the topological derivative is verified.

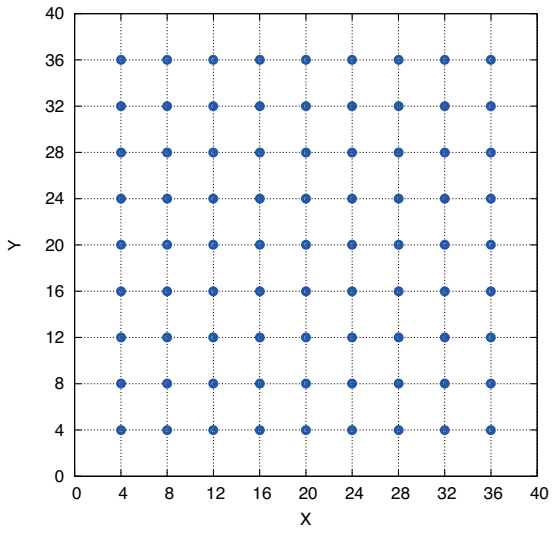

Figure 6.3: Sample points for verifying the topological derivative

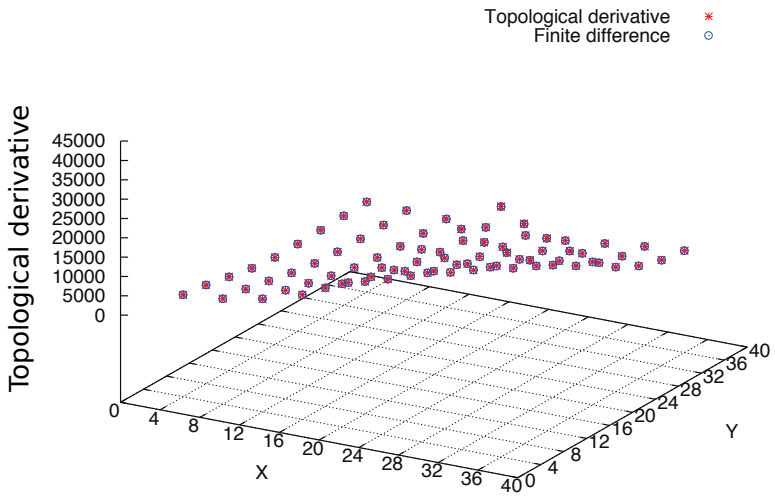

Figure 6.4: Comparison of the topological derivatives obtained by the proposed approach with the one by the finite difference

6.3.2 Numerical Example 2

This example is used to verify the correctness of the derived topological derivative of heat conduction problems with objective function of heat flux defined on design-dependent boundary with heat transfer boundary condition in Eq. (6.25).

The topological derivative (sensitivity) given by Eq. (6.25) is verified by comparing with the one obtained by finite difference method.

We consider a fixed design domain initially filled with material entirely in the region of $2.0\,[\mathrm{m}] \times 2.0\,[\mathrm{m}]$ as shown in Figure 6.5. Temperature boundary condition is given for the boundaries of the top-left and bottom-right corners of the design domain with a prescribed temperature $\bar{u} = 60\,[\mathrm{K}]$, the heat transfer boundary condition is given on boundaries of the top-right and bottom-left corners as well as the newly generated ones, with the ambient temperature $u_\infty = 40\,[\mathrm{K}]$ and the heat transfer coefficient $h = 0.002\,[\mathrm{W/(m^2{\cdot}K)}]$. The thermal conductivity of the domain is assumed as $k = 1.0\,[\mathrm{W/(m{\cdot}K)}]$.

We compare the topological derivative values calculated by Eq. (6.25) with the approximate values calculated by finite difference of the values of the objective

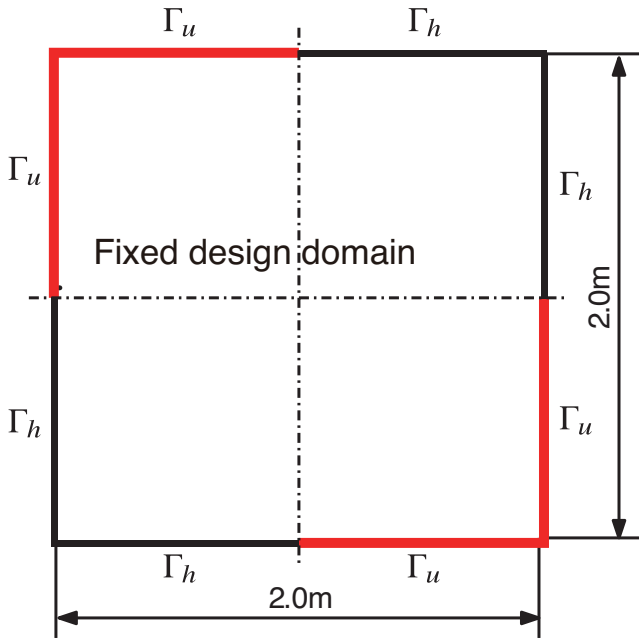

Figure 6.5: Fixed design domain used to verify the topological derivative expression.

functions both for the original domain and the domain from which a small circular hole is actually deleted.

The objective function is defined as

$$F = \int_{\Gamma_h \cup \Gamma\varepsilon} (q - \hat{q})^2 \, d\Gamma, \tag{6.28}$$

where $\Gamma\varepsilon$ denotes the boundary of the deleted area and $\hat{q} = 15.0\,[\mathrm{W/(m^2 \cdot K)}]$ is the target heat flux.

The boundary of the square domain is discretized uniformly with $40 \times 4 = 160$ quadratic conforming elements. Also, $40 \times 40 = 1600$ grids are generated in the fixed design domain. The topological derivative values are calculated at the two rows of internal grid points shown in Figure 6.6.

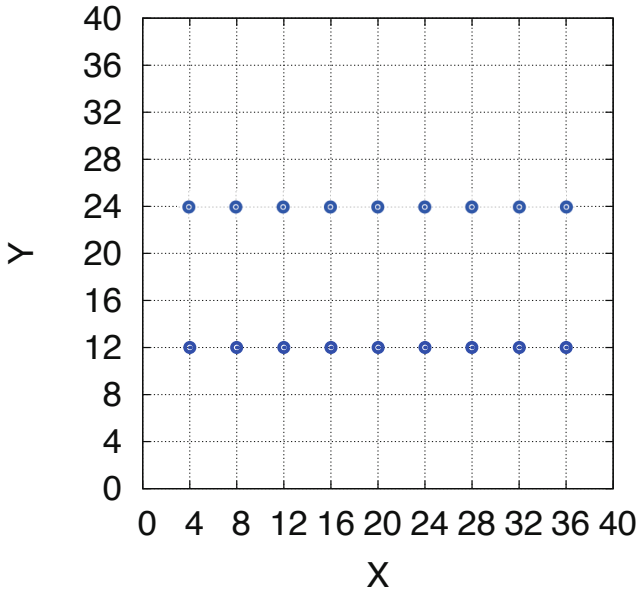

Figure 6.6: Sample points for verifying the topological derivative expression.

The approximate values of the topological derivative is calculated by the following formula:

$$F'_{\text{approx}} = \frac{F_{\text{original}} - F_{\text{hole}}}{2\pi\varepsilon^*}, \tag{6.29}$$

where F_{original} and F_{hole} denote the values of the objective function before and after the hole is created. $\varepsilon^* = 0.0001\,[\text{m}]$ is the radius of the hole, and the boundary of the hole is divided into 32 quadratic elements when F_{hole} is calculated using the boundary element method. The topological derivative obtained using the expression in Eq. (6.25) and those obtained by the finite difference method at the sample points of $Y = 12$ and $Y = 24$ are plotted as Figure 6.7 and Figure 6.8, individually. From these two figures we can find that the topological sensitivity values obtained using the proposed approach are in very good agreement with those obtained with the finite difference formula, thus the present formula of the topological derivative is verified.

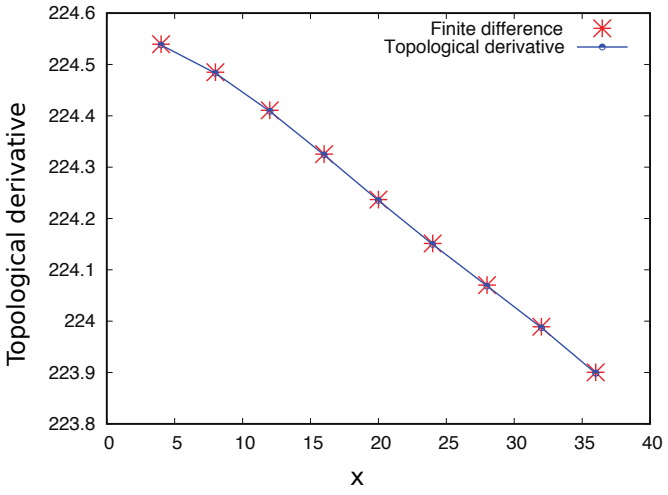

Figure 6.7: Comparison of the topological derivatives obtained by its present explicit expression with those obtained by the finite difference scheme at the sample points of $Y = 12$.

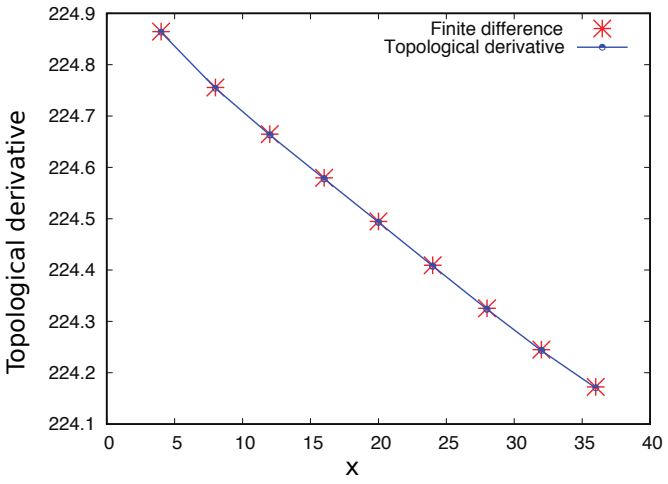

Figure 6.8: Comparison of the topological derivatives obtained by its present explicit expression with those obtained by the finite difference scheme at the sample points of $Y = 24$.

6.4 Numerical examples for the topological optimizations

6.4.1 Numerical Example 1

In this example a topology optimization based on the present topological derivative is presented in Eq. (6.18).. We consider a fixed design domain of $4.0\,[\mathrm{m}] \times 4.0\,[\mathrm{m}]$. The thermal conductivity of the domain is $k = 1.0\,[\mathrm{W/(m{\cdot}K)}]$. This can be realised by setting the level set function as 1 in the fixed design domain. The boundary condition is set as shown in Figure 6.9. Each edge of the square has a temperature prescribed boundary Γ_u of length $0.8\,[\mathrm{m}]$ and the rest of the boundaries are the heat transfer boundaries. The temperature is given as $\bar{u} = 100[\mathrm{K}]$ on Γ_u and the heat transfer coefficient and the ambient temperature on the heat transfer boundaries are set as $h = 1.0\,[\mathrm{W/(m^2{\cdot}K)}]$ and $u_\infty = 0[\mathrm{K}]$, respectively. These boundaries are set as non-design boundaries which does not move in the optimisation process.

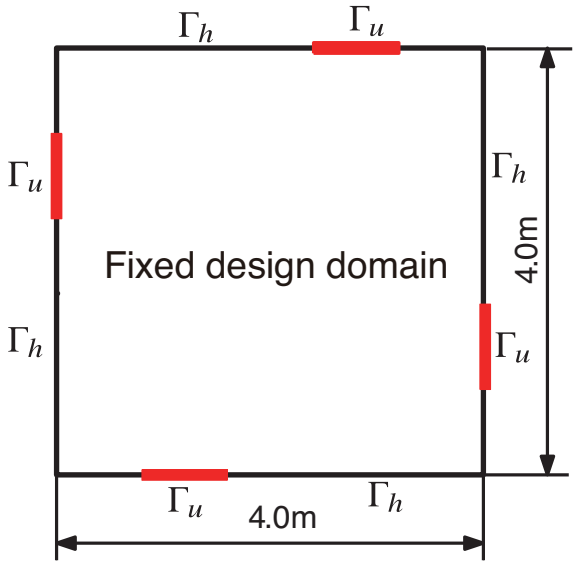

Figure 6.9: Fixed design domain for example 2

The objective function for this example is defined as

$$F = \int_{\Gamma_h \bigcup \Gamma_\varepsilon} (u - \hat{u})^2 \, d\Gamma, \tag{6.30}$$

where $\hat{u}$ is the target temperature prescribed as $\hat{u} = 10$[K]. In this example, we explore the number and the shape of holes inside the fixed design domain which minimise the objective function 6.30. We assume that the boundary condition on the holes is given as the heat transfer one with the same h and u_∞ as ones on Γ_h (Figure 6.9). The area constraint $G_{\max}$ is set to be 80% of the fixed design domain. The regularization parameter is set as $\tau = 5.0 \times 10^{-1}$. The proportional coefficient and the fictitious time interval are given as $K = 10.0$ and $\Delta t = 0.2$, respectively. The boundary element for the computations of the topological derivative are generated automatically at every step of the optimisation by searching iso-surface of zero-value of the level set function.

Figure 6.10 shows the history of the objective function and the area fraction of the material. One observes that the value of the objective function does not change during the first several steps. This is because no holes appear during these steps. The distribution of the level set function is, however, changing during these steps. Once the holes are created, the value of the objective function decreased sharply. One also observes a sharp increase of the objective function at 6th step of the optimization, which is caused by the area constraint. The objective function starts to decrease shortly before the area constraint is satisfied. The value of the objective function finally converges to 78.1897% of its initial value and the area fraction filled with materials is lower than its prescribed value ($G_{\max}$ =80% of the initial value). Figure 6.10 shows that the convergence of the objective function is slow after the 40th step. The convergence can be improved by adjusting the parameters: the parameter K in the reaction diffusion equation and the time increment Δt. The parameters are, for now, determined by numerical experiments. We may address, in our future publications, an efficient criteria for the parameters.

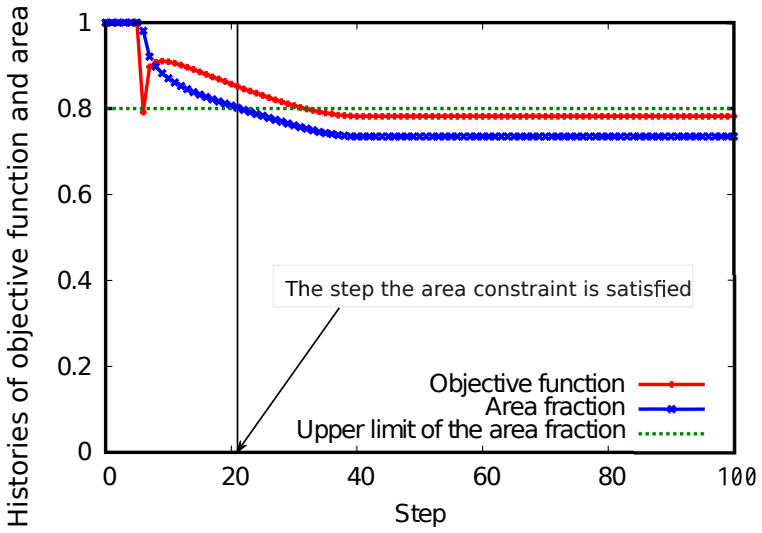

Figure 6.10: History of the objective function (normalized by the initial value) and the area fraction.

Figure 6.11 shows material configurations at some steps of the optimization. 4 holes are created at the 6 steps and the holes become larger step by step. The holes are considered to work as heat absorbers since the boundary condition on the holes are set as the heat transfer one, which can also be confirmed by the fact that the heat flux vectors cross the holes (Figures 6.12).

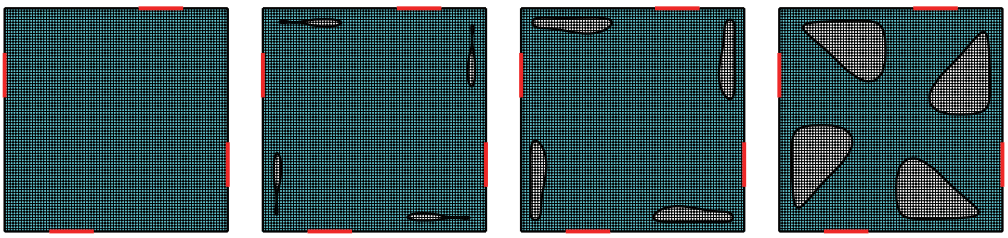

Figure 6.11: Material configurations at steps 0, 6, 7 and 100.

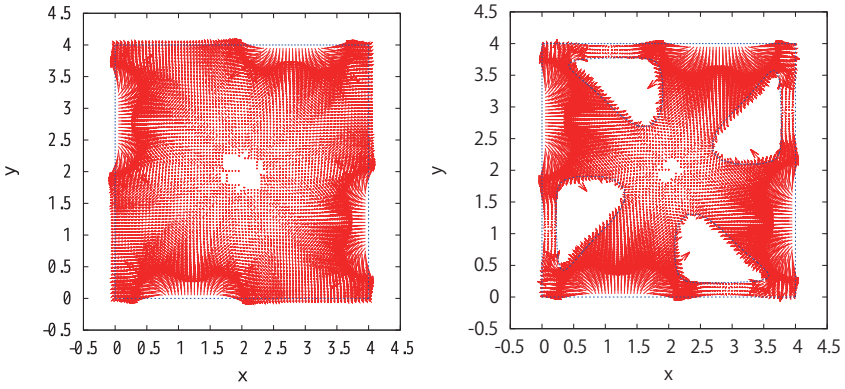

Figure 6.12: Heat flux for (left:) the initial configuration and (right:) the optimized configuration.

Figure 6.13 shows temperature distributions at some steps of the optimization. Since the objective function is defined also on the hole boundaries, the temperature in the entire domain is decreased to near the target temperature $\hat{u}$.

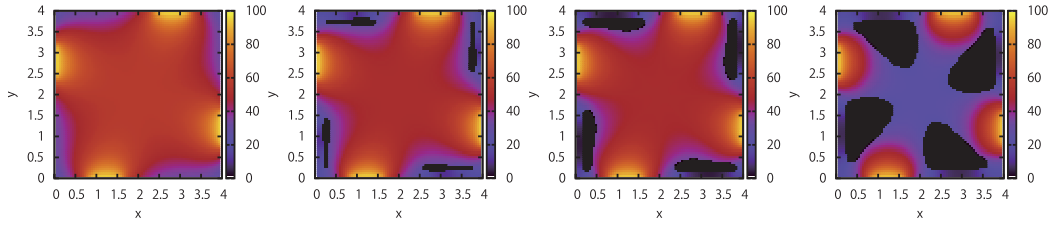

Figure 6.13: Temperature distributions at steps 0, 6, 7 and 100.

Let us discuss now the effect of the regularization parameter τ to the optimal configurations. In Figure 6.14, the optimal configurations obtained with different values of the regularization parameter, $\tau = 7.5 \times 10^{-2}$, 1.25×10^{-1}, 2.5×10^{-1} and 1.0 are shown.

As the regularization parameter increases, the boundary of the holes become smooth. Thus, the regularization parameter can be set according to the manufacturing requirement. Also, the holes are allocated near the boundary of the fixed design domain when the regularization parameter is small, which is caused by the boundary condition for the level set function. Note that in the limit of $\tau \to \infty$, the optimal distribution of the level set function is equal to a constant in the whole fixed design

domain. Since the Dirichlet boundary condition $\phi = 1$ is given on the non-design boundary, the constant will be 1, which gives no hole in the fixed design domain. In the case of $\tau \to 0$, the optimal distribution of the level set function depends only on the topological derivative and the penalty term for the volume constraint λ. Since the topological derivative is known to be smooth for thermal problems and $\lambda = \text{const.}$ is used in this study, it is reasonable for the optimal configurations to have smooth boundaries even in the case of $\tau \to 0$. We have confirmed that the numerical test with $\tau = 1.0 \times 10^{-12}$ gives almost the same configuration as the one obtained by the test with $\tau = 7.5 \times 10^{-2}$. The choice of the regularization parameter value, of course, affects the minimized value of the objective function $F_{\min}$, which is summarized in Table 6.1. In this example, a smaller τ gives smaller objective function, which is not consistent with our previous result [137]. This is, however, reasonable since the smaller τ gives holes with more complexed boundary, which results in a large perimeter of the holes. Indeed, the objective function normalized by the perimeter of holes seems to be comparable regardless of the choice of τ. Also, readers may find that the minimum value of the objective function F_min is great than 1.0. This is because with the generation of holes, the evaluated length of boundary increased. This can be normalized by the length of the boundary.

Note that, strictly speaking, $F_{\min} / \int_{\Gamma_h} d\Gamma$ is not minimized in this case because the length of boundary is not considered in the topological derivatives at the beginning. Minimization of the normalized objective function $F_{\min} / \int_{\Gamma_h} d\Gamma$ can be achieved using the modified topological derivative $\mathscr{T}_{\text{mod.}}$ as follows:

$$\mathscr{T}_{\text{mod.}} = \left(\frac{F}{\int_{\Gamma_h} d\Gamma} \right)' = \frac{\mathscr{T}}{\int_{\Gamma_h} d\Gamma} - \frac{F}{\left(\int_{\Gamma_h} d\Gamma \right)^2}. \tag{6.31}$$

Numerical examples with Eq. (6.31) will be addressed in our future publications. Certainly, the use of $F_{\min} / \int_{\Gamma_h} d\Gamma$ here is enough to examine the history of objective function.

Let us consider now the case that the ambient temperature outside the fixed design domain is higher than that in the holes. We here consider the same settings

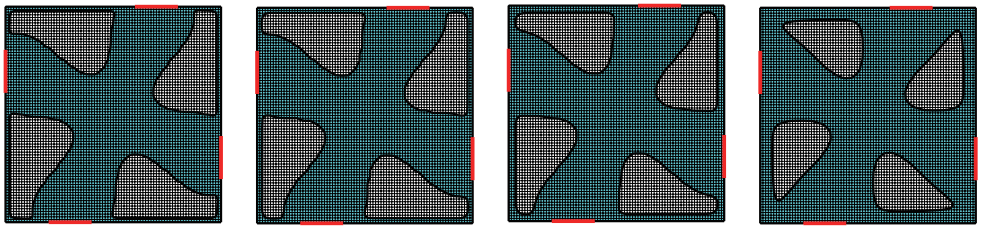

Figure 6.14: Various optimal configurations for the regularization parameters: $\tau = 7.5 \times 10^{-2}$, $\tau = 1.25 \times 10^{-1}$, $\tau = 2.5 \times 10^{-1}$ and $\tau = 1.0$.

Table 6.1: The minimum values of the objective functions for different regularization parameters τ.

τ	min. value of the objective func $F_{\min}$.	$F_{\min} / \int_{\Gamma_h} d\Gamma$
7.5×10^{-2}	104.765 %	48.8%
1.25×10^{-1}	100.688 %	46.9%
2.5×10^{-1}	94.7702 %	44.8%
1.0	78.1897 %	37.1%

as the previous one except that the ambient temperature outside the fixed design domain Γ_h is increased to 30[K].

Figure 6.15 shows the history of the material configurations at the optimization steps 5, 27, 29 and 100. Comparing these results with the ones in Figure 6.11, one finds that the cavities are connected each other and the perimeter of the cavity becomes larger. This is reasonable since the cavity is more capable to relieve heat than the boundary of the fixed design domain. This can also be confirmed from Figure 6.16 where the heat flux for the optimized configuration in this settings.

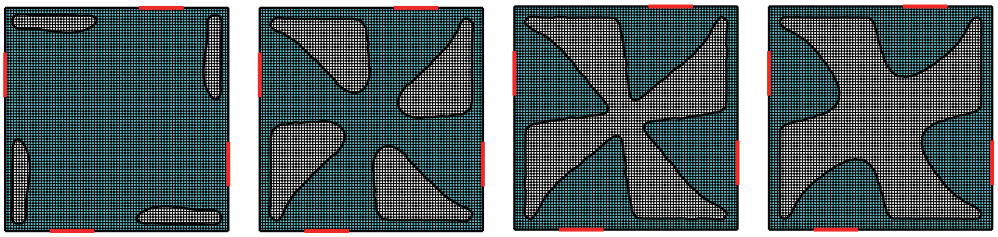

Figure 6.15: Material configurations at steps 5, 27, 29 and 100 in the case that the ambient temperature outside the fixed design domain is higher than that inside the "hole".

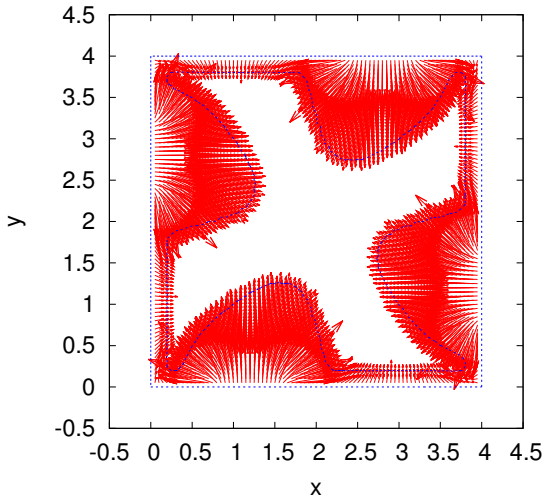

Figure 6.16: Heat flux for the optimized configuration for the case that the ambient temperature outside the fixed design domain is higher than that inside the cavity.

The objective function normalized by its initial value in this case is shown in Figure 6.18. Readers may find that the objective function dropped sharply at the fist several steps. It is because large area is removed. Also, at step 29, it reached the lowermost value, but its area is not satisfied. Thus, the optimization continued and last converged with area 52% shown in Figure 6.17 being satisfied. Figure 6.19 shows the temperature fields for this case. One can confirm that the temperature around the boundary of the cavity is reduced to the target temperature $\hat{u} = 20$[K].

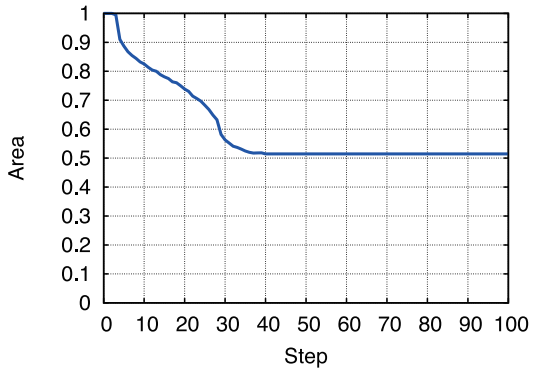

Figure 6.17: Area percentage for topology optimization example

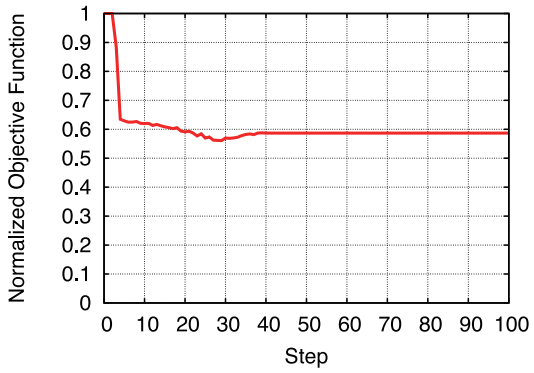

Figure 6.18: Normalised objective function for topology optimization example.

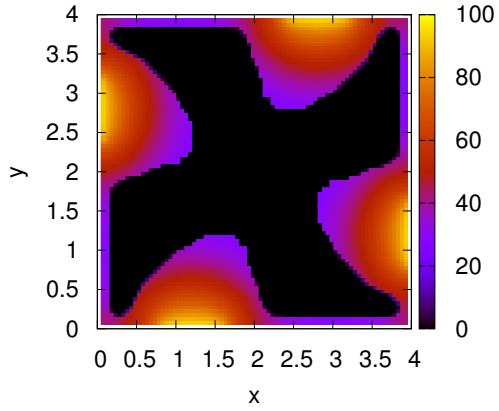

Figure 6.19: Temperature distribution for the optimized configuration for the case that the ambient temperature outside the fixed design domain is higher than that inside the cavity.

Thus, the proposed method can also deal with the the case that ambient temperature in the hole is different from that outside the fixed design domain.

6.4.2 Numerical Example 2

In this example we consider a topology optimization using the derived topological sensitivity as presented in Eq. (6.25). The fixed design domain is a material-filled square region of $2.0\,[\mathrm{m}] \times 2.0\,[\mathrm{m}]$ shown as Figure 6.20. The thermal conductivity is $k = 1.0\,[\mathrm{W/(m{\cdot}K)}]$.

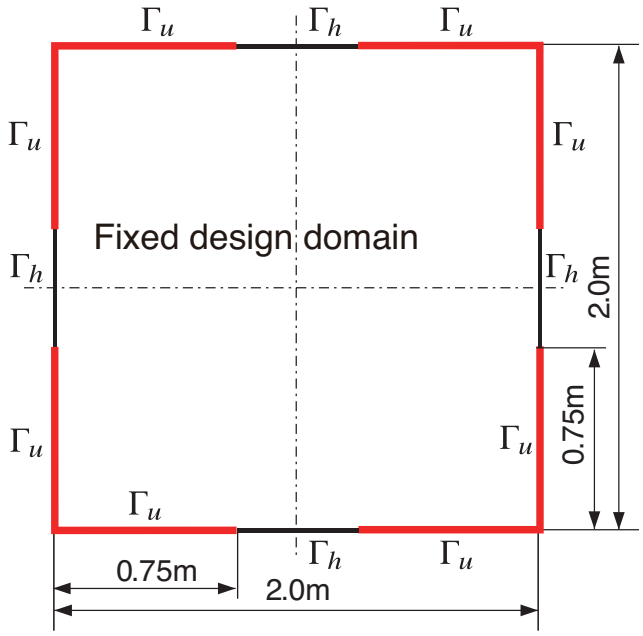

Figure 6.20: Fixed design domain for topology optimization example.

Temperature boundary condition is given for the boundaries of four corners of the fixed design domain with the same prescribed temperature $\bar{u} = 50\,[\mathrm{K}]$. The heat transfer boundary condition is given on the middle part of each edge of the design domain and the newly generated ones in optimization process, with the ambient temperature $u_\infty = 45\,[\mathrm{K}]$ and the heat transfer coefficient $h = 5.0\,[\mathrm{W/(m^2{\cdot}K)}]$.

This example concerns an objective function defined as

$$F = \int_{\Gamma_{all}} (q - \hat{q})^2 \, d\Gamma, \tag{6.32}$$

where Γ_{all} denotes all the boundary of the design domain and the target heat flux is given as $\hat{q} = 5.0\,[\mathrm{W/(m^2 \cdot K)}]$.

The boundary of the square domain is discretized uniformly with $40 \times 4 = 160$ quadratic conforming elements. the area constraint $G_{\max}$ is set as 80% of the area of the fixed design domain. Also, $K = 10$ and $\Delta t = 0.22$ are used. The regularization term is set as $\tau = 5.0 \times 10^{-1}$.

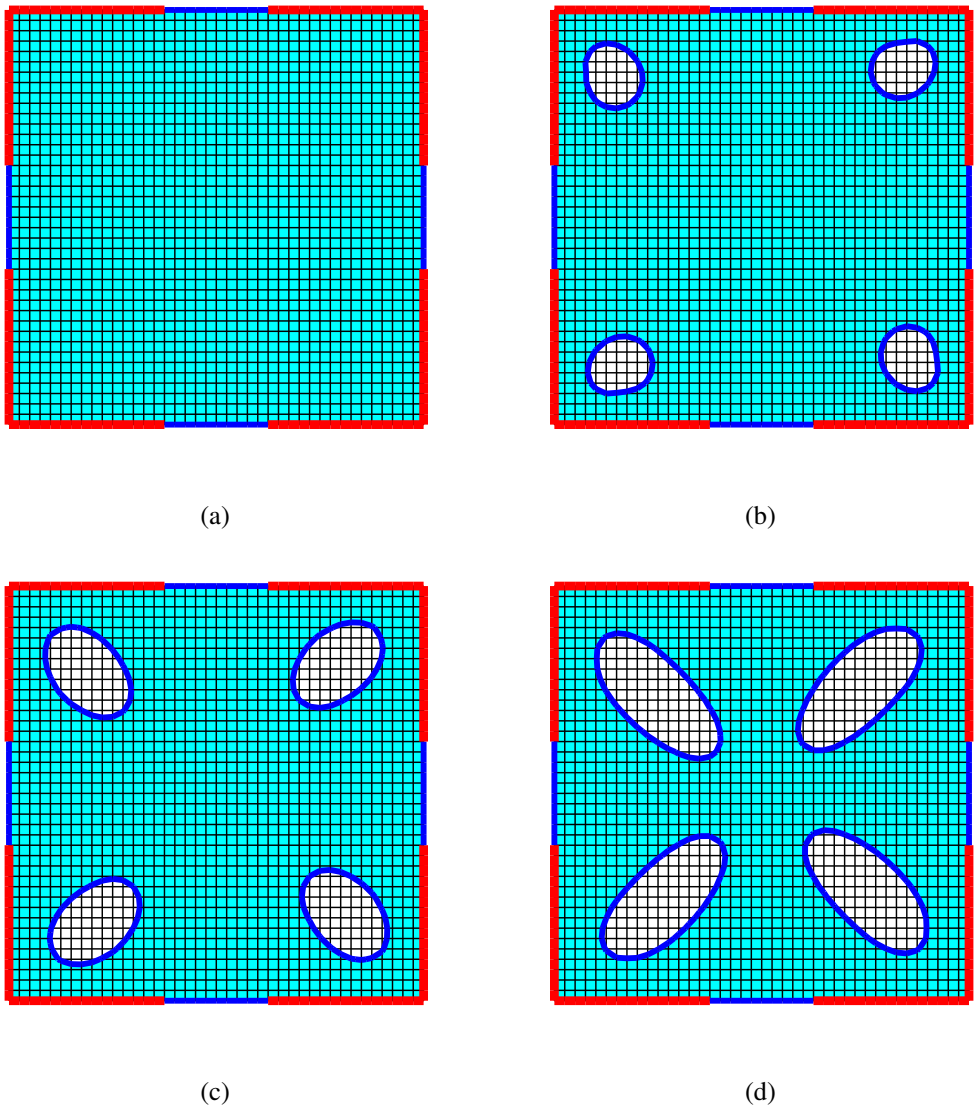

(a) (b)

(c) (d)

Figure 6.21: The obtained configurations: (a) Initial configuration, (b) Configuration at step 20, (c) Configuration at step 40, (d) Optimal configuration

The initial configuration, intermediate configurations and optimal configuration are obtained and shown in Figure 6.21. We can find that the material on the corners are removed and new boundaries are generated, later the boundaries are generated more closer to the center of the fixed design domain. This indicates the heat flux gets closer to the target heat flux in unit length. We show in Figure 6.23 the history of the objective function normalize by the length of the defined boundaries to find the value when the optimal configuration is obtained, as well as in Figure 6.22 the history of the area to check if it is less than the area constraint.

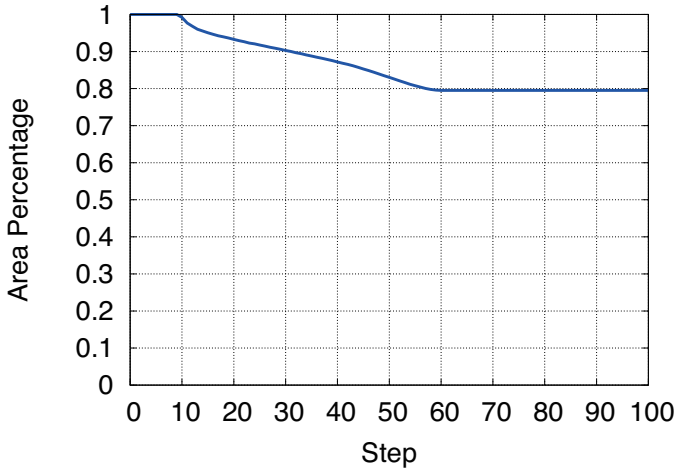

Figure 6.22: Area percentage for topology optimization example

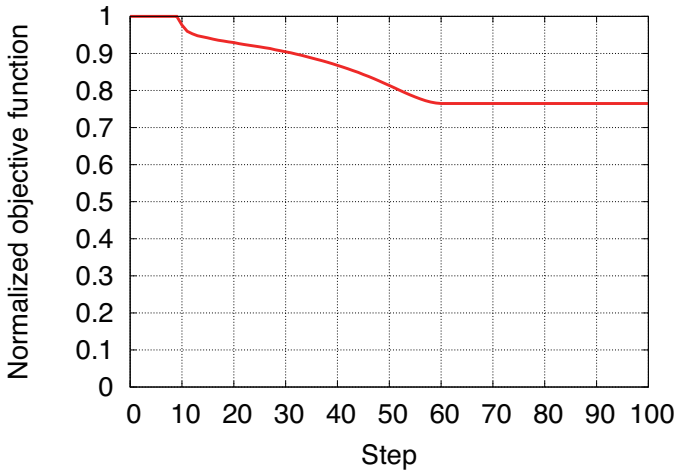

Figure 6.23: Normalised objective function for topology optimization example.

The area constraint is satisfied shown in Figure 6.22. And corresponding normalized objective function finally converged to 76.5% of its initial value shown in Figure 6.23.

6.5 Conclusions

In this chapter, we presented a new level set-based topology optimization method for two-dimensional heat conduction problems using the boundary element method. Analytically the topological derivative (sensitivity) expressions are derived under the heat transfer boundary condition for the objective function as of temperature and the objective function as of heat flux, both with the morphing boundary estimated. Both topological derivative (sensitivity) expressions are verified through corresponding numerical examples. The correctness of the derived topological derivative (sensitivity) expressions are demonstrated by calculating those values at the internal points in comparison with those obtained by finite difference scheme. The same time, topology optimizations using the topological sensitivities have been built and applied in many numerical examples for various boundary conditions and objective functions. It is emphasized that, with the present approach, the morphing heat transfer boundary can be considered in the estimation of objective functions.

Chapter 7

Conclusions

This dissertation proposed a level set-based topology optimization for two dimensional heat conduction problems using boundary element method. Basically, three topological derivatives (sensitivities) are newly derived for heat conduction problems with topology of insulating boundary and heat transfer boundary. The achievement are listed as follows:

1. Topological sensitivity for the topology of insulating boundary combining with boundary element method in two-dimensional heat problems is derived. The topological sensitivity expression has been verified and the level set-based topology optimization using this topological sensitivity has been proposed and applied to some numerical examples, through which it has been proved an effective method. Besides, the proposed method is not a mesh-dependent method and initial configuration does not influence the optimal configuration.

2. Topological derivative (sensitivity) for the topology of heat transfer boundary combing with boundary element method in two-dimensional heat problems is derived. The topological sensitivity has been proved correct by comparing with the values obtained by finite difference method. The topology optimization with this topological sensitivity has been built and applied to a few numerical examples. Topology optimization for two-dimensional heat

problems with various boundary condition and values are implemented and various optimal configurations are obtained. Beside, various configurations are obtained for different regularization parameter values, by which, the role of regularization parameter has been tested.

3. Topological sensitivities for the topology of heat transfer boundary with the morphing boundaries of topology defined in the objective function of temperature and the objective function of heat flux are derived. The morphing boundaries are included in the definition as the newly generated boundaries can be also evaluated as a whole. The topological sensitivities have also been verified through the comparison with the ones obtained using finite difference scheme. The topology optimization with two sensitivities individually has been built and a few numerical results are obtained and the diverse optimal configurations are obtained with different regularization parameter values.

In conclusion, the level set-based topology optimization for two-dimensional heat problems using boundary element method for topology under insulating boundary, heat transfer boundary, as well as morphing boundary considered in the objective function of temperature and the objective function of heat flux, are proposed and proved available. This proposed method avoided the checkerboard and intermediate density problem and the zigzag boundaries when using finite element method. Moreover, This method can obtain various configurations by adjusting the regularization term. Consequently, This method will definitely help in structural design of heat conduction devices. However, it is limited to two-dimensional case. Thus, we suggeste extend the topology optimization to three-dimensional case. Nevertheless, as the topology optimization using boundary element has an advantage of easily handling the mesh comparing with using finite element method, it is suggested not just for heat conduction problems, but also for other physical problems, such as mechanics, acoustics and some multiphysical problems. Moreover, it is especially adoptable for the objective function defined on boundaries, since boundary element method is boundary-treatment method.

Bibliography

[1] W. Prager, A note on discretized Michell structures, Computer Methods in Applied Mechanics and Engineering 3.3 (1974): 349-355.

[2] W. Achtziger, Multiple-load truss topology and sizing optimization: some properties of minimax compliance, Journal of Optimization Theory and Applications 98.2 (1998): 255-280.

[3] T. Amago, Sizing optimization using response surface method in FOA, R&D Review of Toyota CRDL 37.1 (2002): 1-7.

[4] A. Kaabeche, M. Belhamel, and R. Ibtiouen, Sizing optimization of grid-independent hybrid photovoltaic/wind power generation system, Energy 36.2 (2011): 1214-1222.

[5] J. Lagorse, D. Paire, and A. Miraoui, Sizing optimization of a stand-alone street lighting system powered by a hybrid system using fuel cell, PV and battery, Renewable Energy 34.3 (2009): 683-691.

[6] Y. Ding, Shape optimization of structures: a literature survey, Computers & Structures 24.6 (1986): 985-1004.

[7] O. C. Zienkiewicz, and J. S. Campbell, Shape optimization and sequential linear programming, Optimum structural design (1973): 109-126.

[8] J. Sokolowski, and J.P. Zolésio, Introduction to shape optimization, Springer Berlin Heidelberg (1992).

[9] R. T. Haftka, and R. V. Grandhi, Structural shape optimization-a survey, Computer Methods in Applied Mechanics and Engineering 57.1 (1986): 91-106.

[10] M. P. Bendsøe, and N. Kikuchi, Generating optimal topologies in structural

design using a homogenization method, Computer methods in applied mechanics and engineering 71.2 (1988): 197-224.

[11] M. P. Bendsøe and O. Sigmund, Topology optimization-Theory, Methods and Applications, Springer-Verlag Berlin Heidelberg (2003).

M. P. Bendsøe, and O. Sigmund, Topology optimization: theory, methods and applications (2003).

[12] P. Duysinx, and M. P. Bendsøe, Topology optimization of continuum structures with local stress constraints, International journal for numerical methods in engineering 43.8 (1998): 1453-1478.

[13] O. Sigmund, On the design of compliant mechanisms using topology optimization, Journal of Structural Mechanics 25.4 (1997): 493-524.

[14] S. Nishiwaki, M. I. Frecker, S. Min, and N. Kikuchi, Topology optimization of compliant mechanisms using the homogenization method, International Journal for Numerical Methods in Engineering 42 (1998): 535-559.

[15] G. I. N. Rozvany, M. P. Bendsøe, and U. Kirsch, Layout optimization of structures, Applied Mechanics Reviews 48.2 (1995): 41-119.

[16] G. I. N. Rozvany, Some shortcomings in Michell's truss theory, Structural Optimization 12.4 (1996): 244-250.

[17] B. Descamps, Truss Layout Optimization, Computational Design of Lightweight Structures (2014): 1-32.

[18] G. I. N. Rozvany, Partial relaxation of the orthogonality requirement for classical Michell trusses, Structural optimization 13.4 (1997): 271-274.

[19] G. I. N. Rozvany, and T. Birker, Generalized Michell structures-exact least-weight truss layouts for combined stress and displacement constraints: Part I-General theory for plane trusses, Structural optimization 9.3-4 (1995): 178-188.

[20] Y. M. Xie and G. P. Steven, Basic evolutionary structural optimization, Springer London (1997).

[21] S. Osher, and J. A. Sethian, Fronts propagating with curvature-dependent

speed: algorithms based on Hamilton-Jacobi formulations, Journal of computational physics 79.1 (1988): 12-49.

[22] T. E. Bruns, and D. A. Tortorelli, Topology optimization of non-linear elastic structures and compliant mechanisms, Computer Methods in Applied Mechanics and Engineering 190.26 (2001): 3443-3459.

[23] G. P. Steven, Q. Li, and Y. M. Xie, Multicriteria optimization that minimizes maximum stress and maximizes stiffness, Computers & structures 80.27 (2002): 2433-2448.

[24] K. Suzuki, and N. Kikuchi, A homogenization method for shape and topology optimization, Computer methods in applied mechanics and engineering 93.3 (1991): 291-318.

[25] Z. D. Ma, N. Kikuchi, and H. C. Cheng, Topological design for vibrating structures, Computer methods in applied mechanics and engineering 121.1 (1995): 259-280.

[26] J. Du and N. Olhoff, Minimization of sound radiation from vibrating bimaterial structures using topology optimization, Structural and Multidisciplinary Optimization 33.4-5 (2007): 305-321.

[27] X. Y. Yang, Y. M. Xie, G. P. Steven and O. M. Querin, Topology optimization for frequencies using an evolutionary method, Journal of Structural Engineering 125.12 (1999): 1432-1438.

[28] G. H. Yoon, J. S. Jensen and O. Sigmund, Topology optimization of acoustic-structure interaction problems using a mixed finite element formulation, International journal for numerical methods in engineering 70.9 (2007): 1049-1075.

[29] W. Eddie, and M. Berggren, Topology optimization of an acoustic horn, Computer methods in applied mechanics and engineering 196.1 (2006): 420-436.

[30] J. Haslinger, A. Hillebrand, T. Kärkkäinen and M. Miettinen, Optimization of conducting structures by using the homogenization method, Structural and multidisciplinary optimization 24.2 (2002): 125-140.

[31] Q. Li, G. P. Steven, O. M. Querin and Y. M. Xie, Shape and topology design for heat conduction by evolutionary structural optimization, International Journal of Heat and Mass Transfer 42.17 (1999): 3361-3371.

[32] A. Iga, S. Nishiwaki, K. Izui and M. Yoshimura, Topology optimization for thermal conductors considering design-dependent effects, including heat conduction and convection, International Journal of Heat and Mass Transfer 52.11 (2009): 2721-2732.

[33] J. M. Johnson, and Y. Rahmat-Samii, Genetic algorithms and method of moments (GA/MOM) for the design of integrated antennas, IEEE Transactions on Antennas and Propagation 47.10 (1999): 1606-1614.

[34] D. S. Weile, E. Michielssen and D. E. Goldberg, Genetic algorithm design of Pareto optimal broadband microwave absorbers, IEEE Transactions on 3Electromagnetic Compatibility 8.3 (1996): 518-525.

[35] Z. Li, Y. E. Erdemli, J. L. Volakis and P. Y. Papalambros, Design optimization of conformal antennas by integrating stochastic algorithms with the hybrid finite-element method, IEEE Transactions on Antennas and Propagation 50.5 (2002): 676-684.

[36] A. Diop, I. Faye, I. Ly, and D. Seck, Shape and Topological Optimization for Electromagnetism Problems, Contemporary Engineering Science 3.8 (2010): 373-394.

[37] A. R. Díaaz, and N. Kikuchi, Solutions to shape and topology eigenvalue optimization problems using a homogenization method, International Journal for Numerical Methods in Engineering 35.7 (1992): 1487-1502.

[38] A. R. Diaz, and M. P. Bendsøe, Shape optimization of structures for multiple loading conditions using a homogenization method, Structural Optimization 4.1 (1992): 17-22.

[39] E. C. N. Silva, S. Nishiwaki, J. S. O. Fonseca and N. Kikuchi, Optimization methods applied to material and flextensional actuator design using the homogenization method, Computer Methods in Applied Mechanics and En-

gineering 172.1 (1999): 241-271.

[40] L. Tartar, An introduction to the homogenization method in optimal design. Optimal shape design, Springer Berlin Heidelberg (2000).

[41] G. Allaire, Shape optimization by the homogenization method, Springer Science & Business Media 146 (2002).

[42] J. Yoo, N. Kikuchi, and J. L. Volakis, Structural optimization in magnetic devices by the homogenization design method, IEEE Transactions on Magnetics 36.3 (2000): 574-580.

[43] J. Francu, Homogenization of linear elasticity equations, Aplikace matematiky 27.2 (1982): 96-117.

[44] O. A. Oleĭnik, G. A. Iosif'yan, and G. P. Panasenko, Asymptotic expansion of solutions of the system of elasticity theory in perforated domains, Mathematics of the USSR-Sbornik 48.1 (1984): 19.

[45] F. Campelo, J. A. Ramırez, and H. Igarashi, A survey of topology optimization in electromagnetics: considerations and current trends, (2010).

[46] O. Sigmund and J. Petersson, Numerical instabilities in topology optimization: a survey on procedures dealing with checkerboards, mesh-dependencies and local minima, Structural optimization 16.1 (1998): 68-75.

[47] A. Diaz, and O. Sigmund, Checkerboard patterns in layout optimization, Structural optimization 10.1 (1995): 40-45.

[48] F. Brezzi and M. Fortin, Mixed and hybrid finite element methods, Springer Series in Computational Mathematics 15 (1991).

[49] I. Babuška and R. Narasimhan, The Babuška-Brezzi condition and the patch test: an example, Computer methods in applied mechanics and engineering 140.1 (1997): 183-199.

[50] C. S. Jog and R. B. Haber, Stability of finite element models for distributed-parameter optimization and topology design, Computer methods in applied mechanics and engineering 130.3 (1996): 203-226.

[51] M. P. Bendsøe, Optimal shape design as a material distribution problem,

Structural optimization 1.4 (1989): 193-202.

[52] G. I. N. Rozvany, Aims, scope, methods, history and unified terminology of computer-aided topology optimization in structural mechanics, Structural and Multidisciplinary Optimization 21.2 (2001): 90-108.

[53] G. Kiziltas, D. Psychoudakis, J. L. Volakis and N. Kikuchi, Topology design optimization of dielectric substrates for bandwidth improvement of a patch antenna, IEEE Transactions on Antennas and Propagation 51.10 (2003): 2732-2743.

[54] C. G. Pedersen, J. J. Lund, L. Damkilde and A. S. A. Kristensen, Topology optimization-Improved checker-board filtering with sharp contours, Nordic Seminar on Computational Mechanics (2006).

[55] T. E. Bruns, A reevaluation of the SIMP method with filtering and an alternative formulation for solid-void topology optimization, Structural and Multidisciplinary Optimization 30.6 (2005): 428-436.

[56] M. P. Bendsøe and O. Sigmund, Material interpolation schemes in topology optimization, Archive of applied mechanics 69.9-10 (1999): 635-654.

[57] R. B. Haber, C. S. Jog and M. P. Bendsøe, A new approach to variable-topology shape design using a constraint on perimeter, Structural Optimization 11.1-2 (1996): 1-12.

[58] J. Petersson and O. Sigmund, Slope constrained topology optimization, International Journal for Numerical Methods in Engineering 41.8 (1998): 1417-1434.

[59] M. Zhou, Y. K. Shyy and H. L. Thomas, Checkerboard and minimum member size control in topology optimization, Structural and Multidisciplinary Optimization 21.2 (2001): 152-158.

[60] T. Borrvall, Topology optimization of elastic continua using restriction, Archives of Computational Methods in Engineering 8.4 (2001): 351-385.

[61] Q. Xia and M. Y. Wang, Topology optimization of thermoelastic structures using level set method, Computational Mechanics 42.6 (2008): 837-857.

[62] T. Borrvall and J. Petersson, Topology optimization using regularized intermediate density control, Computer Methods in Applied Mechanics and Engineering 190.37 (2001): 4911-4928.

[63] Y. M. Xie and G. P. Steven, Evolutionary structural optimization for dynamic problems, Computers & Structures 58.6 (1996): 1067-1073.

[64] D. N. Chu, Y. M. Xie, A. Hira and G. P. Steven, Evolutionary structural optimization for problems with stiffness constraints, Finite Elements in Analysis and Design 21.4 (1996): 239-251.

[65] O. M. Querin, G. P. Steven and Y. M. Xie, Evolutionary structural optimisation (ESO) using a bidirectional algorithm, Engineering Computations 15.8 (1998): 1031-1048.

[66] V. Young, O. M. Querin, G. P. Steven and Y. M. Xie, 3D and multiple load case bi-directional evolutionary structural optimization (BESO), Structural optimization 18.2-3 (1999): 183-192.

[67] X. Huang and Y. M. Xie, Bi-directional evolutionary topology optimization of continuum structures with one or multiple materials, Computational Mechanics 43.3 (2009): 393-401.

[68] X. Huang and M. Xie, Evolutionary topology optimization of continuum structures: methods and applications, John Wiley & Sons (2010).

[69] Y. M. Xie, Z. H. Zuo, X. Huang, J. W. Tang, B. Zhao and P. Felicetti, Architecture and urban design through evolutionary structural optimisation algorithms, Proceedings of the International Symposium on Algorithmic Design for Architecture and Urban Design 22 (2011).

[70] P. Tanskanen, The evolutionary structural optimization method: theoretical aspects, Computer methods in applied mechanics and engineering 191.47 (2002): 5485-5498.

[71] Q. Li, G. P. Steven and Y. M. Xie, A simple checkerboard suppression algorithm for evolutionary structural optimization, Structural and Multidisciplinary Optimization 22.3 (2001): 230-239.

[72] J. A. Sethian, Curvature and the evolution of fronts, Communications in Mathematical Physics 101.4 (1985): 487-499.

[73] Y. C. Chang, T. Y. Hou, B. Merriman and S. Osher, A level set formulation of Eulerian interface capturing methods for incompressible fluid flows, Journal of computational Physics 124.2 (1996): 449-464.

[74] M. Sussman, P. Smereka and S. Osher, A level set approach for computing solutions to incompressible two-phase flow, Journal of Computational physics 114.1 (1994): 146-159.

[75] M. Sussman and E. G. Puckett, A coupled level set and volume-of-fluid method for computing 3D and axisymmetric incompressible two-phase flows, Journal of Computational Physics 162.2 (2000): 301-337.

[76] J. C. Ye, Y. Bresler and P. Moulin, A self-referencing level-set method for image reconstruction from sparse Fourier samples, International Journal of Computer Vision 50.3 (2002): 253-270.

[77] K. Van Den Doel and U. M. Ascher, On level set regularization for highly ill-posed distributed parameter estimation problems, Journal of Computational Physics 216.2 (2006): 707-723.

[78] R. Tsai and S. Osher, Review article: Level set methods and their applications in image science, Communications in Mathematical Sciences 1.4 (2003): 1-20.

[79] J. A. Sethian, Level set methods and fast marching methods, Journal of Computing and Information Technology 11.1 (2003): 1-2.

[80] J. A. Sethian and A. Wiegmann, Structural boundary design via level set and immersed interface methods, Journal of computational physics 163.2 (2000): 489-528.

[81] D. Adalsteinsson and J. A. Sethian, A fast level set method for propagating interfaces, Journal of computational physics 118.2 (1995): 269-277.

[82] S. J. Osher and F. Santosa, Level set methods for optimization problems involving geometry and constraints: I. Frequencies of a two-density inhomoge-

neous drum, Journal of Computational Physics 171.1 (2001): 272-288.

[83] T. Belytschko, S. P. Xiao and C. Parimi, Topology optimization with implicit functions and regularization, International Journal for Numerical Methods in Engineering 57.8 (2003): 1177-1196.

[84] J. Dolbow and T. Belytschko, A finite element method for crack growth without remeshing, International Journal for Numerical Methods in Engineering 46.1 (1999): 131-150.

[85] T. Belytschko, C. Parimi, N. Moës, N. Sukumar and S. Usui, Structured extended finite element methods for solids defined by implicit surfaces, International journal for numerical methods in engineering 56.4 (2003): 609-635.

[86] M. Y. Wang, X. Wang and D. Guo, A level set method for structural topology optimization, Computer methods in applied mechanics and engineering 192.1 (2003): 227-246.

[87] M. Y. Wang and X. Wang, "Color" level sets: a multi-phase method for structural topology optimization with multiple materials, Computer Methods in Applied Mechanics and Engineering 193.6 (2004): 469-496.

[88] Q. Xia, M. Y. Wang, S. Wang and S. Chen, Semi-Lagrange method for level-set-based structural topology and shape optimization, Structural and multidisciplinary optimization 31.6 (2006): 419-429.

[89] S. Y. Wang, K. M. Lim, B. C. Khoo and M. Y. Wang, An extended level set method for shape and topology optimization, Journal of Computational Physics 221.1 (2007): 395-421.

[90] G. Allaire, F. Jouve, and A. M. Toader, A level-set method for shape optimization, Comptes Rendus Mathematique 334.12 (2002): 1125-1130.

[91] G. Allaire, F. Jouve, and A. M. Toader, Structural optimization using sensitivity analysis and a level-set method, Journal of computational physics 194.1 (2004): 363-393.

[92] G. Allaire, F. De, F. Jouve and A. Toader, Structural optimization using topological and shape sensitivity via a level set method, Control and cybernetics

34 (2005): 59-80.

[93] G. Allaire and F. Jouve, Coupling the level set method and the topological gradient in structural optimization, IUTAM symposium on topological design optimization of structures, machines and materials, Springer Netherlands (2006).

[94] H. A. Eschenauer, V. V. Kobelev and A. Schumacher, Bubble method for topology and shape optimization of structures, Structural optimization 8.1 (1994): 42-51.

[95] J. Céa, S. Garreau, P. Guillaume and M. Masmoudi, The shape and topological optimizations connection, Computer Methods in Applied Mechanics and Engineering 188.4 (2000): 713-726.

[96] S. Garreau, P. Guillaume and M. Masmoudi, The topological asymptotic for PDE systems: the elasticity case, SIAM journal on control and optimization 39.6 (2001): 1756-1778.

[97] T. Yamada, K. Izui, S. Nishiwaki and A. Takezawa, A topology optimization method based on the level set method incorporating a fictitious interface energy, Computer Methods in Applied Mechanics and Engineering 199.45 (2010): 2876-2891.

[98] T. Yamada, K. Izui and S. Nishiwaki, A level set-based topology optimization method for maximizing thermal diffusivity in problems including design-dependent effects, Journal of Mechanical Design 133.3 (2011): 031011.

[99] J. W. Cahn and J. E. Hilliard, Free energy of a nonuniform system. I. Interfacial free energy, The Journal of chemical physics 28.2 (1958): 258-267.

[100] S. M. Allen and J. W. Cahn, A microscopic theory for antiphase boundary motion and its application to antiphase domain coarsening, Acta Metallurgica 27.6 (1979): 1085-1095.

[101] K. Izui, K. Yokota, T. Yamada, S. Nishiwaki and M. Yoshimura, A Structural Optimization Method for Universal Design of Compliant Mechanism Scissors ASME 2009 International Design Engineering Technical Conferences

and Computers and Information in Engineering Conference, American Society of Mechanical Engineers, (2009): 871-880.

[102] N. Bakhtiary, P. Allinger, M. Friedrich, F. Mulfinger, J. Sauter, O. Müller and M. Puchinger, A new approach for sizing, shape and topology optimization, SAE Technical Paper (1996).

[103] S. Zhou, W. Li, Y. Chen, G. Sun and Q. Li, Topology optimization for negative permeability metamaterials using level-set algorithm, Acta Materialia 59.7 (2011): 2624-2636.

[104] A. P. Cisilino, Topology optimization of 2D potential problems using boundary elements, Computer Modeling in Engineering and Sciences 15.2 (2006): 99.

[105] X. Xing and M. Y. Wang, Topology optimization with level set method based on streamline diffusion finite element method. 8th World Congress on Structural and Multidisciplinary Optimization. Lisbon, Portugal (2009).

[106] T. Matsumoto, T. Yamada, T. Takahashi, C. J. Zheng and S. Harada, Acoustic design shape and topology sensitivity formulations based on adjoint method and BEM, CMES 1.1 (2009):1-19.

[107] T. Matsumoto, T. Yamada, S. Shichi and T. Takahashi, A study on topology optimization using level-set function and BEM, Boundary Elements and Other Mesh Reduction Methods XXXIV (2012): 123-133.

[108] W. Hackbusch and Z. P. Nowak, On the fast matrix multiplication in the boundary element method by panel clustering, Numerische Mathematik 54.4 (1989): 463-491.

[109] L. Gaul, M. Kögl and M. Wagner, Boundary element methods for engineers and scientists: an introductory course with advanced topics, Springer (2003).

[110] M. A. Jaswon and G. T. Symm, Integral equation methods in potential theory and elastostatics, London: Academic Press (1977).

[111] S. L. Crouch, A. M. Starfield and F. J. Rizzo, Boundary element methods in solid mechanics, Journal of Applied Mechanics 50 (1983): 704.

[112] T. A. Cruse, Recent advances in boundary element analysis methods, Computer methods in applied mechanics and engineering 62.3 (1987): 227-244.

[113] C. L. Tan and R. T. Fenner, Three-dimensional stress analysis by the boundary integral equation method, The Journal of Strain Analysis for Engineering Design 13.4 (1978): 213-219.

[114] N. Nishimura, Fast multipole accelerated boundary integral equation methods, Applied Mechanics Reviews 55.4 (2005): 299-324.

[115] M. Bebendorf, Hierarchical LU decomposition-based preconditioners for BEM, Computing, 74.3 (2005): 225-247.

[116] H. C. Wu, The Karush-Kuhn-Tucker optimality conditions in an optimization problem with interval-valued objective function, European Journal of Operational Research 176.1 (2007): 46-59.

[117] S. Yamasaki, S. Nishiwaki, T. Yamada, K. Izui and M. Yoshimura, A structural optimization method based on the level set method using a new geometry based reinitialization scheme, International journal for numerical methods in engineering 83.12 (2010): 1580-1624.

[118] S. P. Van Der Pijl, S. Segal, C. Vuik and P. Wesseling, A mass conserving Level-Set method for modelling of multi-phase flows, International journal for numerical methods in fluids 47.4 (2005): 339-361.

[119] H. Ishii, A boundary value problem of the Dirichlet type for Hamilton-Jacobi equations, Annali della Scuola Normale Superiore di Pisa-Classe di Scienze 16.1 (1989): 105-135.

[120] I. C. Dolcetta, On a discrete approximation of the Hamilton-Jacobi equation of dynamic programming, Applied Mathematics and Optimization 10.1 (1983): 367-377.

[121] N. F. Britton, Reaction-diffusion equations and their applications to biology, Academic Press (1986).

[122] J. Smoller, Shock waves and reaction-diffusion equations. Springer Science & Business Media 258 (1994).

[123] D. T. Gillespie, A general method for numerically simulating the stochastic time evolution of coupled chemical reactions, Journal of computational physics 22.4 (1976): 403-434.

[124] M. L. Williams, Stress singularities resulting from various boundary conditions, Journal of Applied Mechanics 19.4 (1952): 526-528.

[125] K. E. Atkinson, An introduction to numerical analysis, John Wiley & Sons (2008).

[126] K. J. Bathe and E. L. Wilson, Numerical methods in finite element analysis (1976).

[127] A. Quarteroni and A. Valli, Numerical approximation of partial differential equations, Springer Science & Business Media 23 (2008).

[128] E. Godlewski and P. A. Raviart, Numerical approximation of hyperbolic systems of conservation laws, Springer Science & Business Media 118 (2013).

[129] W. V. Petryshyn, Direct and iterative methods for the solution of linear operator equations in Hilbert space, Transactions of the American Mathematical Society (1962): 136-175.

[130] C. A. Brebbia and J. Dominguez, Boundary elements: an introductory course, WIT press (1996).

[131] P. Hunter and A. Pullan, Fem/bem notes, Department of Engineering Science, The University of Auckland, New Zealand (2001).

[132] T. Matsumoto, T. Yamada, S. Shichi and T. Takahashi, A study on topology optimization using level-set function and BEM, Boundary Elements and Other Mesh Reduction Methods XXXIV, WIT Press, (2012): 123-133.

[133] C. A. Brebbia and S. Walker, Boundary element techniques in engineering, Elsevier, (2013).

[134] W. M. Rohsenow, J. P. Hartnett and E. N. Ganic, Handbook of heat transfer fundamentals (1985).

[135] A. M. Papadopoulos, State of the art in thermal insulation materials and aims for future developments, Energy and Buildings 37.1 (2005): 77-86.

[136] A. S. Thom, Momentum, mass and heat exchange of plant communities, Vegetation and the Atmosphere 1 (1975): 57-109.

[137] G. X. Jing, T. Matsumoto, T. Takahashi, H. Isakari and T. Yamada, Topology optimization for 2D heat conduction problems using boundary element method and level set method, Transactions of Japan Society for Computational Methods in Engineering 13 (2013): 6.

[138] G. X. Jing, H. Isakari, T. Matsumoto, T. Yamada and T. Takahashi, Level set-based topology optimization for 2D heat conduction problems using BEM with objective function defined on design-dependent boundary with heat transfer boundary condition, Engineering Analysis with Boundary Elements 61 (2015): 61-70.

[139] G. X. Jing, H. Isakari, T. Matsumoto, T. Takahashi and T. Yamada, Topological sensitivity of objective function defined on morphing boundaries of two dimensional heat conduction problems, WIT Transactions on Modelling and Simulation, Boundary Elements and Other Mesh Reduction Methods XXXVII 57 (2014): 3-11.

[140] G. X. Jing, H. Isakari, T. Matsumoto, T. Takahashi and T. Yamada, Level Set-Based Topology Optimization of Two Dimensional Heat Conduction Problems using the Boundary Element Method, Proceedings of the Twelfth International Conference on Computational Structures Technology (2014): 193.

[141] G. X. Jing, H. Isakari, T. Matsumoto, T. Yamada and T. Takahashi, Topology optimisation for heat conduction problems in 2D with heat transfer boundary condition and heat flux objective function defined on morphing boundaries using BEM, Proceedings of the 38th International Conference on Boundary Elements and Other Mesh Reduction Methods (2015).

[142] G. X. Jing, T. Matsumoto, T. Yamada, T. Takahashi and H. Isakari, Identification of optimum topologies of heat conducting media in 2D using level set method and BEM, The 8th International Conference on Inverse Problem in Engineering, Poland, (2014).

[143] G. X. Jing, H. Isakari, T. Matsumoto, T. Takahashi and T. Yamada, Topological sensitivity of objective function defined on morphing boundaries of two dimensional heat conduction problems, The 37th International Conference on Boundary Elements and Other Mesh Reduction Methods, UK, (2014).

[144] G. X. Jing, T. Matsumoto, T. Takahashi, H. Isakari and T. Yamada, A topology optimization for 2D heat conduction problems using BEM, JSME 26th Computational Mechanics Division Conference (CMD2013), Saga, Japan, (2013).

[145] G. X. Jing, H. Isakari, T. Matsumoto, T. Takahashi and Takayuki Yamada Level set-based topology optimisation for two-dimensional heat problems using boundary element method with heat transfer boundary conditions, The Twelfth International Conference on Computational Structures Technology, Italy, (2014).

[146] G. X. Jing, H. Isakari, T. Takahashi, T. Yamada and T. Matsumoto, Topology optimization of two-dimensional thermal problem using BEM under heat transfer boundary condition, Japan Society of Computational Engineering and Science 19 (2014).